Master's Theses and Doctoral Dissertations

Master's Theses, and Doctoral Dissertations, and Graduate Capstone Projects

8-2008

Studies of polymers in fouling release coating science

Haoran Chen
Eastern Michigan University

Recommended Citation

Studies of Polymers in Fouling release coating science

by

Haoran Chen

Thesis

Submitted to the Department of Polymer & Coating

Eastern Michigan University

in partial fulfillment of the requirements

for the degree of

MASTER OF SCIENCE

in

Polymer and Coating science, College of Technology

Thesis committee:

Weidian Shen, PhD

John Texter, PhD, Chair

August, 2008

Ypsilanti, Michigan

ACKNOWLEDGMENTS

The author would like to express his heartfelt gratitude to Professor John Texter for his thoughtful supervision, resourceful advice, and patient guidance throughout the course of this work.

The author is earnestly grateful to all committee members for their time and efforts on reviewing this thesis.

The author would like to gratefully convey his acknowledgment to all his friends for their contributions to this work. Forgetting their assistance is none forgivable.

The author wishes to express his appreciation to his parents for their understanding and endless support through the duration of his studies. He is forever indebted to them.

ABSTRACT

In chapter one, we describe our studies of the solubility properties of two biocides in F127 aqueous solutions. One is zinc omadine and the other is C9211. The partition coefficients of these two biocides were also determined from the analytical results.

In chapter two, we conducted phase related studies of a triblock copolymer, PEO_{400}-PBO_{55}-PEO_{400} in aqueous solution. The phase diagram features of PEO_{400}-PBO_{55}-PEO_{400} in water are compared with those of F127. We believe the lack of a lower gel to liquid transition boundary in this system is because of the relatively longer PEO segments relative to the PBO segment.

In chapter three, we successfully prepared and characterized a polymerizable macromonomer, PEG-PS-DVB. A preliminary application of the polymer was investigated and nanoparticles were prepared by microemulsion polymerization. According to the characterizations, the nanoparticles have crosslinked cores and could be used as "inorganic free" nanofluid. No apparent thermoreversible behaviors were observed for these nanoparticles in water.

TABLE OF COTENTS

LIST OF FIGURES

LIST OF TABLES

Chapter I

Solubility and partition coefficients study of two biocides in F127 aqueous solutions

1.1 Introduction

It has been a major problem for the U.S. Navy and for the maritime shipping industry that bio-fouling, which consists of marine organisms attaching to submerged surfaces, greatly increases fuel needed to maintain a given cruise speed. An efficient way to prevent the attachment of fouling organisms is to use anti-fouling paints to protect the submerged boat surfaces. The principle idea is that the leakage of toxic substances (such as soluble copper, tributyltin [TBT], etc.), which are actual and effective components of anti-fouling paints, can prevent the settlement and growth of marine organisms.[1-3] Anti-fouling paints have been doing a good job although during their application, people found that certain desirable aquatic organisms or non-target organisms are also negatively impacted. With the development of anti-fouling paint industry, highly toxic and less degradable biocides are being replaced by those less toxic and more environmentally friendly biocides. For example, initially TBT was used as a substitute for organomercury, arsenic, or lead boosters in copper-based paints.[4] Later, it was found to be the most toxic substance ever artificially introduced into the aquatic environment. Since 1987, the use of tributyltin (TBT) has been banned and other organic booster biocides been introduced as substitutes for TBT in anti-fouling products.[5, 6] Currently the most commonly used biocides in anti-fouling paints are C9211, zinc pyrithione (zinc omadine) (Fig. 1.1), zineb,

dichlofluanid, chlorothalonil, TCMS (2,3,3,6-tetrachloro-4-methylsulfonyl) pyridine, and

TCMTB [2-(thiocyanomethylthio) benzothiazole].[1, 7] Those biocides are approved for use

by Health and Safety Executive (HSE) in amateur and professional anti-fouling products

marketed in the UK.[2, 8] However, these alternatives to TBT were also found to be toxic;

their contamination in the aquatic environment has been a topic of increasing importance

in recent years.[6]
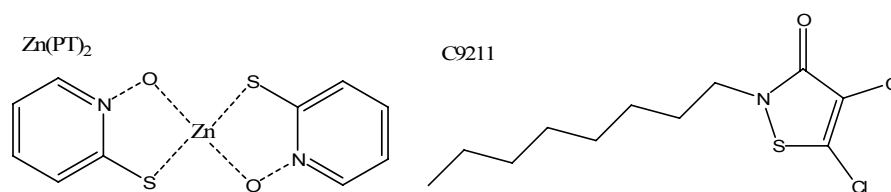
Figure 1.1 Molecular structures of biocides zinc omadine ($Zn(PT)_2$) and C9211.

Recently, many biocide-free anti-fouling paints have been developed to be more

friendly to the environment such as SSC-44, etc, but study has revealed that although

those "biocide-free" anti-fouling paints don't contain the compounds of "prohibited

biocide list," they still leak toxic substance into the environment during application that

are similar to biocides containing anti-fouling paints.[6] Unless totally leak-free anti-

fouling coatings are developed, some biocides, such as zinc omadine and C9211, will still

be used as components in anti-fouling paints.

A review by the UK Health and Safety Executive (HSE) as part of the European

Commission's Biocidal Products derivative (98/8/EC) has led to restrictions in the use of

booster biocides.[7] The results of these restrictions in the UK is that only paints containing

zinc omadine, dichlofluanid, or zineb as the active biocide can be applied on vessels less

than 25 m in length. In addition to these three biocides, Sea-nine 211, chlorothalonil, and Irgarol 1051 containing formulations may also be used on vessels more than 25 m in length.[1]

1.1.1 Zinc omadine and C9211

Zinc omadine ($C_{10}H_8N_2O_2S_2Zn$) has long been known as an effective bactericide, fungicide, and algaecide, and has more recently been used in anti-fouling paints as a booster biocide. Due to its low solubility in water, zinc omadine is also known as an anti-fouling pigment.[8-10]

C9211 has been used as a fungicide, among other targets against mildew. The substance has been chosen for anti-fouling applications by the producer Rohm & Haas through the screening of various isothiazolones using the parameters algae toxicity, barnacle toxicity, and water solubility (slow leaching).[8, 11] Because of its lower persistence in the environment and lower toxicity towards humans than TBT, the company won the "presidential green chemistry award" of the U.S. EPA in the category "designing safer chemicals."

1.1.2 Thermoreversible gel by F127

Many studies have shown that the triblock copolymer F127 (poly(ethylene oxide)-poly(propylene oxide)-poly(ethylene oxide) (PEO_{99}-PPO_{65}-PEO_{99}) in aqueous solution has thermoreversible gel phase behavior.[12-16] It will form gel phases above a certain copolymer concentration and within certain temperature range. This concentration has generally been found to be around 15 wt%,[14] and increasing the concentration decreases the temperature of the liquid-to-gel transition and increases the temperature of the gel-to-liquid transition, as can be seen from the shape of the measured boundaries. The

mechanism of gel formation in F127 has been discussed by others and is still a topic under debate in the literature. Physically, gel formation must be related to micellar packing and volume fraction. As the temperature is increased above the critical micelle temperature, micelles are formed, inevitably increasing the volume fraction occupied by the aggregates. A further increase in the temperature has been shown to increase the micellar volume fraction until it reaches a critical value for cubic close packing.[14, 17] Researchers have attributed gelation to the dehydration of PPO groups in the micelle core,[12] a change in the micellar volume,[17] or a decrease in the critical micelle concentration and increase in the aggregation number.[18] At higher temperatures, a gel-to-liquid transition is observed. The reason for the presence of this transition has been proposed to be due to the unfavorable water-PEO interaction at higher temperatures, resulting in the dehydration and shrinkage of micelle coronas.[17] This would effectively decrease the micellar volume and reduce the total volume fraction to below the critical value. The research group of S. C. Kimi1[17] observed this drop in the micelle volume fraction below the critical value at higher temperatures corresponding to the gel-to-liquid boundary. Others also found that the micellar core radius (~4.4nm) and the aggregation number of the micelles (~50) are independent of micellar concentration and temperature.[19] Below 23°C, the CMC of F127 in water is 2wt.%,[20] so in our research, in order to measure biocide concentration in aqueous solution accurately so as to calculate the corresponding partition coefficient, all F127 containing samples were diluted to less that 2 wt%. This dilution insures that the biocides are released from F127 micelles since the micelles are dissociated.

1.1.3 F127-based fouling release coatings

With the development of the coating industry and the environmental issues increasing, fouling release coatings are more and more popular in recent years.[16, 21, 22] The main purpose of fouling release coatings is to keep a submerged surface from attaching of foulings (mainly biofouling) without any toxic leaking to the environment. The function mechanisms of fouling release coating are quite complex. Generally speaking, the fouling release coatings could be developed by the following materials: (a) low surface free energy materials, which would reduce interactions between bioadhesives and the coating surfaces; (b) high molecular mobility (e.g., low glass transition temperature, Tg) to minimize mechanical locking that takes place when a bioadhesive cures in crevices and surface imperfections; (c) a low modulus material for facilitating breaking of adhesive joints, and (d) chemical and physical stability upon long-term water exposure to prevent an increase in surface free energy and to avoid loss of mass and the development of surface roughness. F127 is very soft and has a low modulus, and our group has been developing fouling release coating on it for years.

1.2 Experimental

Knowledge of the partition coefficient of a biocide in F127 is important for developing a potential formulation and characterizing the performance of the formulation.[23] The partition coefficient indicates the equilibrium loading of the biocides and sets up the initial concentration gradient that will drive biocides release. The release of biocides from micellar liquid crystalline systems has been reported to depend on the hydrophobicity.[24] The biocide release rate can decrease with an increasing hydrophobicity, or the relationship between biocide partitioning and biocide release can

be more complex, making it important to know the partition coefficient. Biological activity can increase parabolically up to a maximum at an optimal partition coefficient.[25] Provided it is the only influencing factor, it may be possible to predict properties such as biological activity for structurally similar compounds from accurate measurements of the partition coefficient of an existing compound. Furthermore, accurate measurement of the partition coefficient of biocides in F127 solutions may allow the calculation of substituent hydrophobicity constants[25] that can be used to estimate the performance and properties of newly discovered analogue biocides that might be completely friendly to the environment.

1.2.1 Materials

Pluronic® F127 is a triblock copolymer PEO_{99}-PPO_{65}-PEO_{99}, with a molecular weight of 12,600; flakes at room temperature and melts at 56°C. It was a gift of BASF and was used as received. The biocide zinc omadine ($Zn(PT)_2$), a white powder, and the biocide C9211 ($C_{11}H_{17}C_{l2}NOS$, 4,5-dichloro-2-octylisothiazol-3(2H)-one), a brown solid. Formic acid and methanol were purchased from Aldrich; all are reagent grade and were used as received. Deionized water, obtained from a purification system located in Sill Hall, EMU, was used for all solutions.

1.2.2 Measurements

Ultraviolet spectroscopy (UV-Vis Jasco-v530), centrifugation, and isothermo water bath (setting at 23°C) were used to measure the solubility of biocide and calculate the partition coefficient between micelle and water (K_{mw}) of each biocide in F127 aqueous solution. All reported experiment data values are measured at 23±1°C.

In the fields of organic and medicinal chemistry, a partition (distribution) coefficient is the ratio of concentrations of a compound in the two phases of a mixture of two

immiscible solvents at equilibrium.[23] In our research, we assume that the micelle core is a relatively hydrophobic phase though the core actually contains both PPO segments and water, and the micelle corona (PEO) and aqueous solvent together comprise a relatively hydrophilic phase. This assumption is common in colloid and medicinal science[14, 26] and is often referred to as the pseudophase approximation. We use the equation below to calculate the micelle–water partition coefficients for the biocides Zn(PT)$_2$ and C9211 in F127 aqueous solutions.[27-29]

$$K_{mw} = \frac{[X]_{core}}{[X]_{aq}} \ldots\ldots\ldots\ldots\ldots\ldots\ldots\ldots\ldots\ldots\ldots\ldots\ldots\ldots\ldots\ldots\ldots\ldots\ldots\ldots\ldots\ldots\ldots \quad (1)$$

This equation works in the case of a dilute system and equilibrium. The partition coefficient, K, is given by the ratio of the concentration of solute in each phase.[28] Ultraviolet spectroscopy (UV-Vis Jasco-v530) was used to measure concentration. For biocides zinc omadine and C9211, the wavelengths of maximum absorption were found to be 267nm and 280nm respectively, in our system. All UV-Vis measurements were conducted at those wavelengths, respectively.

1.2.3 Preparation of standard samples and calibration curve

Our preparation of standard reference samples took account of the phase behavior of F127 in an aqueous environment, the physical properties of the biocides,[30] and the effects of F127's absorption at certain wavelengths. We found there are only minor effects on the biocide UV-Vis absorption spectra caused by the existence of F127.

To make the standard samples, first, a certain amount of biocide is dissolved in specific solvents to get a fixed concentration biocide solution. Then bulk solvent mixtures are used to dilute a certain amount of the fixed concentration biocide solution to get a serial dilution series of the biocide solutions. For example, we use a certain amount of

Zn(PT)$_2$ to make a 0.0395mg/g Zn(PT)$_2$ solution in a specific solvent, 0.175 v/v% formic acid, and 99.825 v/v% methanol and water (CH$_3$OH:H$_2$O=3:7 v/v).[30] We then used the bulk solvent to dilute a certain weight of 0.0395mg/g Zn(PT)$_2$ solution to get a set of serial dilutions of fixed concentration biocide solutions. At a fixed wavelength (for Zn(PT)$_2$) 267nm, we can get serials of readings of absorption. A standard calibration curve is then completed by plotting those readings vs. concentration, as illustrated in Fig. 1.4.

1.2.4 Preparation of field samples and measurement of the concentrations

The preparation of field or actual partitioning samples utilized an isothermal water bath and centrifuge equipment. First, an excess of biocide is placed in a fixed concentration F127 aqueous solution, and then the sample is shaken for 5 to 7 days to get a saturated equilibrium biocide solution. The sample is then centrifuged at 3000 rmp for 5 minutes to separate the excess biocide. The supernatant is then transferred to a new container and centrifuged again to make sure there is no more excess biocide in that sample. This supernatant is then diluted by about 5 to 10 fold with a specific solvent so that the final diluted sample comprises similar components to a corresponding standard sample. An absorption value is then measured for the diluted sample on UV-Vis instrument at the fixed wavelength. From the standard calibration curve, we find the diluted biocide concentration, and we then back-calculate the solubility (concentration) from the total volume dilution.

1.3 Results and discussion

1.3.1 Solubility properties of Zn(PT)$_2$

Spectra of the solvent mixture, F127, and the biocide are shown in Fig. 1.2 and 1.3. Zinc omadine, Zn(PT)$_2$, is illustrated in Fig 1.2, and C9211 in methanol and in water is shown in Fig 1.3. The UV absorption maximum of 267.5 nm and 282 nm for zinc omadine and C9211, respectively, were used for analysis.

Table 1.1 shows the UV absorption of standard samples for Zn(PT)$_2$ at wavelength 267.5 nm at different levels (wt%) of F127. Based on this table, Zn(PT)$_2$ calibration curves in F127 and the mixed solvent were plotted in Fig 1.4. From the figure, we can see that below 25 μg/g (Zn(PT)$_2$/solution), F127 level has little effect on the UV absorption. Since all the actual samples were highly diluted, and in order to minimize any systematic error that might result from using different calibration curves from Fig. 1.4, we prepared another calibration curve for Zn(PT)$_2$ concentration measurement (Fig. 1.5). The standard samples in Fig. 1.5 have no F127, and all the concentration is lower than 14 μg/g.

The calibration curve in Fig 1.5 is Y=0.0401X; here X is the concentration (μg/g) of zinc omadine and Y is the absorption reading value from UV-Vis spectrometer. To check how accurate this curve would be, three samples that have known concentration of Zn(PT)$_2$ were measured the same time, right after the standard sample was done (Table 1.2). According to Table 1.2, we confirmed that the accuracy of the calibration curve Y=0.0401X is good enough for determining the Zn(PT)$_2$ concentration in diluted solutions. Also, to eliminate system error on field Zn(PT)$_2$ samples' measurement as much as possible, three batches of field samples were made at the same time (Table 1.3). Table 1.3 also gives partition coefficient value of Zn(PT)$_2$ between F127 micelles and

water. Those coefficients are quite low when compared with that of other biocides.[14, 26] But the existence of F127 do help to increase the solubility of Zn(PT)$_2$ in F127 aqueous solutions when compared to that in pure water (Fig 1.6).
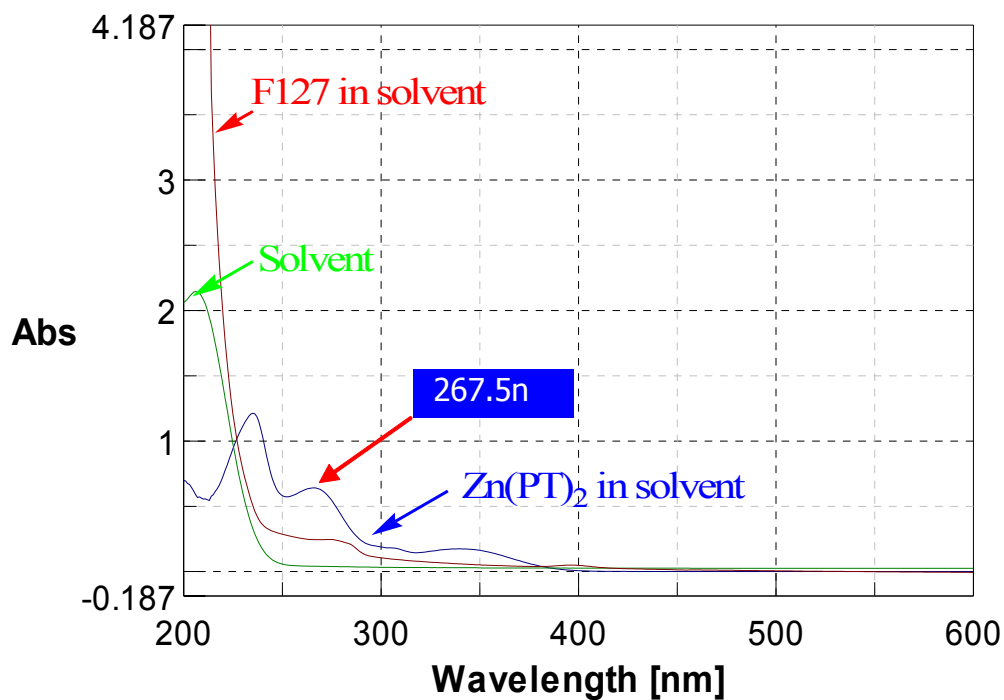
Figure 1.2 UV-Vis spectra of solvent (green curve), F127 (10 wt%, red curve) in mixed solvent, and biocide Zn(PT)$_2$ (blue curve) in mixed solvent. The mixed solvent comprised 0.175 v/v% HCOOH in methanol/water (3:7, v/v).
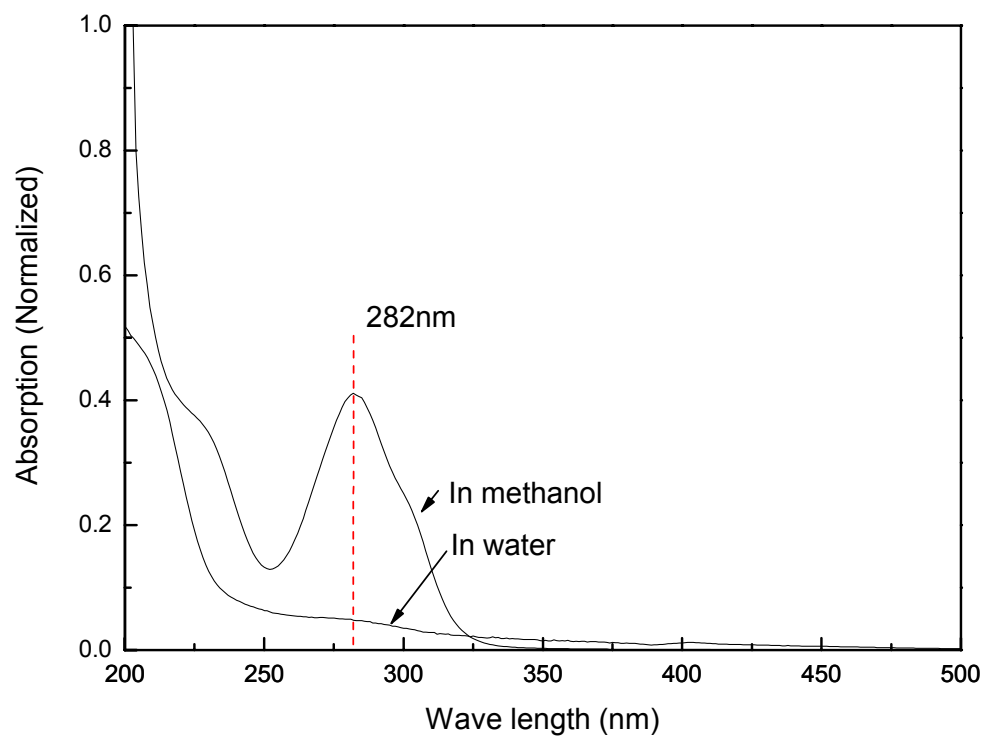
Figure 1.3 UV-Vis spectra of biocide C9211 in methanol and water; the solubility of

C9211 in water is about 6 ppm (0.0006 wt%)[8].

Table 1.1 UV absorption of standard samples of $Zn(PT)_2$ in mixed[30] solvent[a) with different amounts of F127 at 267nm.

F127	$Zn(PT)_2$ (μg/g)/Abs					
(wt%)	39.50	19.69	7.910	3.968	2.468	1.605
0.0	1.571	0.7787	0.3267	0.149	0.1003	0.0634
0.4	1.447	0.7751	0.3464	0.1544	0.0998	0.0676
0.8	1.682	0.8343	0.3386	0.1655	0.1054	0.0684
1.2	1.635	0.7825	0.3511	0.1781	0.1209	0.0847
1.6	1.607	0.8148	0.3535	0.1707	0.1138	0.0763
2.0	1.579	0.8118	0.3561	0.1776	0.1220	0.0863

a) Solvent comprises 0.175% HCOOH in methanol/water (3:7 v/v).
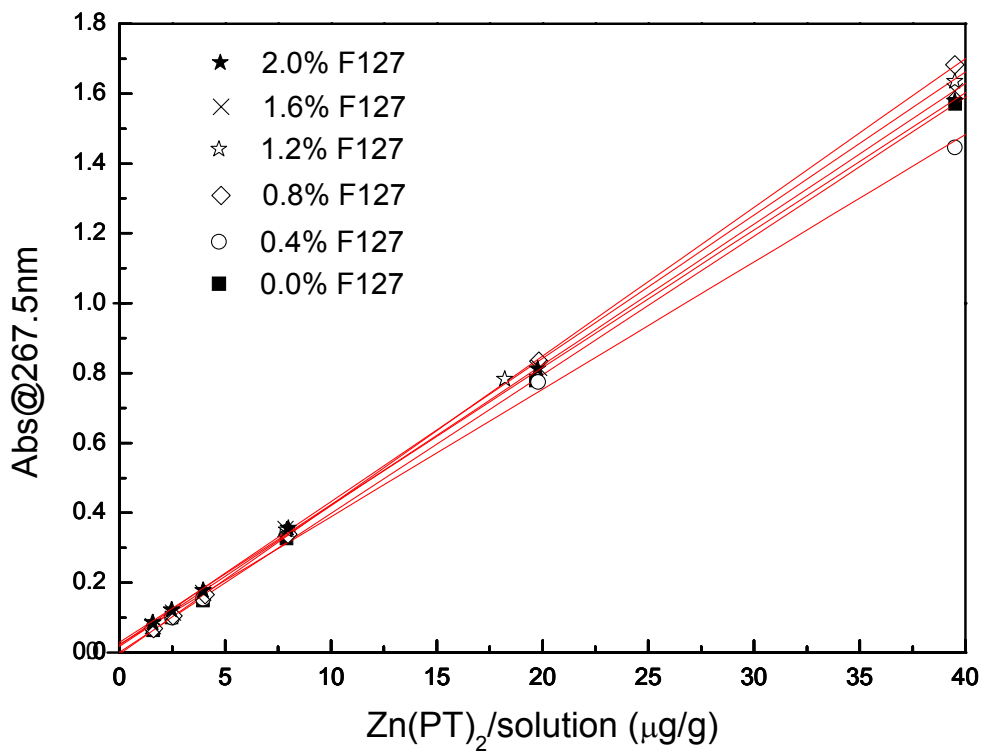
Figure 1.4 Concentration calibration curve of biocide $Zn(PT)_2$ in various solvents that consist of a certain percent of F127, 0.175v/v% formic acid in methanol/water $(CH_3OH:H_2O=3:7 \text{ v/v})^{30}$.
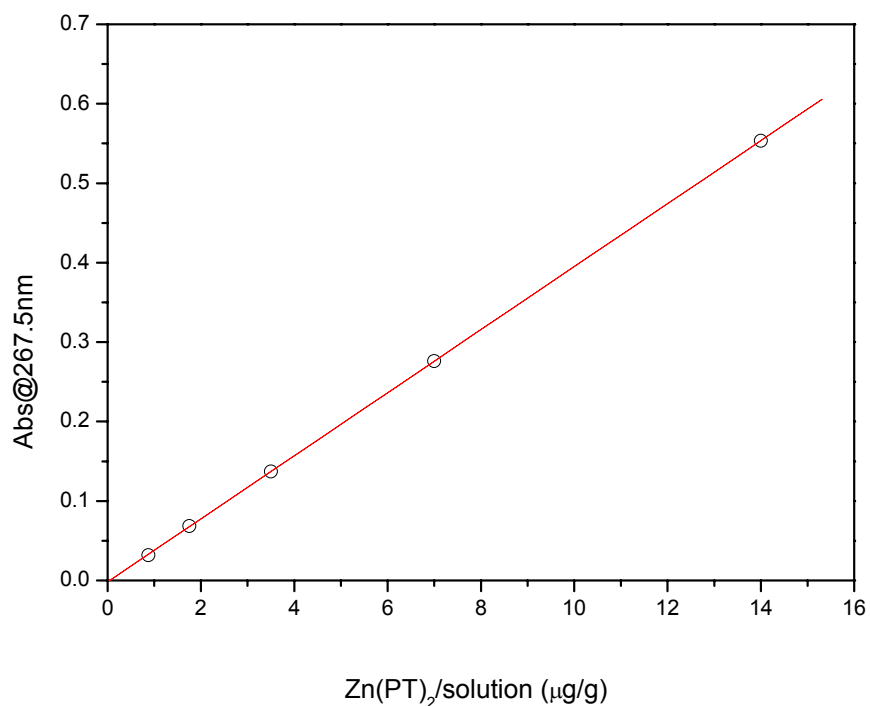
Figure 1.5 Low range $Zn(PT)_2$ concentration calibration curve without F127.

Table 1.2 Comparison of $Zn(PT)_2$ concentration between theoretical and practical value for three known samples

Sample label	F127 (wt%)	Abs	Concentration(µg/g)		
			Theoretical	Actual[a]	Relative[b]
1	0.54	0.5868	12.98	14.2469	0.089
2	1.90	0.3703	6.236	8.6484	0.279
3	0.00	0.1838	2.504	3.4289	0.270

a) Calculation was based on Fig. 1.5 calibration curve.

b) $Relative = |Actual - theoretical| / Actual$

Table 1.3 Zn(PT)$_2$ concentration measurement based on Fig. 1.5 calibration curve

F127	Batch 1		Batch 2		Batch 3		Concentration	St.	K$^{c)}_{mw}$
(wt%)	Dil$^{a)}$	Abs	Dil	Abs	Dil	Abs	(μg/g)$^{b)}$	Dev	
0	10.05	0.0155	9.99	0.0129	9.99	0.0129	3.428	0.31	-------
4	9.97	0.0229	9.98	0.0215	9.97	0.0232	5.592	0.18	16.78
8	9.90	0.0438	9.99	0.0455	10.60	0.0429	11.14	0.24	29.1
12	10.00	0.0661	10.01	0.0642	9.99	0.0647	16.17	0.19	31.96
16	13.47	0.0851	11.43	0.0808	10.93	0.1081	28.96	0.37	47.54

a) Dil for dilution factor. Each sample was diluted before measuring.

b) The concentration has been averaged based on three batch samples results.

c) Kmw is the partition coefficient between micelles and water. The calculations were based on equation (1).
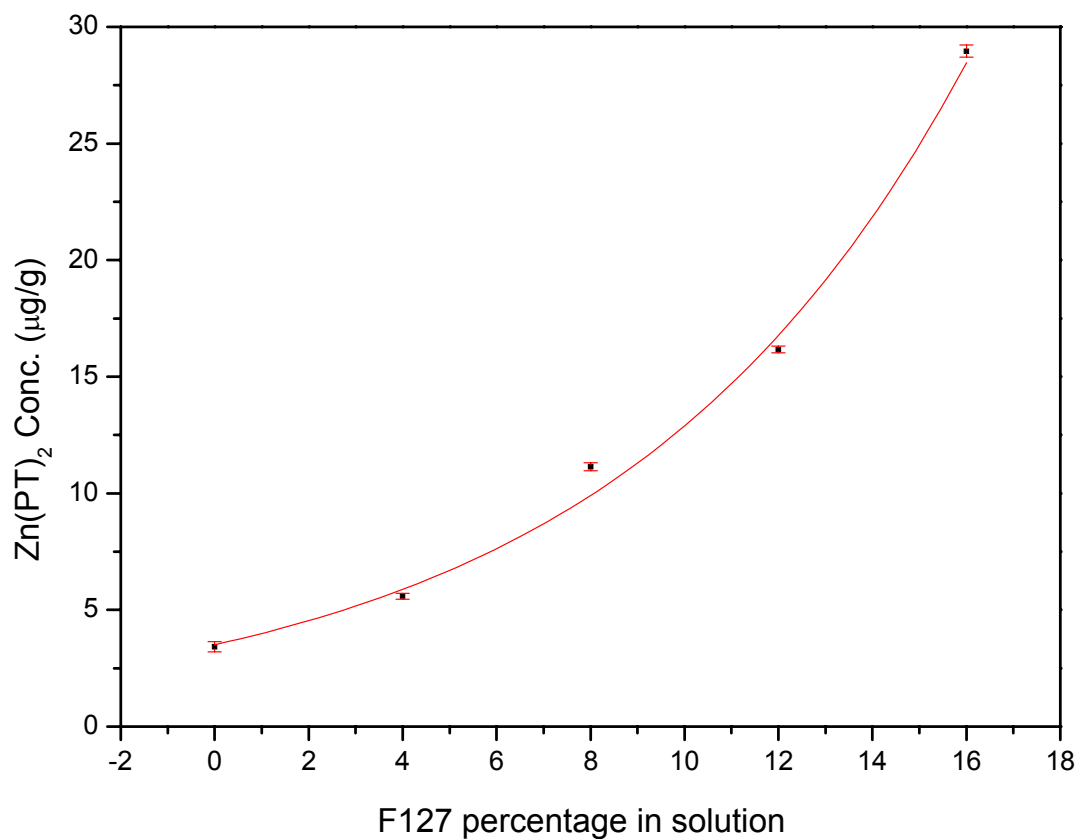
Figure 1.6 Zn(PT)$_2$ concentration as a function of F127 fraction in water solution; red dash is error bar.

The F127 micelles in aqueous solution have a core radius of about 4.4 nm, and the aggregation number of the micelles is around 50. These properties are independent of micellar concentration and temperature.[19] Based on this model, we calculated how many Zn(PT)$_2$ molecules there are in one F127 micelle (Table 1.4) at different levels of F127. According to Table 1.4, it seems that in saturated Zn(PT)$_2$ aqueous F127 solutions, there

is less than one molecule $Zn(PT)_2$ in each F127 micelle. In other words, some F127 micelles are empty even after 5~7 days equilibration processing for $Zn(PT)_2$. This indicates that the solubility of $Zn(PT)_2$ in F127 micellar is quite limited. Even at a very high content of F127 (near its liquid to gel boundary) in the solution at $23 \pm 1^{\circ}C$, the solubility of $Zn(PT)_2$ is still not much (29µg/g), even though zinc omadine is still a broad-range antimicrobial agent with very high activity. The scientific data on algae toxicity indicate inhibitory activity at concentrations as low as 0.01µg/g for $Zn(PT)_2$.[8] Acute toxicity and embryotoxicity[31] towards fish was found at concentrations of 0.003µg/g and 0.01µg/g, respectively. From this point of view, Table 1.3 and Fig 1.6 show that $Zn(PT)_2$ could still be a very efficient antimicrobial agent when incorporated with F127 in water.

Table 1.4 $Zn(PT)_2$ quantitative molecular distribution in F127 aqueous micelles.

F127 (wt%)	In water (µg).	Total (µg)	In micelle (µg)	$N_{Zn(PT)2}$ micelle^{-1}
0.0	3.4283	3.4283	0.0000	----
4.0	3.2912	5.5917	2.3005	0.11
8.0	3.1541	11.1353	7.9813	0.20
12.0	3.0169	16.1664	13.1495	0.22
16.0	2.8798	28.9567	26.0769	0.32

1.3.2 Solubility properties of C9211

C9211 has very limited solubility in pure water, which is around 6ppm.[8] Fig. 1.7 is a standard concentration calibration curve for C9211; based on this curve, three batches of filed samples were measured (Table 1.5). Table 1.6 was calculated based on both Table 1.5 and Fig. 1.7. As we can see that in Table 1.4 and Table 1.6, two biocides' partition coefficients respectively between F127 micelle and water K_{mw} have been calculated. As we have mentioned, the calculation was based on equation 1. For example, $[X]_{aq}$ is equal to the concentration where the sample contains zero percent of F127, while $[X]_{core}$ is calculated from $[X]_{aq}$ and the total $[X]$. Roughly the difference between $[X]$ and $[X]_{aq}$ is due to the introduction of F127, so that $[X]_{core}= ([X] - [X]_{aq})/[F127]$ approximately. In other words, we calculated or estimated those partition coefficients K_{mw} (Table 1.3 and Table 1.5) based on the biocides' concentration in F127 and the concentration in aqueous phase. Moreover, the quantitative molecular distribution in F127 aqueous micelles (Table 1.4 and Table 1.6) were calculated based on the F127's molecular weight (126,00), the biocides' concentration in F127, and the concentration of F127 in the solution. Tables 1.5 and 1.6 indicate that in aqueous solution, the existence of F127 greatly helps to increase the solubility of biocide C9211 (Fig 1.8). This indicates that the interaction between F127 micelles and C9211 molecular is strong and according to Table 1.6, at room temperature, each F127 micelle can hold more than 5 C9211 molecules.
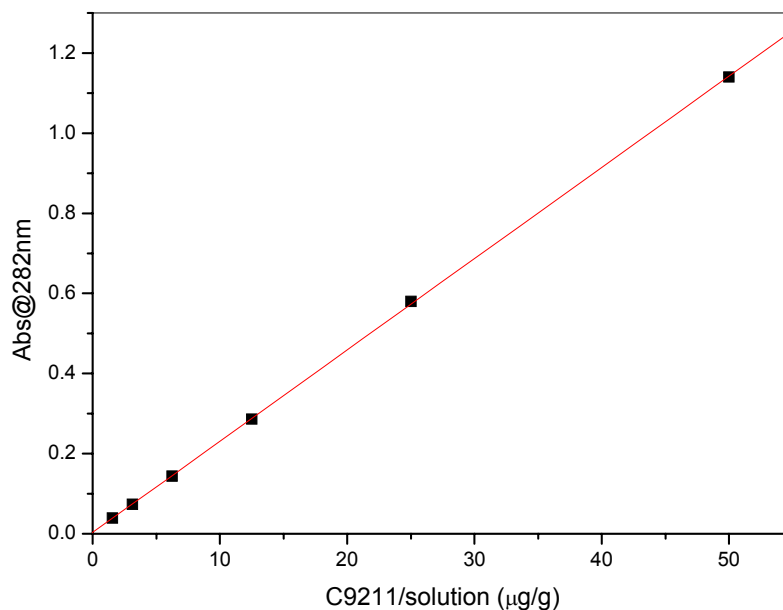
Figure 1.7 Concentration calibration curve of biocide C9211 in methanol solvent.

Table 1.5 C9211 concentration measurement

F127	Batch 1		Batch 2		Batch 3		Concentration	St.	K_{mw}[c]
(wt%)	Dil[a]	Abs	Dil	Abs	Dil	Abs	$(\mu g/g)$[b]	Dev	
0	9.99	0.0172	9.98	0.0166	9.99	0.0122	6.93	1.0	-------
4	10.05	0.0938	9.99	0.127	9.71	0.117	50.41	6.0	157.9
8	10.05	0.273	10.04	0.278	10.03	0.397	143.6	25.9	247.6
12	9.99	0.429	10.02	0.756	9.85	0.753	290.6	68.6	342.2
16	9.93	0.758	9.99	0.811	9.90	0.912	371.8	28.1	330.2

a) Dil for dilution factor. Each sample was diluted before measuring.

b) The concentration is an average value based on three batch samples results.

c) K_{mw} is partition coefficient between micelles and water.

Table 1.6 C9211 quantitative molecular number distribution in F127 aqueous micelles.

F127 (wt%)	In water (μg).	Total (μg)	In micelle (μg)	N_{C9211} micelle^{-1}
0.0	6.93	6.93	0.00	----
4.0	6.65	50.41	43.76	2.4
8.0	6.37	143.6	137.2	3.8
12.0	6.10	290.6	284.5	5.3
16.0	5.82	371.8	366.0	5.1
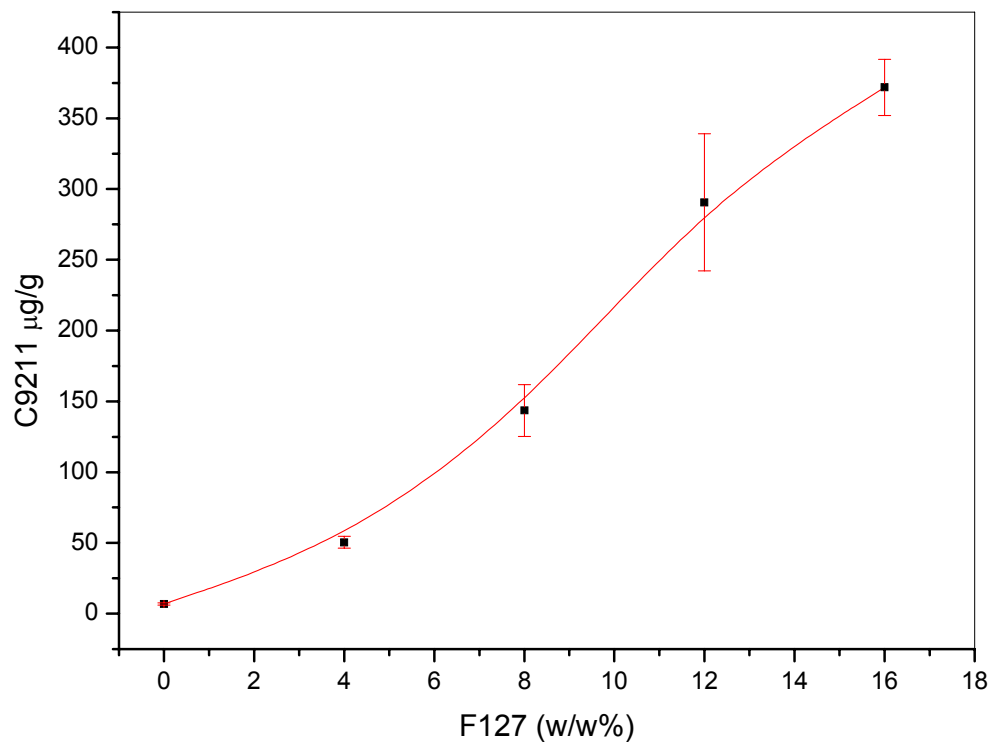
Figure 1.8 C9211 concentration as a function of F127 fraction in water solution.

1.4 Conclusions:

The solubility properties of two biocides, zinc omadine and C9211, in F127 aqueous solutions were studied by simply using UV-Vis spectrometry. The partition coefficients of those two biocides were determined based on the analytical results. The triblock copolymer F127 can help to increase both $Zn(PT)_2$ and C9211's solubility in water. It seems that the $Zn(PT)_2$ is immiscible with F127 aqueous solution for there are still empty micelles in the saturated $Zn(PT)_2$ solutions containing a certain amount of F127. The C9211's apparent micelle–water partition coefficient is much higher than that of $Zn(PT)_2$. Its quantitative molecular distribution in F127 aqueous micelles shows that when saturated, each F127 micelle can hold around 5 C9211 molecules. Hopefully those results are important for assessing the feasibility and the potential industrial performance of possible anti-fouling coating formulations.

Chapter II

Phase study of a triblock copolymer PEO_{400}-PBO_{55}-PEO_{400} in aqueous solution

2.1. Introduction

Much work has been done on studying triblock copolymers of poly(ethylene oxide) (PEO) and poly(propylene oxide) (PPO).[20, 32-34] Much additional work in the field of biochemistry and drug delivery on PEO has established that PEO has novel properties in retarding the adsorption of proteins.[35-38] This retardation has made PEO very popular in formulating drug delivery systems.[39]

More fundamentally, studies of the various structures of PEO-PPO-PEO micelles in various solutions have shown that such triblock copolymer micelles generally form cubic lattice gels or lyotropic crystalline phases when the conditions are appropriate.[40, 41] What's more, the gels formed by PEO-PPO-PEO triblock copolymers are thermoreversible, where gel phases form from solution as temperature is increased. However, when it comes to PEO-PBO-PEO triblock copolymers, much less work has been disclosed than with PEO-PPO-PEO systems. It is easily understood that PEO-PBO-PEO is more difficult to be synthesized due to the lower reactivity of 1,2-butylene oxide than that of ethylene oxide.

Nevertheless, there are several publications on PEO-PBO diblock and PEO-PBO-PEO triblock copolymers. Similar to Pluronic® copolymers, PEO-PBO-PEO copolymers can also form (cubic lattice) gels or lyotropic crystalline phases. Yu et al.[42, 43] synthesized

highly ordered mesoporous silica structures including body-centered cubic (Im3m), 2D hexagonal (p6mm) and lamellar (Lα) symmetries by using hydrophobic poly (butylene oxide) moiety diblock and triblock copolymers as structure-directing templates. Alexandridis et al.[44] also studied the phase behavior of the $PBO_{10}PEO_{17}$ diblock in the presence of water and xylene. They gave a complete phase diagram of the ternary $PBO_{10}PEO_{17}$-water-xylene system. They also reported the effect of solvent quality on reverse micelle formation and water solubilization by PEO-PPO-PEO and PEO-PBO block copolymers in xylene.[45] In another report, Alexandridis et al. found that a PEO-PBO diblock copolymer exhibited a much lower CMC than the corresponding PEO-PBO-PEO block copolymer.[46] This observation is consistent with findings of Helfand and Wasserman,[47] where AB diblock copolymers form domains of the same size (presumably at a similar composition range) as ABBA triblocks (of the same A/B composition but of double the AB molecular weight). Yu et al. also found that for different block architectures, the pore size of mesoporous materials templated by diblock copolymer is much larger than that templated by triblock copolymer.[43]

PPO- and PBO-based copolymers have also been investigated as stabilizers in making PMMA polymer microparticles by spray process with compressed fluids including supercritical or near critical fluids.[48] For example, block copolymer surfactants with either PPO or PBO CO_2-philic groups have been used to stabilize 0.03 wt% PMMA latexes in supercritical and near critical CO_2. The results of that study suggested that PPO and PBO are novel CO_2-philic groups in addition to those stabilizer surfactants based on flourine and silicon.[48]

Although researchers have conducted plenty of investigations on PPO-based copolymers, few data can be found on the phase diagrams of PEO-PBO-PEO triblock copolymers in aqueous solution. Our group has been developing anti-fouling and fouling release coatings for several years[16, 49, 50] based on thermoreversible F127 (PEO_{99}-PPO_{65}-PEO_{99}) gels. The surface of the coating made by F127 is basically PEO, so it has less tendency for the fouling to accumulate. However, one problem is that F127 is too soft and it can't meet the mechanical property requirements of real coating applications.

More rigid (higher modulus) PEO-containing polymers are desired for developing practical fouling release coatings. The triblock copolymer PEO_{400}-PBO_{55}-PEO_{400} has a longer polymer chain than F127 but a similar molecular structure. Moreover, its PBO segment is more hydrophobic than the PPO segment in F127 and has a higher molecular weight.[51] PEO_{400}-PBO_{55}-PEO_{400} should therefore have a higher mechanical modulus and be tougher than F127. In this study, we constructed the phase diagram of the binary water-PEO_{400}-PBO_{55}-PEO_{400} system as a function of temperature and weight fraction. We also carried out thermal characterizations (from DSC and TGA), molecular weight distribution measurements, and NMR experiments.

2.2 Experimental

2.2.1 Materials

The block copolymer PEO_{400}-PBO_{55}-PBO_{400} was prepared by sequential anionic polymerization. Initiator solution was prepared by dissolving freshly cut potassium in freshly distilled diethylene glycol. A portion of this solution served to initiate the polymerization of 1, 2-butylene oxide in an ampoule under vacuum conditions at 50ºC for 3 days and then at 75ºC until polymerization was complete. The molecular weight

calculated from preparative conditions was $M_n = 4000$. The poly(oxybutylene) was then

used to initiate the polymerization of ethylene oxide at about 10ºC raised to 70ºC over a

period of two weeks until conversion was complete (Scheme 2.1). All water used was

deionized.
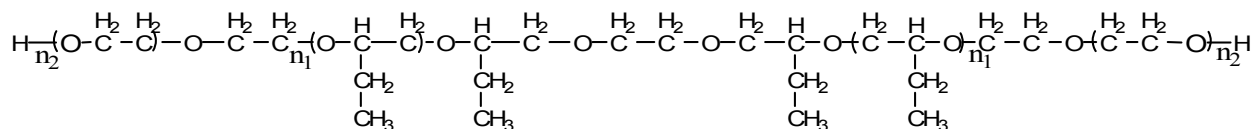
Scheme 2.1 Molecular structure of PEO$_{400}$-PBO$_{55}$-PEO$_{400}$ (n$_1$ is about 28 and n$_2$is

about 400)

2.2.2 Methods

2.2.2.1 DSC, TGA, NMR and GPC measurements

Differential scanning calorimetry (DSC) measurements were done using a 2920

MDSC (TA Instruments, New Castle, Delaware, USA) at a heating rate of 5°C/min; a

heating and cooling cycle was applied when necessary. Thermal gravimetric analysis

(TGA) measurements were done using a TA Instruments Q500 to check the

decomposition temperature of the triblock copolymer. ^{1}H NMR spectra were carried out

at 25°C on a Jeol 400 MHz ^{1}H/^{13}C NMR spectrometer with tetramethylsilane as an

internal standard and CDCl$_3$ as a solvent. Samples for molecular weights analysis were

dissolved in either water or THF and analyzed by using corresponding columned GPC,

which were equipped with autosampler (Waters, 717 plus), HPLC pump at 1 ml/min

(Waters, 515), and four columns (guard, 105 Å, 103 Å, and 100 Å; Polymer Standards

Services) in series. Toluene was used as the internal standard. A calibration curve based on monodisperse PEG (for water) or linear polystyrene (for THF) standards were used in conjunction with a differential refractometer (Waters, 2410). CMC measurements were done through pendant drop method by measuring samples' surface energy as a functional of polymer aqueous concentration. The test utilized a dynamic contact angle (DCA) instrument (FTA200, First Ten Angstroms, Inc).

2.2.2 2 Determination of phase boundaries

Various amounts of PEO_{400}-PBO_{55}-PBO_{400} polymer were put into different PYREX disposable culture tubes, and then appropriate amounts of deionized (DI) water were added to form various concentrations of polymer solution (a water bath was used to help the dissolving process at higher temperature). After different solutions were prepared, the sample tubes were then put into a HAAKE K20 (Haake, Germany) bath (-20°C to +130°C) for phase boundary mapping. The measurements were run slowly enough to ensure the highest possible accuracy of phase status. Evaporation of water into the empty (dead) space in the vials and the higher probability of formation of small bubbles may lead to an increasing error of the measured results at higher temperatures. The water bath temperature settings were changed gradually. After equilibrium, the samples were then examined by ocular inspection for transparency and apparent viscosity. At each temperature it was recorded whether an apparent first order phase change had ensued or not.

Measurements were done under atmospheric pressure, so the seals of the tube caps were broken briefly and often in order to prevent pressurization of the samples, although not for sufficient time to facilitate any significant evaporation from the sample tubes.

2.3. Results and discussion

The phase diagram of our triblock PEO_{400}-PBO_{55}-PEO_{400} in water is illustrated in Fig. 2.1. The most significant feature is that the gel-liquid phase boundary runs from 3.7 wt% at 0ºC and steadily increases with the polymer's increasing weight fraction. When the PEO_{400}-PBO_{55}-PEO_{400} concentration is higher than 9.5 wt%, it becomes very difficult to handle the sample solution (difficult to dissolve the polymer into water) because the upper gel point (Fig. 2.1) at this concentration is so high (>75ºC) that it has to be heated over 75ºC to dissolve the polymer gradually. The liquid or solution phase exhibits a cloud point at about 104°C±1°C all through 3 to 9.6 percent composition range investigated. As we have known, at a given F127 (PEO-PPO-PEO) concentration, it would form a gel phase, and the gel phase would liquidize by heating or cooling it sufficiently (thermoreversible). However, things are changed on the phase behavior aspect for the triblock we studied. The PEO_{400}-PBO_{55}-PEO_{400} polymer would not liquify from cooling the gel phase it formed. When the PEO_{400}-PBO_{55}-PBO_{400} solution's concentration is below 3.7 wt%, it will not have a gel phase, which is similar to F127 except the latter's concentration is higher (18.1 wt% [52]). The system become unstable between -14°C±2°C ~0°C; unstable means if the sample was cooling down from 0°C to -14°C, the sample can flow under shear force (or just flow if the concentration was lower than 3.7 wt%); if the sample was heating up from -14°C to 0°C, the sample can stay in solid opaque phase (Temperature Hysteresis?). Below -14°C, the samples always solidify to opaque state (phase separation). It always melts above 0°C, either to liquid phase (below 3.7 wt%) state, or to gel phase (above 3.7 wt%) state, depending on the sample's concentration.

At higher temperature, the hydrated layer of micelles began to peel off and at the same time the micelles agglomerated together due to the interaction between them. The cloud point we got here is similar to that of aqueous F127, which is around 100°C.[13, 16]
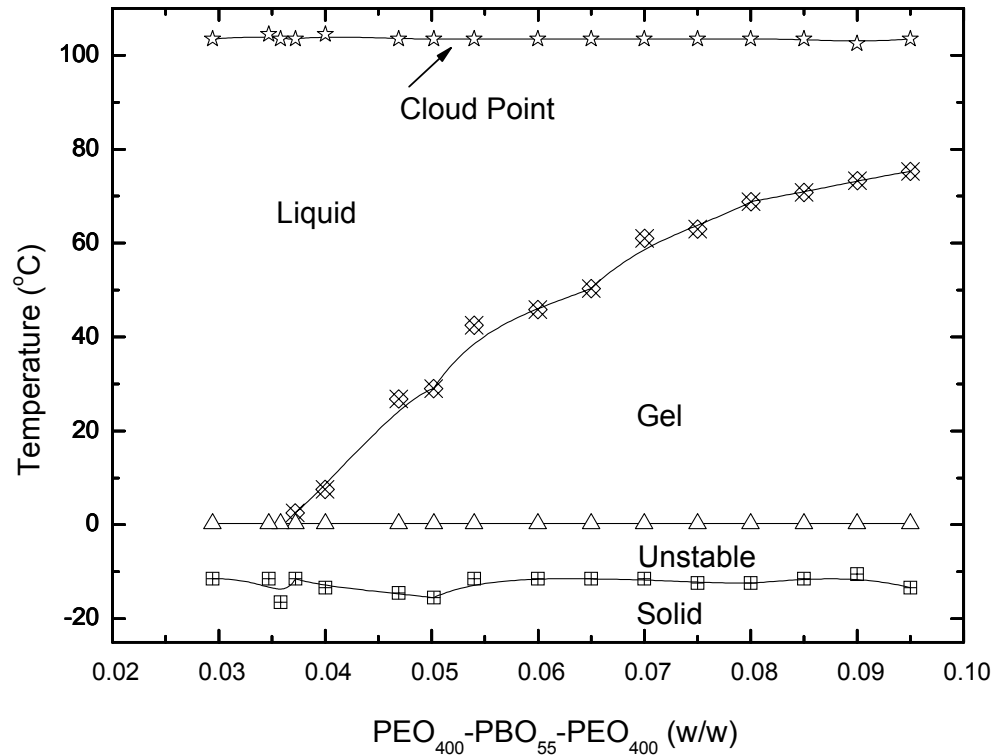
Figure 2.1 PEO_{400}-PBO_{55}-PEO_{400} phase behavior as a function of temperature and weight fraction in aqueous solution.

When compared with PEO_{99}-PPO_{65}-PEO_{99} (F127), the PEO segment in PEO_{400}-PBO_{55}-PEO_{400} is much longer; in other words, the chains will be more flexible. According to Fig. 2.1, we can see that the phase behavior is not as clear as F127 though

in general it is similar to that of F127. With increasing concentration of PEO_{400}-PBO_{55}-PEO_{400}, the gel phase regions are also widened.
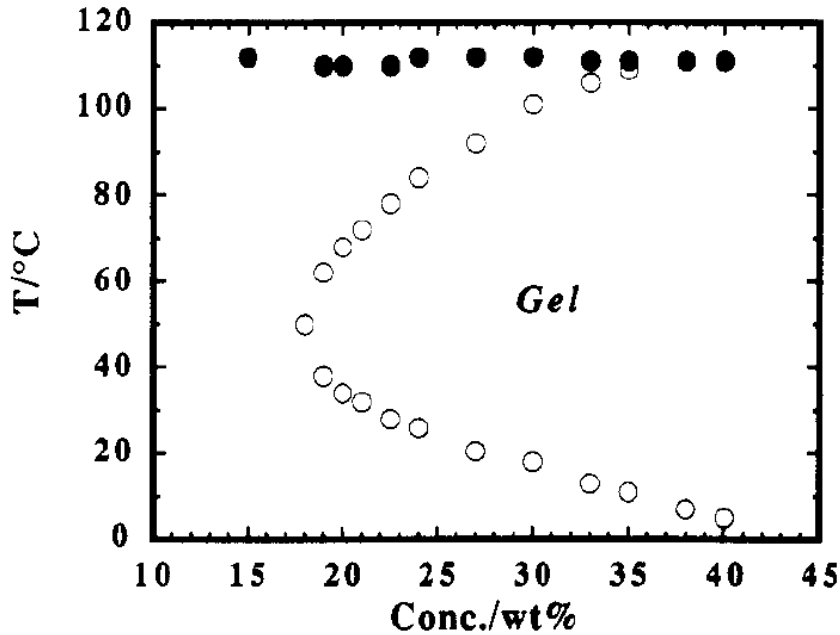
Phase behavior of the PEO_{99}-PPO_{65}-PEO_{99} water system. Solid circles refer to clouding points. (Malmsten, M.; Lindman, B. *Macromolecules* 1992, 25, (20), 5440-5; The figure was taken for comparison purpose only.)

The biggest difference with the phase diagram of F127[52, 53] is that this PEO_{400}-PBO_{55}-PEO_{400} triblock has no lower gel to liquid phase boundary or lower thermoreversible gel boundary (Fig. 2.1). Below $0^{o}C$, the water phase normally would become solid ice. However, the hydrated layers of the polymer micelles would retard the formation of ice crystals. This is probably why we observed an unstable domain (Fig. 2.1). Since there are no special terms to describe this region, we just call it an unstable region for characterization purpose.

Similarly, the relatively longer segment of PEO also affects the other properties of the polymer. Fig. 2.2 is a DSC measurement of the polymer. From the figure, we can see, due to the PBO segment being much shorter than that of the PEO, the polymer appears to have no Tg transition but does have a sharp melting point at 62.4°C. It is known that pure poly(ethylene glycol) has a melting point at around 65°C when the M_n is around 35000,[54] which is almost the same value to that of the 800 units of PEO in the investigated polymer. For similar reasons, the TGA measurement has only one decomposition temperature at around 365°C (Fig. 2.3).

Fig. 2.4 says that the polymer didn't decompose during the phase boundary mapping measurement. The GPC measurements were carried in water and used monodisperse PEG as the standards. From the figure we can see that the polymer molecular weight distribution didn't change much. This means the studied polymer PEG_{400}-PBO_{65}-PEO_{400} is quite stable during the phase diagram mapping.

Pendant drop is a reliable and easy-to-control method to check liquids' surface tension. It needs only small quantities of sample. Fig. 2.5 is CMC measurement of a small molecule surfactant (SDS). The figure shows that the surfactant's CMC is around 0.21 wt% and is quite close to the literature value[55] 0.24 wt%. This shows it is quite an accurate method to determine the CMC of amphiphilic molecule. Gibbs Adsorption isotherm is a model to calculate the packing density of a solute at the interfacial surface. The equation is:

$$\Gamma_2^1 = -\frac{1}{RT}\left(\frac{\partial \gamma}{\partial \ln c_2}\right) \cdots\cdots\cdots\cdots\cdots\cdots\cdots\cdots\cdots\cdots\cdots\cdots\cdots\cdots\cdots\cdots\cdots (2)$$

Here the Γ is the surface excess of solute per unit area, $\dfrac{\partial \gamma}{\partial \ln c_2}$ is the slope of surface

energy vs. logarithm of solute concentration polting. R is constant. T is temperature. According to equation 2, we calculated that the surface excess of SDS in water before CMC is about 4.1 molecule/nm^2.

Figure 2.6 is the CMC measurement of PEG_{400}-PBO_{65}-PEG_{400} in water through pendant drop method. From the figure, the CMC, 0.0164 wt%, can be calculated. Similarly, we calculated that the surface excess of polymer PEG_{400}-PBO_{65}-PEG_{400} is about 1.4 molecule/nm^2. That is to say, the surfactivity of PEG_{400}-PBO_{65}-PEG_{400} is not as strong as SDS. This property probably has much to do with the relative shorter hydrophobic PBO segments. Since there are two long hydrophilic segments in the polymer molecule, it can stay in aqueous solution very stably without going to air-liquid interface necessarily, thus resulting in a weaker surfactivity.
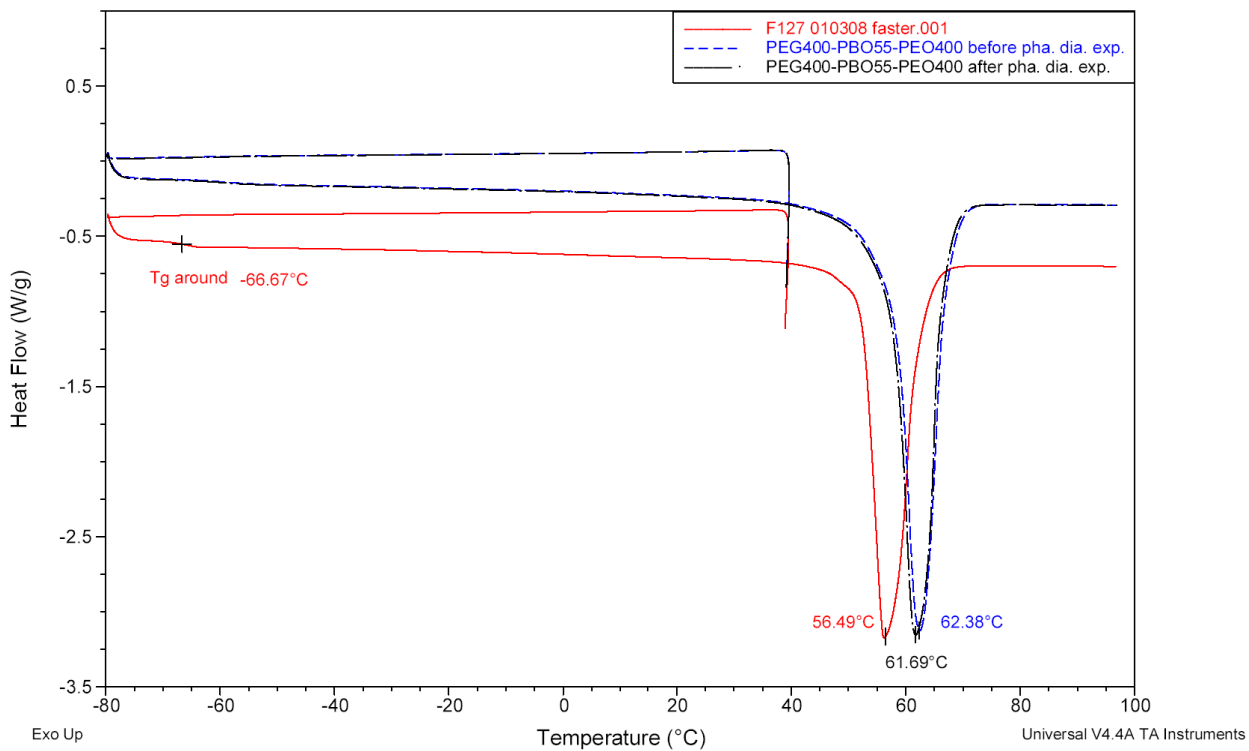
Figure 2.2 GPC measurement of F127 and PEG$_{400}$-PBO$_{55}$-PEO$_{400}$, blue dash and black long dash dot line almost overlapped, indicates that there is no significant change for the polymer before and after phase diagram mapping experiment.
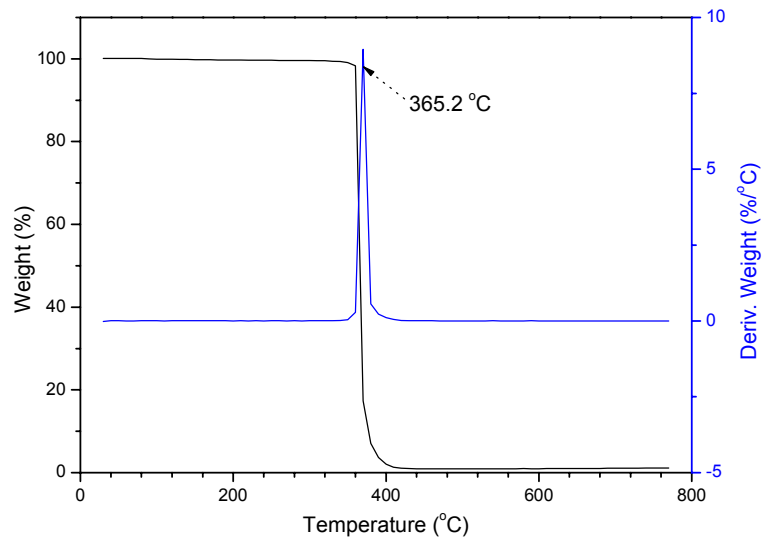
Figure 2.3 TGA measurement of PEO_{400}-PBO_{55}-PEO_{400}; the compound decomposes very homogeneously at 365°C.
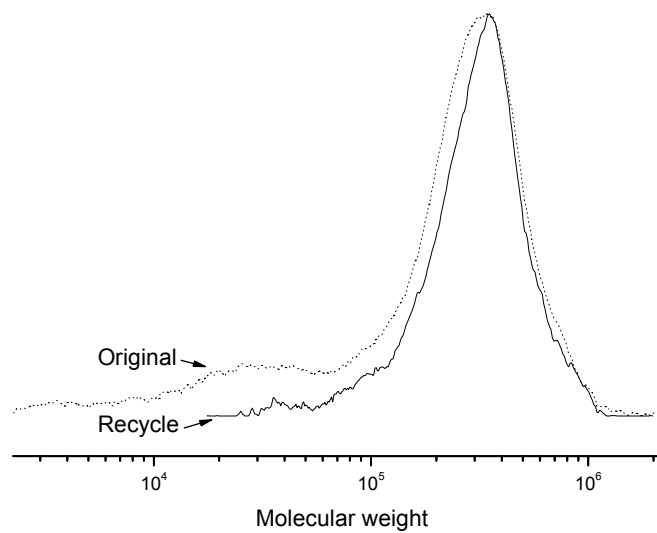
Figure 2.4 GPC measurement of PEO_{400}-PBO_{55}-PEO_{400}: dotted line refers to the original polymer and solid line refers to the polymer recovered by freeze drying after phase mapping experimental.
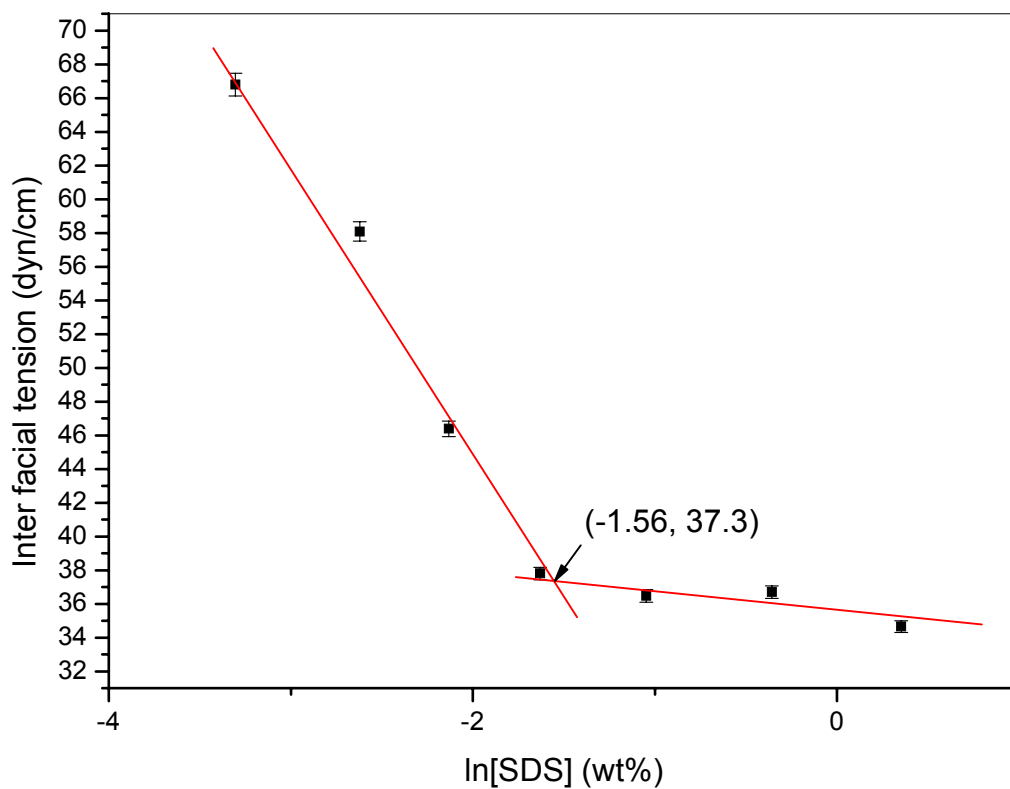
Figure 2.5 CMC measurement of a small molecular surfactant SDS in water through pendant drop method; the CMC of SDS is 0.21 wt% based on the figure (literature value is ~0.24 wt%).
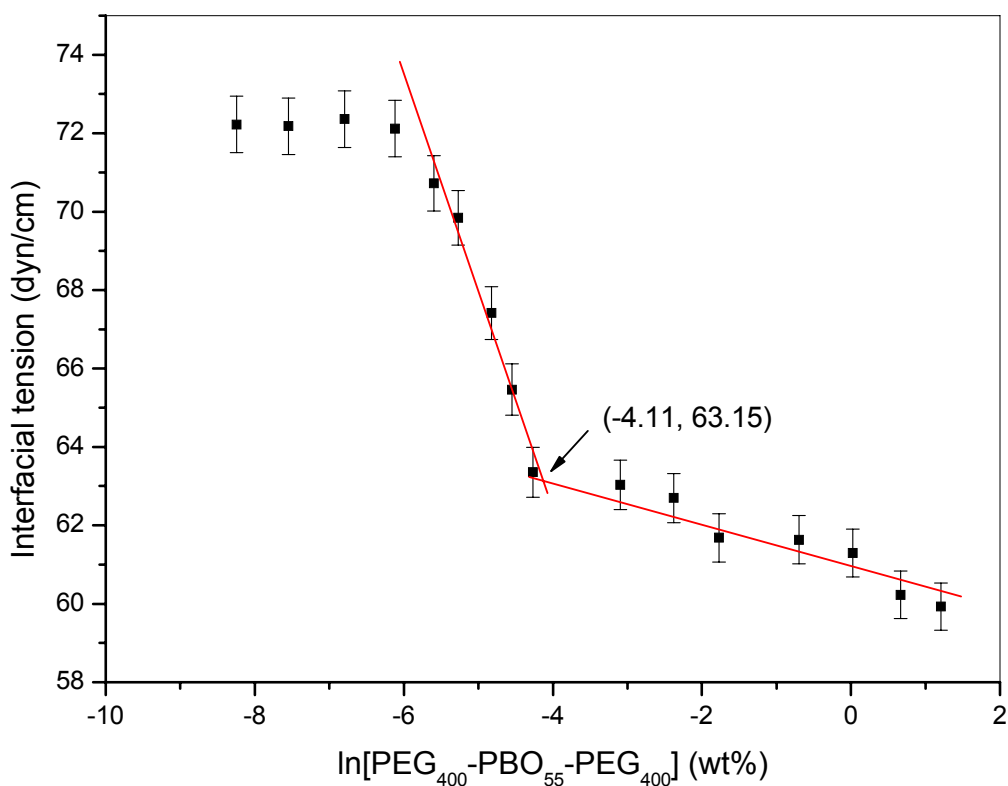
Figure 2.6   CMC measurement of polymer PEG_{400}-PBO_{65}-PEG_{400} in water through pendant drop method; CMC is 0.0164 wt% (no literature value available).

2.4. Conclusions

The phase diagram of PEO_{400}-PBO_{55}-PEO_{400} in water has no lower gel to liquid transition boundary. Instead, the system becomes unstable on cooling until it solidifies with microscopic phase separation and water separating as normal ice at around -14°C. We believe the lack of a lower gel to liquid transition boundary in this system is because of the relatively longer PEO segments, relative to the PBO segment. The polymer does have a well defined T_m (61°C).

The polymer exhibits a well-defined upper gel to liquid transition boundary as the system is heated up from the gel state, as long as the concentration of this triblock copolymer is above 3.6 wt%. This transition boundary steadily widens with increasing triblock weight percent. A cloud point is exhibited at atmospheric pressure when the temperature is raised slightly above 100°C. The polymer's molecular weight distribution is almost the same before and after the phase diagram mapping experiment, and its melting point keeps the same before and after the experiment. The polymer exhibits amphiphilic properties, and its CMC is 0.0164 wt%. But the surfactivity is fairly low due to its molecular structure: two much longer hydrophilic segments on the end and one short hydrophobic segment in the middle.

Chapter III

Synthesis, characterization and preliminary application of polymerizable triblock copolymer poly(ethylene oxide)-b-polystyrene

3.1 Introduction

Our group has been developing advanced fouling release coatings for the U.S. Navy based on thermoreversible tri-block copolymer poly(ethylene oxide)-poly(propylene oxide)-poly(ethylene oxide)(PEO-PPO-PEO).[16, 49, 50, 56] Unlike the anti-fouling coatings that always contain a certain amount of biocide to poison the aquatic bio-film forming organisms to keep the submerged surfaces clean,[7, 8] PEO-PPO-PEO-based fouling release coatings retard protein adsorption.[57-61] However, according to our experience, these Pluronic triblock copolymers are too soft. A higher modulus polymer with a more rigid polymer chain with the same or similar properties as that of Pluronic copolymers is desired to make practical fouling release coatings. F127 is an amphiphilic triblock copolymer. Its molecular chain has a PEO block of 99 ethylene oxide on each end, and of a 65 segment propylene oxide oligomer. The PEO chains are hydrophilic and the PPO chain is hydrophobic. It is known that the F127 in aqueous solution forms micelles, and the micellar core radius is around 4.4 nm, and the aggregation number of the micelles is around 50. Some SANS studies on F127 micelles also found that the core radius and the aggregation number are independent of micellar concentration and temperature.[19] If we could make nanoparticles that have a crosslinked core around 4.4 nm and a PEO corona,

we perhaps could get a similar material to F127 but with much better mechanical properties. Divinylbenzene (DVB) has been used as an efficient crosslinker in coating and material science due to its very high reactivity.[62-65] The reaction of DVB with itself or other monomers is uncontrollable through normal radical polymerization.[66] Polystyrene has a rigid backbone and is hydrophobic. If we could attach one to two DVB repeating units to the end of the copolymer PEO-PS chain, making a polymerizable amphiphilic macromonomer, and then crosslink the macromonomer in microemulsion polymerization, we should be able to get those kinds of nano particles that have a crosslinked core and a PEG-covered corona. This was the main idea in this chapter.

3.1.1 Controlled ("living") radical polymerization (CRP)

In recent years, preparation of polymers with precisely controlled compositions and topologies has been a standard requirement for development of new materials and new applications. Thus, controlled/"living" radical polymerizations (CRPs) have been successfully developed.[67-70] Mechanistically, CRPs are similar to Free radical polymerization (FRP) and proceed through the same intermediates except that in CRPs, the proportion of terminated chains is minimized. Generally, there are three different mechanisms of reversible activation in CRP, which are dissociation-combination, represented by nitroxide mediated polymerization (NMP);[71, 72] degenerative chain transfer, represented by reversible addition-fragmentation chain transfer (RAFT) polymerization;[73, 74] and catalyzed atom transfer, represented by atom transfer radical polymerization (ATRP).[75-78] In our research, we will utilize ATRP technology to prepare our target polymer.

3.1.2 Atom transfer radical polymerization (ATRP)

Since its first appearance in 1995, ATRP has emerged as one of the most powerful

synthetic techniques for preparation of well-defined polymeric materials.

Mechanistically, ATRP originates from a widely used organic reaction known as atom

transfer radical addition (ATRA).[79-81] In this technique, a halogen atom is transferred

homolytically from a dormant halide species to a transition metal complex, forming a free

radical that can quickly be deactivated by a back-transfer of the halogen atom from the

transition metal complex to the organic radical species. The process of ATRP is

illustrated in Scheme 3.1. The activation process includes the participation of both

dormant species and catalyst based activators (lower oxidation state of metal complexes).

The metal complexes with higher oxidation states function as deactivators.
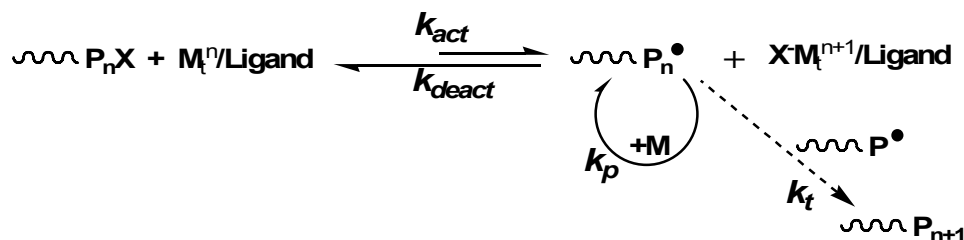
Scheme 3.1 General scheme of ATRP

ATRP has been successfully carried out with the participation of a variety of

transition metals, including Ti,[82] Mo,[83] Re,[84] Fe,[85] Ru,[76] Os,[86] Rh,[87] Co,[88], Ni,[89] Pd,[90] and

Cu.[75] By far, complexes with Cu have been recognized as the most efficient catalysts for

ATRP. Cu can coordinate with various organic ligands forming complexes that display a

wide range of activity for ATRP, and accordingly by selecting an appropriate ligand, it

becomes easy to adjust the dynamic equilibrium between the dormant species and the

propagating radicals.[77, 91] Thus by using Cu-based catalysts, a broad range of monomers can be polymerized by ATRP.

Compared with other CRP methods, ATRP is superior in preparation of polymers with well preserved chain-end functionality,[92] and it is so far one of the most efficient methods for block copolymer synthesis. ATRP is also well-known for its capability of synthesizing polymers with low molecular weight. In addition, a significant advantage of ATRP is that all necessary components are commercially available.[68] In short, ATRP can be applied to a broad range of monomers based on commercially available reagents, providing exceptional control over polymer topology, composition, functionality, and microstructure.

3.1.4 Brief introduction of microemulsion polymerization[93, 94]

A microemulsion is an isotropic, optically transparent or translucent thermodynamically stable system. Usually it is used to synthesize so-called nano polymer particles. These nano particles are typically characterized by diameters between 5 and 100 nm, a narrow size distribution, and a small number of polymer chains per particle.[95, 96] Microemulsion is formed spontaneously by mixing oil and water in the presence of appropriate amounts of surfactant (some times also with co-surfactant) and requires no vigorous agitation or homogenization.

The concept of microemulsion polymerization was firstly reported in the 1980s.[97, 98] The published literature indicates that there is no general scheme for the kinetics of microemulsion polymerization that is valid for all systems. Basically, there are several essential features in microemulsion polymerization:

1. The average number of radicals per particle during the polymerization reaction is between 0.1 and 0.3.

2. The size of the latex particles increases throughout the course of polymerization by ca. 50%. The number of polymeric particles increases with conversion, too.

3. The polymer chains formed in microemulsion latex are highly compressed.

These observations are summarized and extracted in the Candau-Leong-Fitch model,[99] which provided a kinetic scenario for microemulsion polymerization. First of all, microemulsion polymerization proceeds via a continuous particle nucleation mechanism. Polymerization is initiated by the entry of radicals into the monomer-swollen micelles, or by homo-nucleation. These nucleated particles grow by transport of monomer through the outer phase or by particle collision. Due to the transport of monomer to the latex particles, new micelles are formed, and these empty micelles catch free initiator radicals preferentially, which might be due to their number but also an easier permeability for the radicals to diffuse through the surfactant layers. At the end of polymerization, latex particles and a large excess of empty micelles co-exist. Microemulsion polymerization allows the synthesis of ultra-fine polymer latex particles in the size range of 10-50 nm.

3.2 Experimental

3.2.1 Chemicals

Poly(ethylene oxide) monomethoxy ether 5000 (mPEO5000) was purchased from Fluka and dried prior to use by azeotropic distillation from toluene. Ethyl 2-bromopropanoate (E-BrP), 2-bromoisobutyryl bromide, benzyl bromide, N,N,N',N',N'-pentamethyldiethylenetriamine (PMDETA) 4-Methoxyphenol (MEHQ), 2,2'-bipyridine

(Bpy) styrene, anisole, tetrahydrofuran (THF) toluene, ethyl ether, methylene chloride, CuCl, CuBr, ammonium persulphate (APS) triethylamine (TEA), and N,N-dimethyl-4-aminopyridin (DMAP) were all purchased from Aldrich, reagent grade and were used as received. Styrene and DVB were purified (to remove the inhibitor) by passing the monomers through a basic Al_2O_3 column twice. CuBr and CuCl were purified and dried using glacial acetic acid to wash the CuBr or CuCl three times and then using methanol to wash another three times. CuBr or CuCl solid was then transferred to a vial and dried in a vacuum oven at room temperature, and then flush with nitrogen and the vial was then sealed for future use.

3.2.2 Synthesis of polystyrene through ATRP

To practice the ATRP method and test the accuracy of gravimetric conversion measurement (to monitor the monomer conversion), we first carried out the synthesis experiment only with styrene monomer. We tried two similar systems. One was monomer/initiator/CuBr/PMDETA/Toluene system and the other was monomer/initiator/CuCl/Bpy/Anisole system. The respective analytical results (by GPC and gravimetric conversion measurement) on their products indicate that the latter system was better because it was easier to control. We therefore used this system for all subsequent experiments.

A general polystyrene synthesis by an ATRP method in our study is described as follows: a magnetic stirrer, 10 g styrene (96 mmol) as monomer, 0.15 g Bpy (1mmol) as ligand, 5.5 g anisole as solvent, and 0.174 g E-BrP (1mmol) as initiator were put together into a 50 ml round bottom Schlenk flask and bubbled with nitrogen for 30 min. Then 0.096 g CuCl (1mmol) was added as copper(I) into the flask, the flask was sealed by a

rubber stopper, and the reaction mixture was bubbled with nitrogen for another 15min; then the flask was submersed into a 90°C oil bath to start the reaction. When completed, the flask was removed from the bath, cooled and opened, and CH_2Cl_2 was added to dilute the whole mixture. Also, the flask was backfilled with air to fully oxidize the copper(I) to copper(II). (This will result in precipitation, because copper(II) is not soluble in organic solvent.) Then the mixture was passed through a neutral alumina column to get rid of copper ligand complex. The filtrate was poured into methanol to get a white product, PS. The product polymer was washed several times and the final sample was dried in a vacuum oven at 50°C.

3.2.3 Preparation of macroinitiator mPEO-Br[100, 101]

First, poly(ethylene oxide) monomethoxy ether 5000 (mPEO5000) was dried through an azeotropic distillation process, using toluene as solvent. This mPEO was refluxed in a Dean Stark apparatus for 6 hours, and then the solution was precipitated in cold ethyl ether. The white precipitate was placed in a vacuum oven overnight at 50°C to dry the mPEG. Then a round bottom three-necked flask was prepared as a reactor, equipped with condenser, gas outlet/inlet, dropping funnel, and magnetic stirring. N,N-Dimethyl-4-aminopyridin (DMAP) (0.915 g; 7.5 mmol) together with triethylamine (TEA) (0.505 g; 5.0 mmol) were dissolved in 20 ml CH_2Cl_2 in the reactor and cooled to 0°C in an ice bath. 2-bromoisobutyryl bromide (2.875 g; 12.5 mmol) in 20ml CH_2Cl_2 was slowly added to the flask while stirring. To the yellow dispersion that formed, mPEGO5000 (25 g; 5 mmol) was added in 100ml CH_2Cl_2 dropwise. The whole process was done under the protection of nitrogen. After the complete addition of mPEG CH_2Cl_2 solution, the ice bath was removed and stirring was continued for 18 h at room temperature. Then the

mixture was filtered and the excess solvent was evaporated at room temperature. The mixture was then poured into cold diethyl ether to isolate the final product. The final product was dried in a vacuum oven at room temperature and stored as a white powder in a nitrogen-protected vial for future use.

3.2.4 Preparation of PEO-b-PS Diblock Copolymer[100]

The PEO-b-PS diblock copolymer preparation was similar to polystyrene preparation. mPEO-Br (2 g; 0.4 mmol) as initiator, Bpy (0.1246 g; 0.8 mmol) as ligand, anisole (8 g) as solvent, and styrene (4 g; about 40 mmol) were added to a 50 ml round bottom flask, and nitrogen was bubbled through the mixture for 30 min to get rid of oxygen. Then CuCl (0.04 g; 0.4 mmol) was added. The flask was sealed with a rubber stopper and purged with nitrogen for about 15 min. The flask was then immersed in a 100°C oil bath, stirring until the reaction was completed. In our research, the monomer and initiator were always set to 100 to 1 molar ratio. So 1 percent monomer conversion means that the same amount of monomer as initiator was reacted to the formed polymer chain, theoretically. So depending on the expected polymer chain length, the reaction time was different. After the reaction was completed, it was cooled down to room temperature and diluted with CH_2Cl_2. The flask was then backfilled with air to oxidize all of the copper(I) to copper(II). Then the mixture was passed through a neutral alumina column to remove the copper ligand complex. The filtrate was poured into cold diethyl ether to provide a white precipitate. The isolated polymer was washed with diethyl ether several times, and the product was dried in a vacuum oven at room temperature. The yield was about 65 wt% on the basis of the theoretical product weight corresponding to the styrene conversion estimated gravimetrically. The product was stored in a desiccator for future use.

3.2.5 Preparation of PEO-PS-DVB polymerizable Copolymer

The previously prepared PEO-PS was used as macroinitiator, and the same ATRP method was used to make the polymerizable copolymer PEO-PS-DVB. The living PEO-PS (2.6 g; 0.4 mmol) as initiator, Bpy (0.623 g; 0.8 mmol) as ligand, anisole (8 g) as solvent, and DVB (5.21 g; 40 mmol) were added to a 50 ml round bottom flask and purged with nitrogen for 30 min to get rid of oxygen. The flask was sealed with a rubber stopper and then CuCl (0.04 g; 0.4 mmol) was added while continuing to bubble nitrogen through the mixture for another 15 min. The flask was then immersed in a $100^{o}C$ oil bath and stirred till the reaction was completed. Depending on the expected polymer chain length, the reaction time was different. After the reaction was completed, the system was cooled to room temperature and diluted with CH_2Cl_2. 4-Methoxyphenol (MEHQ; 1000ppm) was added as an inhibitor to prevent the pendant vinyl groups of any DVB segments from reacting. The flask was backfilled with air to oxidize the copper(I) to copper(II). Then the mixture was passed down a neutral alumina column to remove the copper ligand complex. The filtrate was poured into cold diethyl ether to obtain a white precipitate. The isolated polymer was washed with diethyl ether several times and the product was dried in a vacuum oven at room temperature. The product was stored in a desiccator in the dark for future use.

3.2.6 Characterization and Measurements

Monomer conversion measurements were conducted during each synthesis based on a gravimetric method described as follows. At a specific time during the experiment, a certain amount of reaction mixture was withdrawn through a syringe and transferred to a pre-weighted clean aluminum dish. The total weight was recorded after recording the pan

and the dish was then put into a vacuum oven for drying the sample (to constant weights) at about 30°C. From the weight difference, the monomer conversion was calculated. ^{1}H NMR spectra were measured at 25°C on a JEOL 400 MHz ^{1}H/^{13}C NMR spectrometer with tetramethylsilane as an internal standard and CDCl$_3$ as a solvent. Samples for molecular weight analysis were dissolved in either water or THF and analyzed by using corresponding columned GPC. The GPC system was equipped with an autosampler (Waters, 717 plus), HPLC pump at 1 ml/min (Waters, 515), and four columns (guard, 105 Å, 103 Å, and 100 Å; Polymer Standards Services) in series. Toluene was used as the internal standard. A calibration curve based on monodisperse PEG (for water as solvent) or linear polystyrene (for THF as solvent) standards was used in conjunction with a differential refractometer (Waters, 2410). Dr. Haifeng Gao of Carnegie Mellon University conducted the GPC measurements. Ms. Michelle Bruck of CAS-MI did the GPC analysis in THF-based on an HP 1050 series HPLC with an HP 1047A RI detector and three Phenogel columns in a series as a set for a molecular weight of 500 to 1,000,000.

Differential scanning calorimetry (DSC) measurements were done using a 2920 MDSC (TA Instruments, New Castle, Delaware, USA) at a heating rate of 5°C/min. Thermal gravimetric analysis (TGA) measurements were done using a TA Instruments Q500 under nitrogen atmosphere. Particle size measurements were done with a 90 Plus Particle Size analyzer (Brookhaven Instruments Corporation) based on dynamic light scattering. TEM experiments were conducted by Dr. Zhiming Qiu on a JEOL 3011 microscope at the University of Michigan Electron Microbeam Analysis Laboratory (EMAL), at the operating voltage of 200 kV. CMC measurements were done through

pendant drop method, similar to the procedure in the Chapter II experimental section (2.2.1).

3.2.7 Preliminary application of PEO-PS-DVB polymerizable triblock Copolymer

3.2.7.1 Phase diagram mapping

In order to design microemulsion polymerization using PEG-PS-DVB together with DVB/St in aqueous media, a phase diagram of the PEG-PS, water, DVB/St pseudo ternary system was determined by visual titration of DVB/St with PEO-PS solutions in sealed culture tubes or vials with PTFE-coated rubber liners at fixed temperature. There were only 1~3 repeating DVB units in our PEG-PS-DVB products backbone, and what's more, the PEG-PS is much easier to store and make compared to the PEG-PS-DVB polymer. We actually mapped the pseudo ternary phase diagram of PEG-PS, DVB/St, water instead of mapping PEG-PS-DVB, DVB/St, water pseudo ternary phase diagram. We assumed that the phase behavior (microemulsion L_1 domain boundary) has no significant difference between PEG-PS and its corresponding derivative, PEG-PS-DVB, in water and DVB/St pseudo ternary system.

3.2.7.2 Microemulsion polymerization in L_1 domain[102]

After we determined the microemulsion L_1 domain (oil in water) boundary of PEG-PS in the water and DVB/St ternary system, we continued to do bulk microemulsion polymerization of PEG-PS-DVB in water together with DVB/St (40/60). The procedure is described as follows: PEG-PS$_7$-DVB$_2$ (1.0823 g) was added to 9.9625g water in a 25 ml round bottom flask to form a 10.9 wt% polymer solution. Then 0.1130g DVB/St (40/60) monomer was added to the mixture (1.13wt% of the whole reaction mixture), and the reactants were stirred for 15 min until the system turned to a clear and transparent

solution. Ammonium persulphate (APS; 150 µl 41mg/ml; 1% mole ratio relative to the vinyl groups) aqueous solution was added as an initiator (a corresponding amount of compensational APS was included due to the inhibitor in the PEG-PS$_7$-DVB$_2$). The flask was then immersed in a 60°C oil bath for 25 h. The final solution was still clear. Rotary evaporation were to remove the excess water in the solution until a clear gel formed in the flask; the flask was then placed in a vacuum oven overnight to dry at 50°C. Product (0.9612 g) was collected, and the yield was 80%. The final product was stored in a vial in a desiccator at room temperature.

3.3 Results and Discussion

3.3.1 Synthesis and characterization

To carry out the ATRP reaction smoothly before we actually made our target molecule, we first executed a model reaction simply using styrene as monomer. During this model experiment, we monitored the styrene conversion by a gravimetric method described and illustrated in Fig. 3.1. We will show the accuracy of this seemingly rough procedure (monitoring the monomer conversion by gravimetric method; conversion usually is done by GC). From Fig 3.1, we see that with the reaction going on, the monomer conversion is no longer linear after 8 reaction hours. This behavior probably results from the concentration variation of two different copper species Cu(I)/Cu(II).[103] We also did GPC measurement on some samples in Fig. 3.1 (letter labeled). GPC results showed that those samples were monodispersed and had a low polydispersity, which is one of the features of ATRP ("living" polymerization). So if the monomer and initiator were set at a certain ratio, the conversion of monomer as well as the molecular structure could be predicted as a function of reaction time. That is to say, we could control the

polymer backbone length by simply controlling the reaction time. We did CMC measurements on several diblock copolymers of our product (Fig. 3.14 to Fig. 3.19). All of the four tested polymers exhibited amphiphilic properties. However, further studies on the starting material (Fig. 3.18 and Fig 3.19) indicate that the surfactivities are original from the impurities in PEG. The surface excess area calculation based on Gibbs Adsorption isotherm model (Chapter 2, equation 2) shows that all their surfactivities are not strong (Table 3.3). The higher CMC value (Fig. 3.15) is most likely due to the impurity of the unreacted PEG. During the synthesis of diblock copolymer PEG-PS, there was impurity of PEG. Most of the tested CMC of the polymers are between 0.01 wt% to 0.008 wt%. This information will be useful for conducting microemulsion polymerization in our study later.
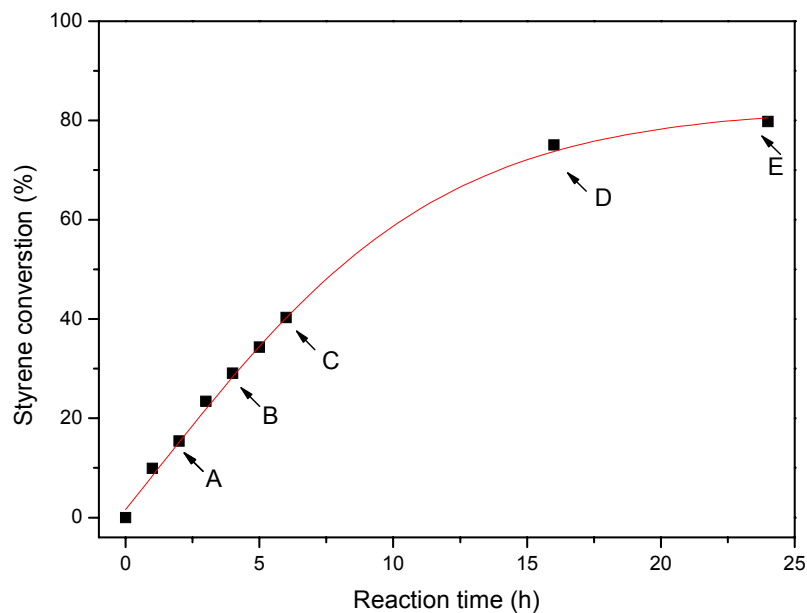
Figure 3.1 Styrene (080906) monomer conversion as a function of reaction time.

We then started to make our target molecule, which is a polymerizable triblock copolymer PEG-PS-DVB; Scheme 3.1 illustrates the synthesis route. At each step we isolate and dry the product before continuing to the next.
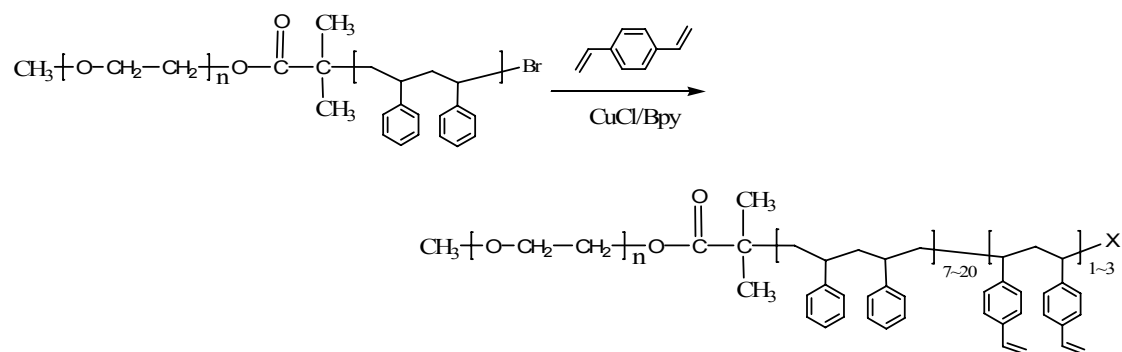
Macroinitiator Foumation:
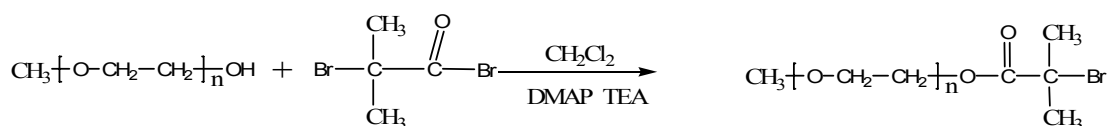
Styrene Block Polymerization:
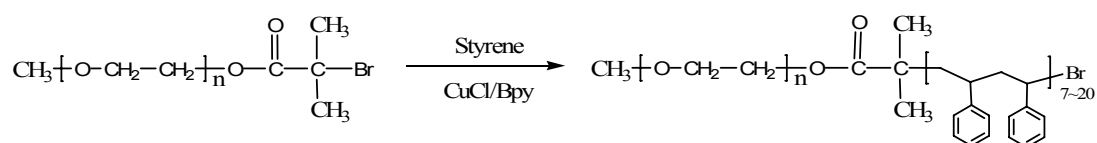
DVB Doping:

Scheme 3.1 Procedure of making polymerizable copolymer PEG-PS-DVB.

Fig. 3.2 and Fig 3.3 are NMR spectra for our starting material poly(ethylene oxide) monomethoxy ether (mPEG) and its functionalization product 2-bromoisobutyryl polyethylene glycolate (mPEG-Br), respectively. Theoretically, for mPEG, there should be only protons between 3.3~3.9ppm. Fig. 3.2 contains two spectra, which were conducted in different batch experiments. The mPEG (090806) sample was directly purchased from Aldrich without any purification process, while the sample mPEG (092806) was purified (dried) through an azeotropic distillation process, which in this

procedure uses toluene as solvent, and refluxing in a Dean Stark apparatus for 6 hours following precipitation in cold diethyl ether, The white precipitate is dried in a vacuum oven overnight at 50^oC. However, both samples were not completely pure according to their NMR. Protons around 2.0ppm and 2.5ppm were attributed to the impurity of the raw material mPEG. CH_3O- and $-CH_2-CH_2-O-$ protons were identified at 3.3ppm and 3.4~3.8ppm, respectively. Based on the integration area of CH_3O- and $-CH_2-CH_2-O-$ protons, we calculated that the raw mPEG from Aldrich has a $-CH_2-CH_2-O-$ repeating unit number of 103.8 (090806) or 105.4 (092806). Since all of our target molecules will be derived from this mPEG, and to simplify the subsequent calculation and minimize the system error as well, we took 104 as our raw material molecular chain length (PEO repeating units). In other words, we assume the raw mPEG backbone has 104 $-CH_2-CH_2-O-$ repeating units unless otherwise mentioned.
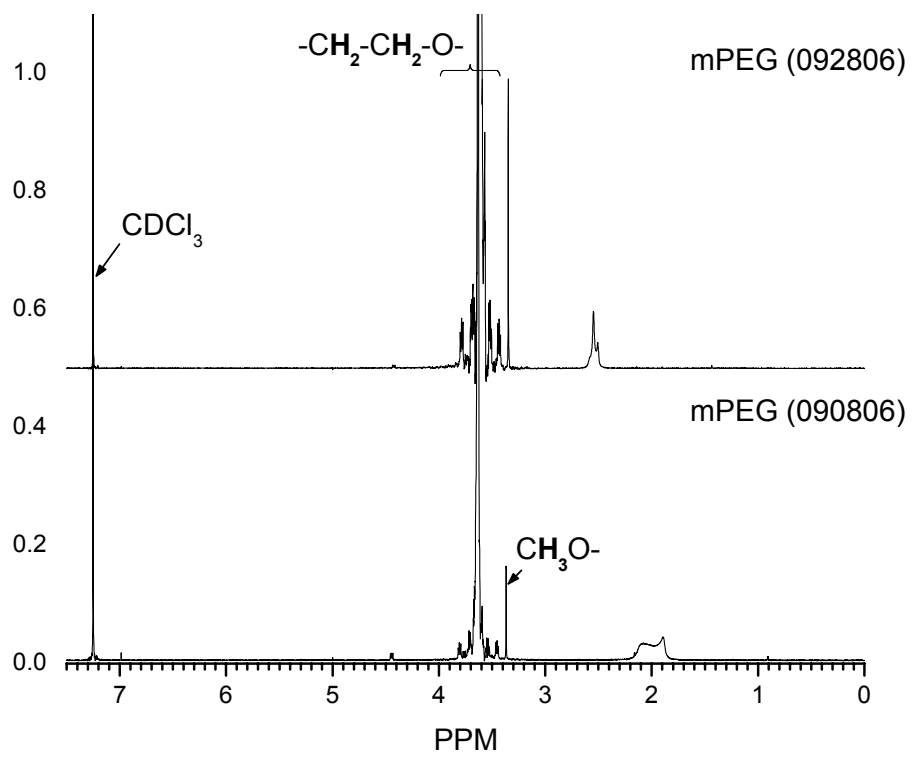
Figure 3.2 NMR spectra of poly(ethylene oxide) monomethoxy ether (mPEG).
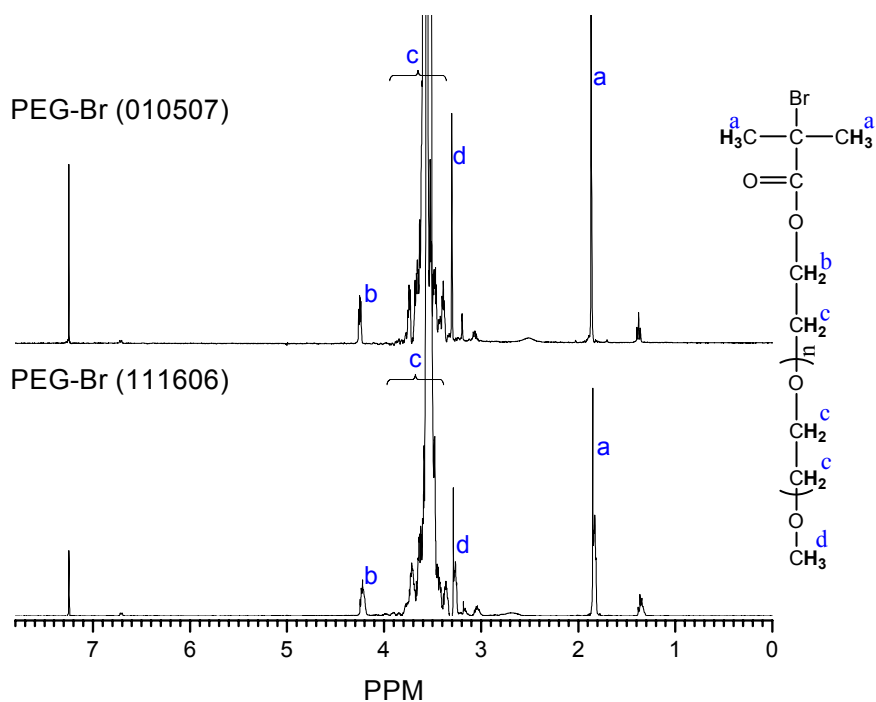
Figure 3.3 NMR spectra of 2-bromoisobutyryl polyethylene glycolate (mPEG-Br).

After the esterification reaction (mPEG and 2-bromoisobutyryl bromide), we got the

end hydroxyl group functionalized to bromine, which would initiate the subsequent

ATRP reaction. The proton attribution is illustrated in Fig. 3.3. Apparently, if all mPEG

hydroxyl groups get brominated, the selective integration area ration of a, b, and d would

be 6:2:3. But, in fact, the actual ratio is always different; for example, for product 010507,

the ratio of a, b, and d is 6:2.17:2.91, and for another mPEG-Br (111606) sample, the

ratio of a, b, and d is 6:1.98:3.66. The reason the ratios are not 6:2:3 is that it's impossible

to get a 100% functionalization for mPEG hydroxyl group to bromine, and the impurity

(such as residual 2-bromoisobutyryl bromide) would also affect the integration area. Fig

3.3 confirmed that we now have mono functionalized bromine mPEG. Based on the 111606 sample's NMR, around 82% mPEG was transformed to mPEG-Br.

The next step to our target molecule is making the diblock copolymer PEG-PS through ATRP. Many researchers have made or are making PEG-PS block copolymers.[104, 105] The difference between us and those researchers is that we are trying to make a very short (around 10) polystyrene segment instead of 100 or more. A study of F127 shows that in aqueous solutions, PEG_{99}-PPO_{65}-PEG_{99} will form micelles that have PPO cores around 8 nm in diameter, containing about 50 F127 molecules.[19] The micellar core diameter and aggregation number are independent of temperature and concentration. Our idea was to make an alternate material to F127 that has similar thermoreversible properties in aqueous solution but has a higher mechanical modulus.

Fig. 3.4 to Fig. 3.7 illustrate the serial NMR spectra from the starting material to the final product. We have already interpreted the mPEG and mPEG-Br NMR spectra, and now we will just explain Fig. 3.6 and Fig. 3.7. In both spectra, protons around 1.0 ppm and 1.3~2.5 ppm are attributed to many groups (include solvents impurity and residual TEA, etc.), so those two regions are not accurate for identifying chemical groups or for calculating polymer backbone structures. But we noticed that protons from 3.3 to 3.9 ppm, 5.2 ppm and 5.8 ppm, and 6.8 ppm and 7.1 ppm are exclusively due to PEG, DVB, and styrene. This makes those peaks and their integration ideal for calculation and identification purposes. For example, Fig. 3.6 has much greater 6.8 ppm and 7.1 ppm proton intensities and much smaller 4.3 ppm proton intensity than Fig. 3.5. These aspects indicate that polystyrene had been grown from the mPEG chain successfully. Similarly, the appearance of 5.2 ppm and 5.6 ppm protons in Fig. 3.7 indicates that DVB has been

added onto PEG-PS polymer chain. Further calculation shows that the polystyrene segment in 092707 sample has 7.1 repeating styrene units. The sample was labeled as PEG-PS$_7$. The calculation was based on the integration areas of the 3.3 to 3.9 ppm, 5.2 ppm, and 5.8 ppm, 6.8 ppm and 7.1 ppm proton peaks. For example, in Fig. 3.6, the area of 3.3 to 3.8ppm is 88.5, while it is 7.5 for the 6.8 ppm and 7.1 ppm peaks taken together. There are roughly 104 -(CH_2-CH_2-O)- units in the mPEG segment, and the 6.8 ppm, 7.1 ppm peaks are due to the benzene ring protons in styrene, so we have the following proportionating:

$$\frac{4 \times 104}{5 \times n} = \frac{88.5}{7.5} \cdots (1)$$

where n is the number of styrene in the PS segment, and from the equation, n equals 7.1 approximately. There are two ways to calculate the number of DVB. In Fig 3.7, the relative integration areas of 3.3 to 3.8 ppm, 5.2 ppm, 5.6 ppm together, and 6.8 ppm, 7.1 ppm together are 101.5, 0.87 and 10.834 respectively. It has been mentioned that 5.2 ppm and 5.6 ppm is due to the pendant vinyl group, so we can list two equations as follow:

$$\frac{4 \times 104}{5 \times (7.1 + x)} = \frac{101.5}{10.834} \cdots (2) \quad or \quad \frac{2x}{5 \times (7.1 + x)} = \frac{0.87}{10.834} \cdots (3)$$

where x means the number of DVB in polymer backbone. In equation 2, x equals 1.8 approximately while it is 1.78 in equation 3. Actually peak 5.2ppm and 5.8ppm are quite tiny and the integration area might have significant error, so usually we use equation 2 instead of 3 when calculating DVB repeating numbers. The PEG-PS-DVB (100807) sample was finally labeled as PEG-PS$_7$-DVB$_2$.
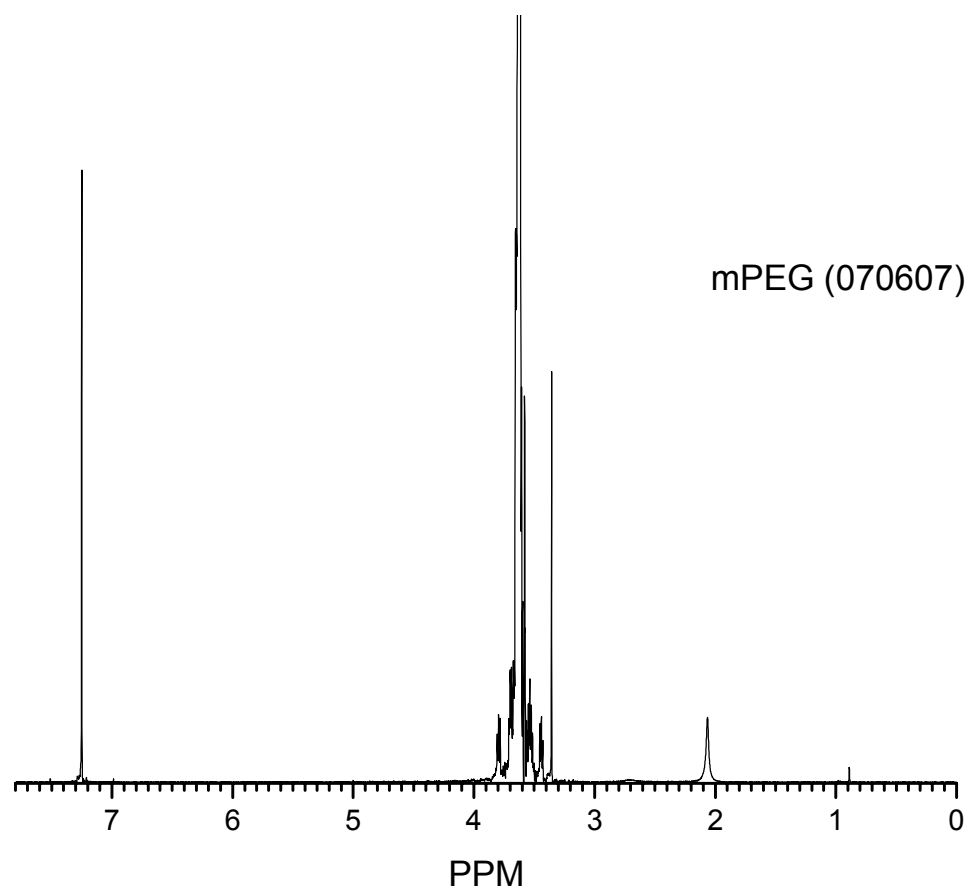
mPEG (070607)

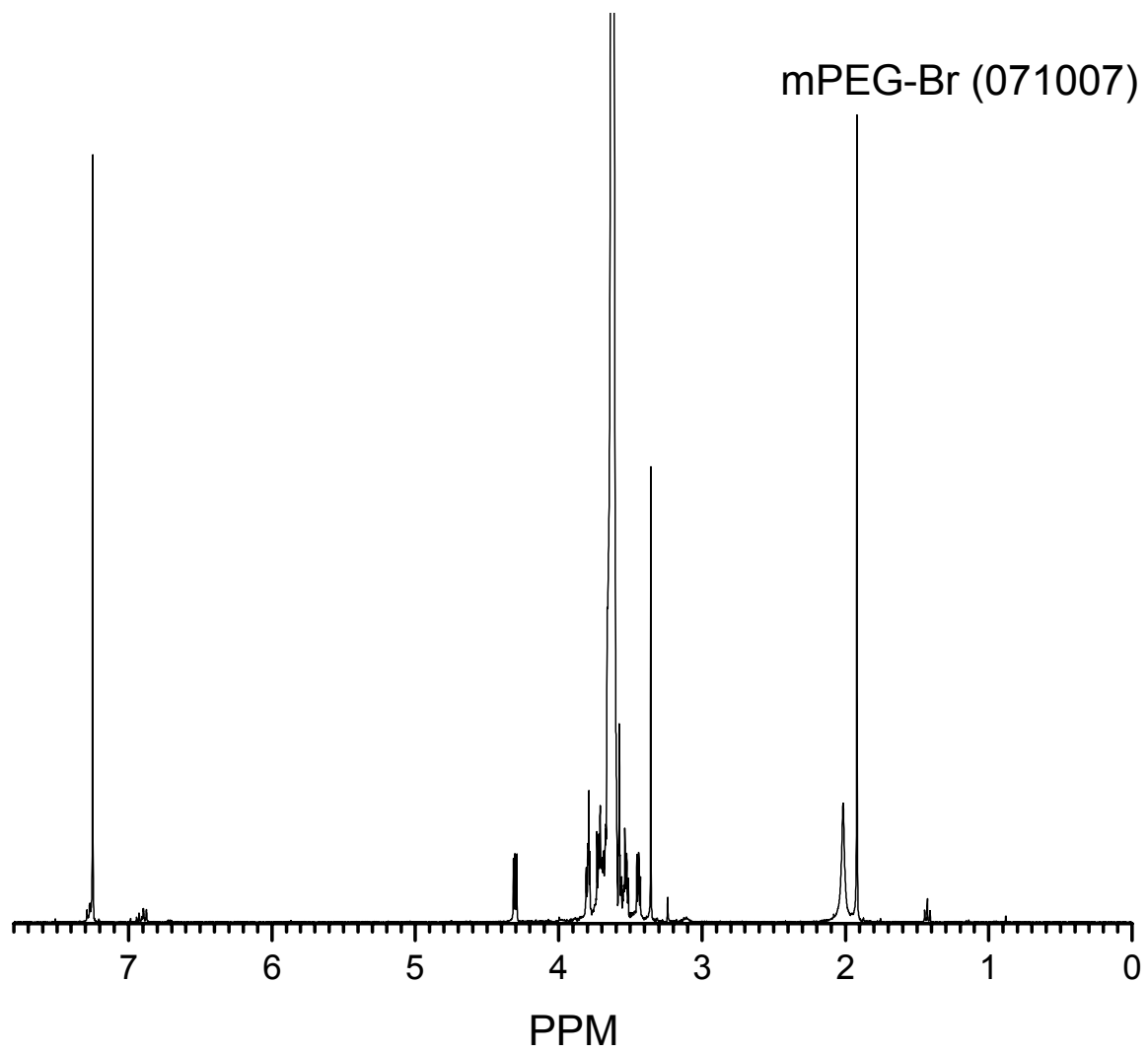Figure 3.4 NMR spectrum of mPEG (070607).

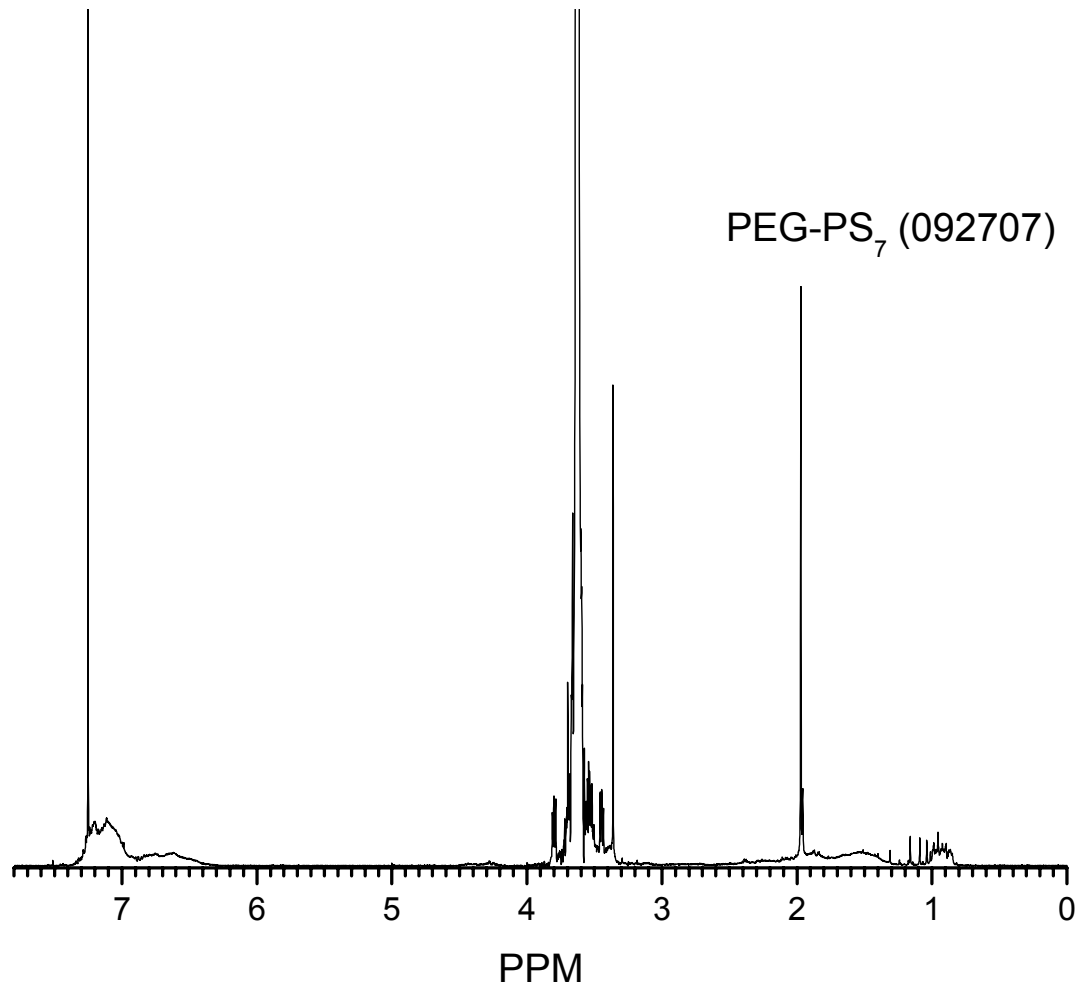Figure 3.5 NMR of mPEG-Br (071007).
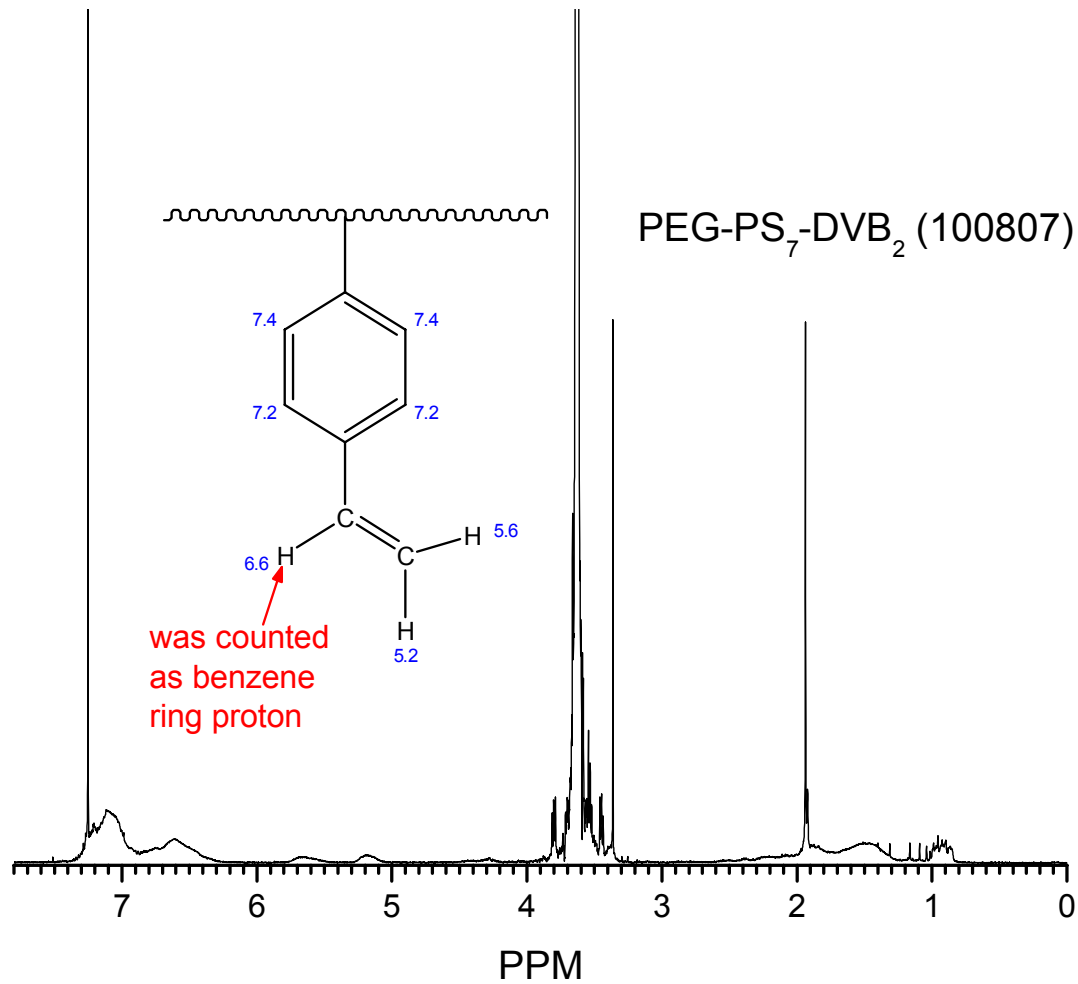
Figure 3.6 PEG-PS$_7$ (092707) NMR spectrum.

Figure 3.7 PEG-PS$_7$-DVB$_2$ (100807) NMR spectrum. (The blue shifts are simulated by ChemDraw software.)

In addition to NMR measurement, GPC measurements as well as monomer conversion measurements on a gravimetric basis were also conducted in order to control and monitor the product's structure and stoichiometry. Fig. 3.8 is a styrene monomer conversion on gravimetric basis vs. reaction time curve. The slope of the linear fit line

(red line) is 1.01. The y-intercept is 2.97. In this chapter, the experiment section, we have mentioned that all the ATRP experiments in this research have monomer to initiator ratios of 100:1 unless noted otherwise. Together with the Fig. 3.8, we can conclude that the PEG-PS molecular structure could be controlled by reaction time as long as the experimental conditions are kept as same (as in the Fig. 3.8 experiment). And the growing polystyrene segment's "length" (repeating unit) is just the reaction time in hours, e.g., the total reaction time of 010907 experiment was 11.5h, so the "length" of PS segment in the product polymer PEG-PS should be 11.5. Fig. 3.9 is another conversion vs. reaction time curve (the error bar result from three repeating experiments' results) on gravimetric basis. The monomer was DVB and the initiator was the product 010907, which is PEG-PS. The experimental conditions were the same as in the 010907 (styrene was monomer) experiment, but from Fig. 3.9 we can see that the reaction speed was much higher than in the 010907 experiment. This is easy to understand if we consider that DVB has a higher reactivity than that of styrene under same reaction conditions.[66] From Fig. 3.9 we see that the monomer conversion is 5.6 percent when the reaction time is 3 h. Again, please note that 5.6 percent theoretically means we have 5.6 DVB units in our product since the monomer to initiator ratio was 100:1.

Table 3.1 is a comprehensive comparison of conversions on a gravimetric basis, NMR analysis and GPC measurements (Fig. 3.10). From the table, we can see that the GPC measurement is quite consistent with the conversion measurements and NMR calculations. Table 3.1 also confirms that the conversion on gravimetric basis and NMR calculations are quite consistent. Fig. 3.10 is an apparent result of GPC measurement in related to polymers listed in Table 3.1.
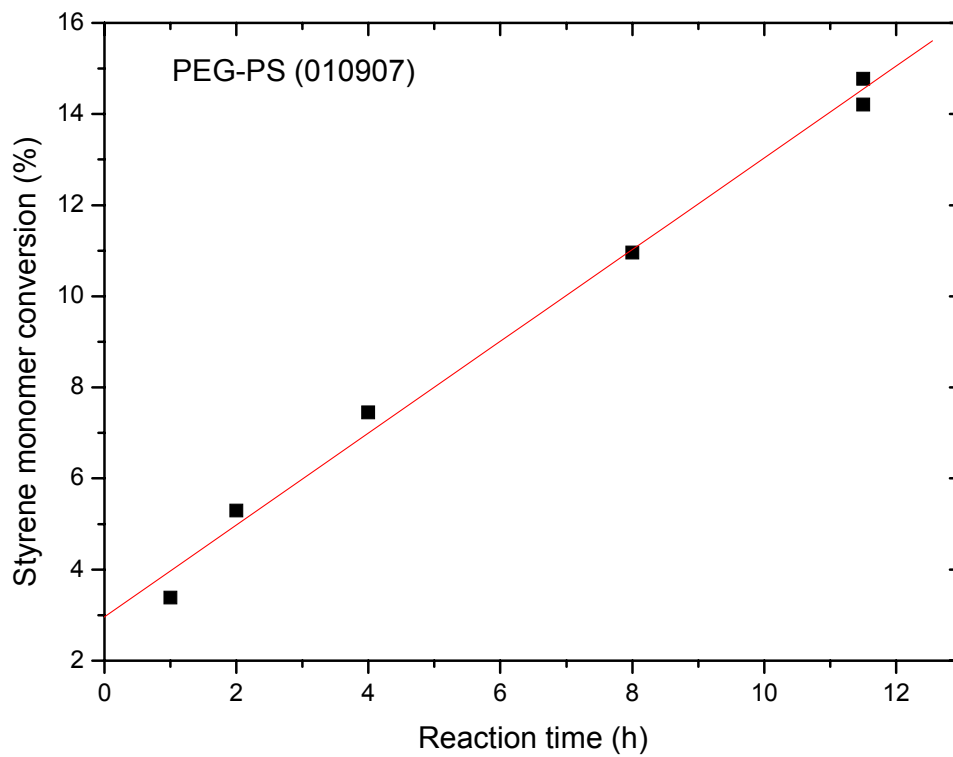
Figure 3.8 Styrene monomer conversions (010907) as a function of reaction time in ATRP. 3 percent conversion at 0 h reaction (supposed to be zero) times indicates there were errors in that measurements.
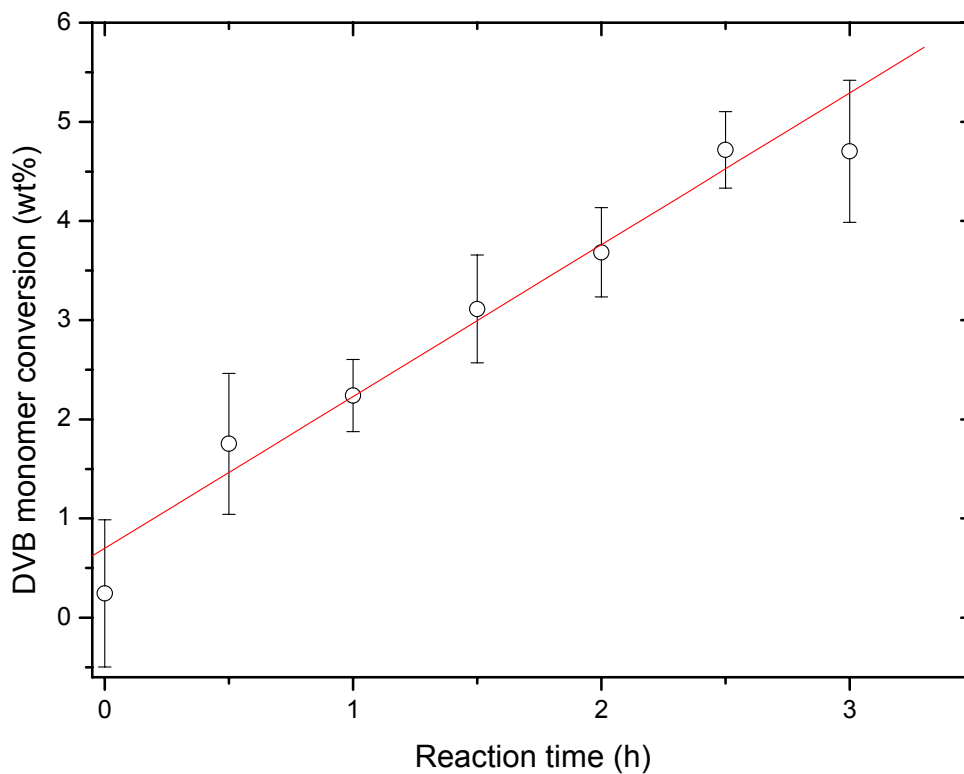
Figure 3.9 DVB monomer conversion as a function of reaction time; the initiator was PEG-PS$_{13}$ (010907). This figure resulted from three experiments run under the same conditions, and the conversions represent averages of the three DVB conversions. All three runs used a ratio of DVB/Bpy/CuCl/PEG-PS-X=100/2/1/1.

Table 3.1 Comparison between monomer conversion measurements on gravimetric basis,

NMR analysis and GPC measurements

Sample	Conversion[a] (%)	Num[b]	ΔMn[c]	Mn[d]	Polydispersity[d]
mPEG5000 (Aldrich)	0	0		6.10E3	1.04
PEG-PS$_{13}$(010907)	11.5	12.7	1320	7.53E3	1.06
PEG-PS$_{13}$-DVB$_6$(012207)	5.3	5.6	728	8.01E3	1.08

a) The conversion specially refers to corresponding monomer, e.g., 3rd row refers to styrene while 4th row refers to DVB. Data from correspond Conversion vs Reaction time curve.

b) The Num refers to corresponding monomer repeating units' number. Data from correspond NMR spectra.

c) ΔMn means the variation of Mn results from the monomer grafting compared to its precursor. Data were calculated from monomer repeating units' number.

d) Polydispersity is from GPC measurement.
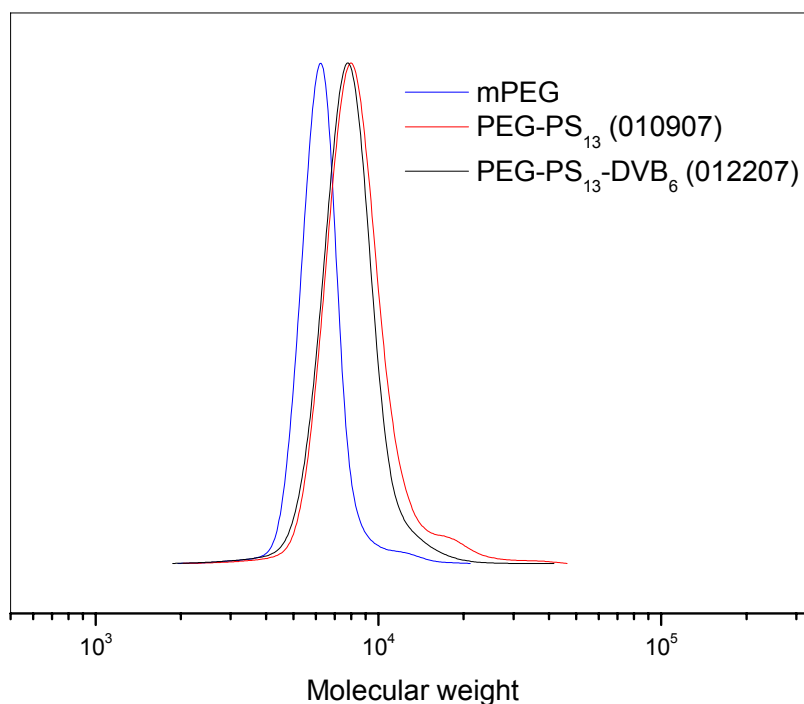
Figure 3.10 GPC measurement for polymers in Table 3.1.

The above discussion shows the high consistency in different experiment steps'
products. Actually, in a single experiment, the consistency is also very high based on
experiment data. Table 3.2 lists various data for comparison in a single experiment
(051707). This table indicates that all samples from a different time interval had very
narrow polydispersity, which reflected that the polymerization was quite "living." It
confirmed again that we could make products of a designed molecular structure by this
method. Fig 3.11 is the apparent molecular weight distribution that displays the gradual
molecular weight increase as a function of reaction time in experiment 051707. Fig. 3.12
showed that the ATRP method keeps its linearity fairly well even with a 40 h reaction
time.

Table 3.2 Gravimetric conversion and GPC measurement of sample PEG-PS (051707).

Reaction time (h)	Conversion (%)[a]	$Mn^{[b]}$	$Mn^{[c]}$	Polydispersity[c]
0	0.77	6600	6600	1.04
5	7.51	7400	7200	1.04
17	16.78	8300	8300	1.05
26	22.45	8800	8900	1.05
38	28.84	9500	9600	1.06

a) Data derived from gravimetric analysis

b) Data calculated from conversion data, since 1% conversion correspond to 1 monomer addition to the polymer backbone.

c) Data original from GPC measurement.
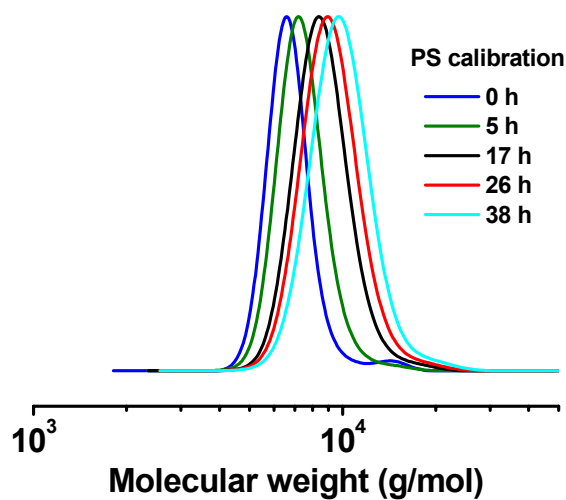
Figure 3.11 Molecular weight increasing as a function of reaction time for mPEG-PS (051707) product.

Table 3.3 Surface excess information of different polymers in water

Samples	Γ(mol/m2)	Γ' molecule/nm^2	σ(A2/molecule)
SDS	6.9E-06	4.1	24.2
PEG (070607)	8.2E-07	0.5	203
PEG-Br (071007)	2.9E-06	1.7	58
PEG-PS$_{7.3}$ (090507)	2.4E-06	1.4	73.9
PEG-PS$_{13}$ (030507)	9.9E-07	0.6	167.5
PEG-PS$_{20}$ (050907)	3.2E-06	1.4	71.1
PEG-PS$_{22}$ (041607)	1.3E-06	0.7	138.1
PEG$_{400}$-PBO$_{65}$-PEG$_{400}$	2.0E-06	1.4	74.0
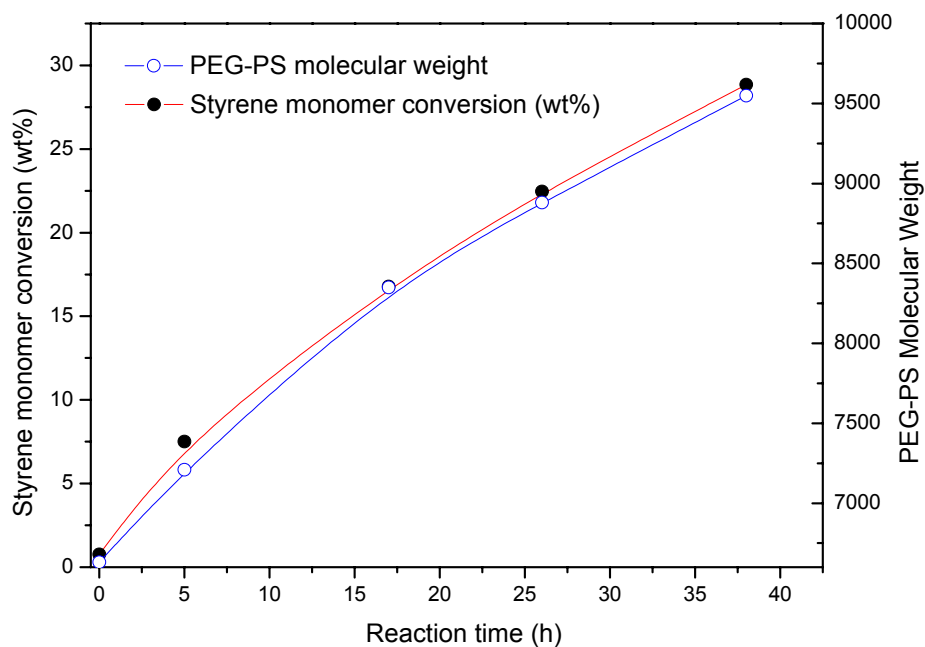
Figure 3.12 PEG-PS (051707) syntheses: PEG-PS molecular weight and styrene monomer conversion as a function of reaction time.

During the preparation of polymerizable triblock copolymer having designed molecular structure, we found it was necessary to add a certain amount of inhibitor into the final product (PEG-PS-DVB) to keep it from reacting either during isolation or storage. Failure to do so would result in crosslinked material that would not dissolve in the organic solvent in which the product was made. Probably this is because of the high reactivity of DVB so that PEG-PS-DVB reacts by some thermal or photochemical pathway even in the solid state. Anyway, even after auto crosslinking, the product was still dispersible in aqueous solution and formed nanoparticles (Fig. 3.13). And we noticed that all the particle sizes are no less than 100nm in diameter, which seems too big when compared to the size of F127 micelles in aqueous solution. Consequently, we decided to remake the PS segment in the polymer shorter so that smaller size micelles could be formed when dissolving the product (PEG-PS-DVB) in water. Our experiences also indicated that the DVB segment couldn't be too long; otherwise, the product PEG-PS-DVB became very unstable. Later we aimed to make macromonomers that have only 2 DVB units.
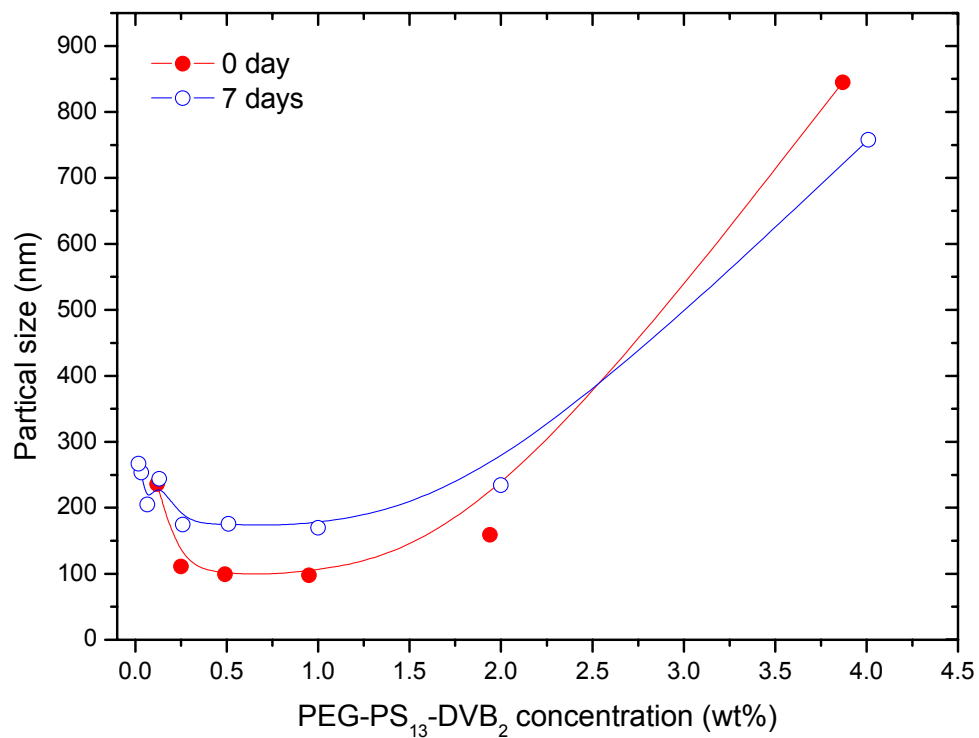
Figure 3.13 Polymer PEG-PS$_{13}$-DVB$_2$ (082707) in aqueous solution forms particles without the protection of inhibitor during isolating and storing.
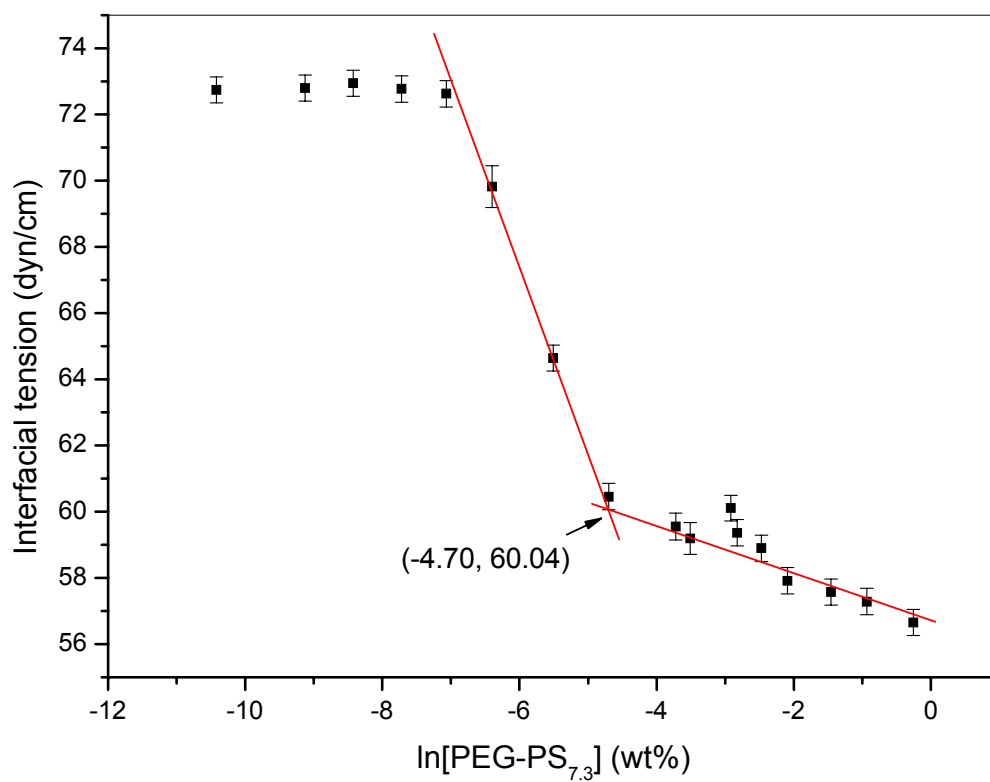
Figure 3.14 CMC measurement of polymer PEG-PS$_{7.3}$ (092507) in water through pendant drop method; CMC is 0.00910 wt%.
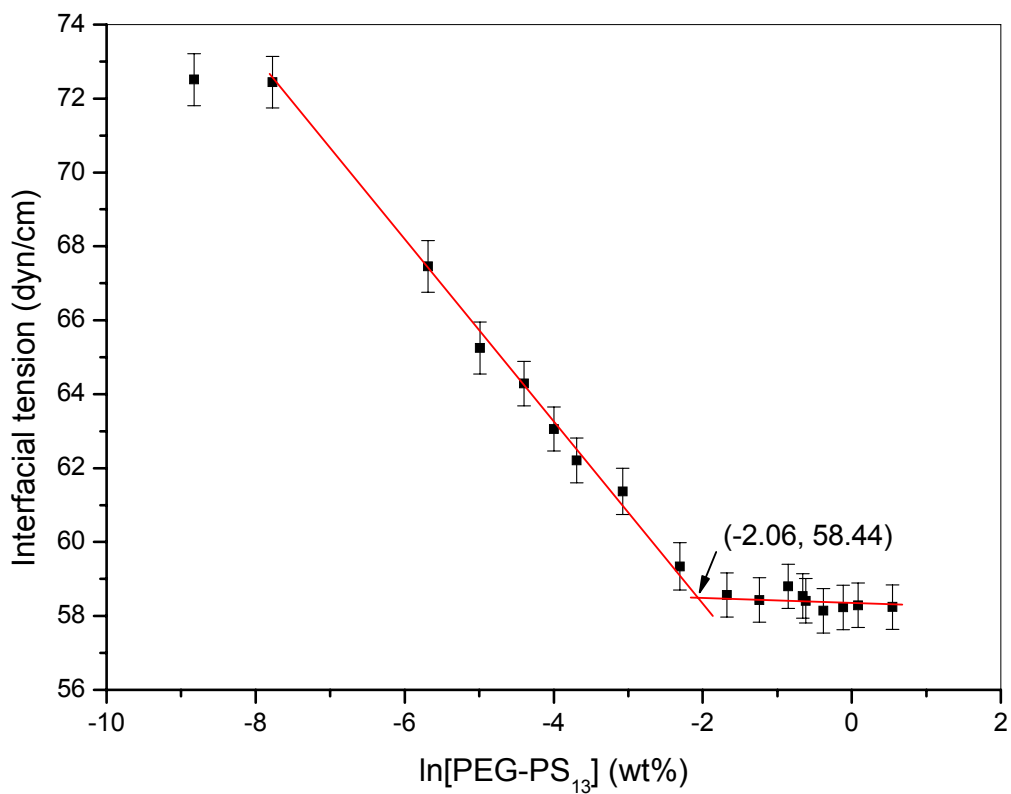
Figure 3.15 CMC measurement of polymer PEG-PS$_{13}$ (030507) in water through pendant drop method; CMC is 0.13 wt%.
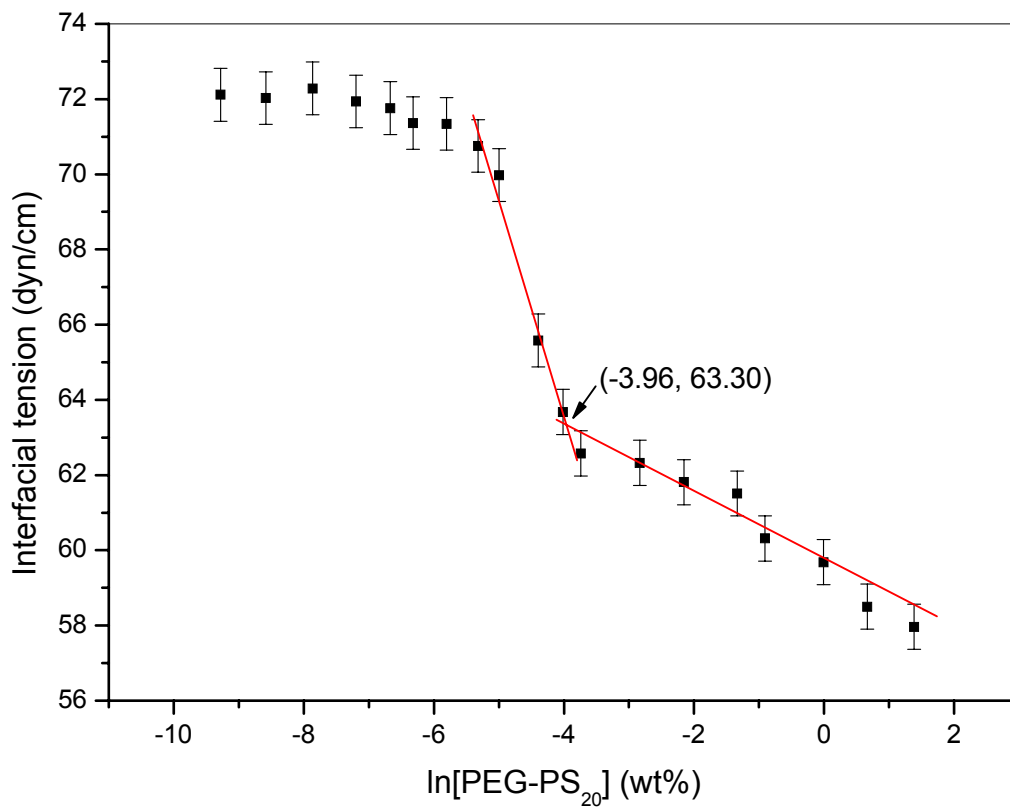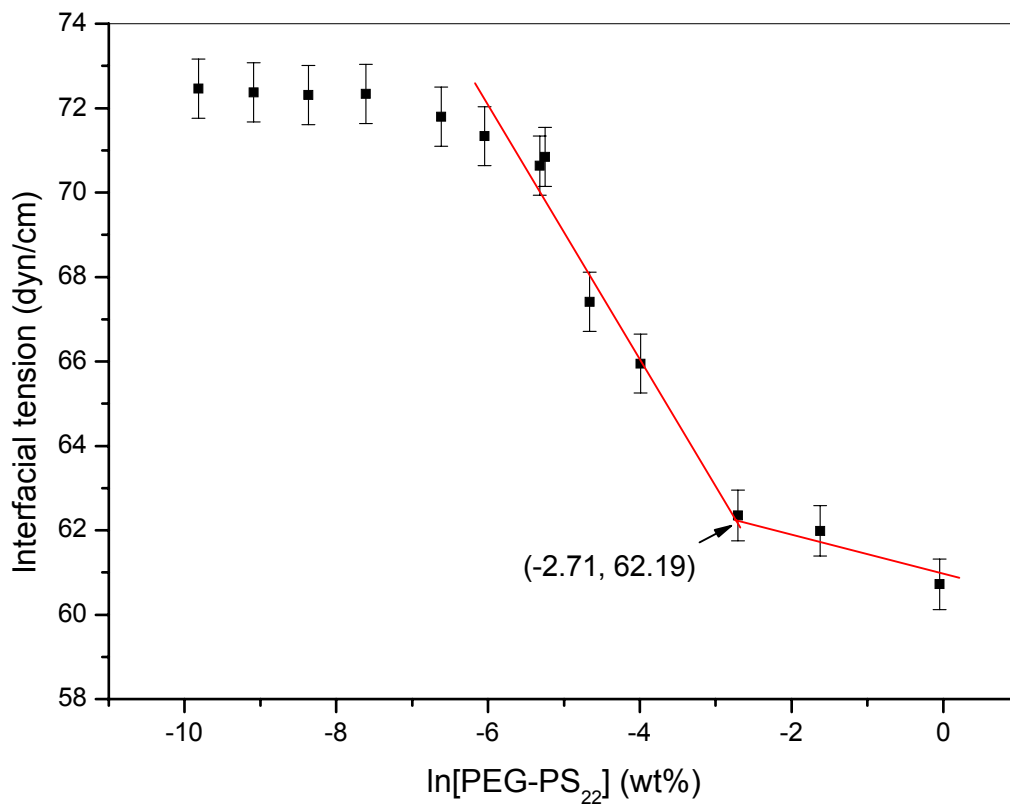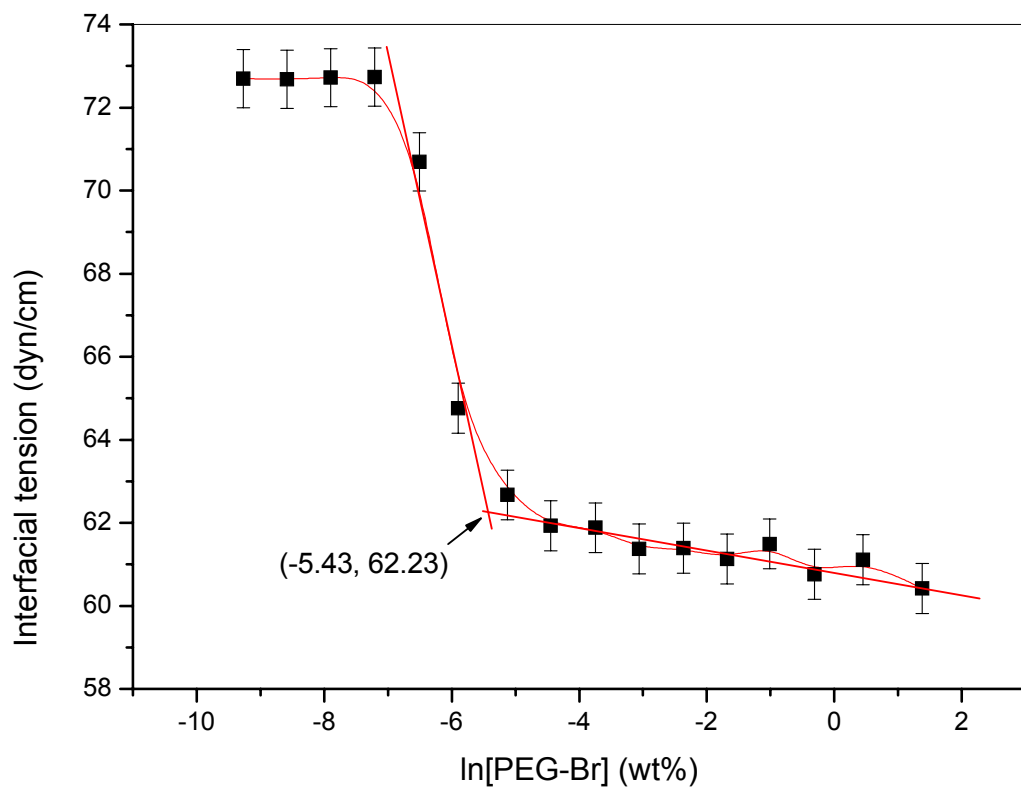
Figure 3.16   CMC measurement of polymer PEG-PS$_{20}$ (050907) in water through pendant drop method; CMC is 0.0191 wt%.

Figure 3.17   CMC measurement of polymer PEG-PS$_{22}$ (041607) in water through pendant drop method; CMC is 0.0665 wt%.

Figure 3.18 CMC measurement of polymer PEG-Br (071007) in water through pendant
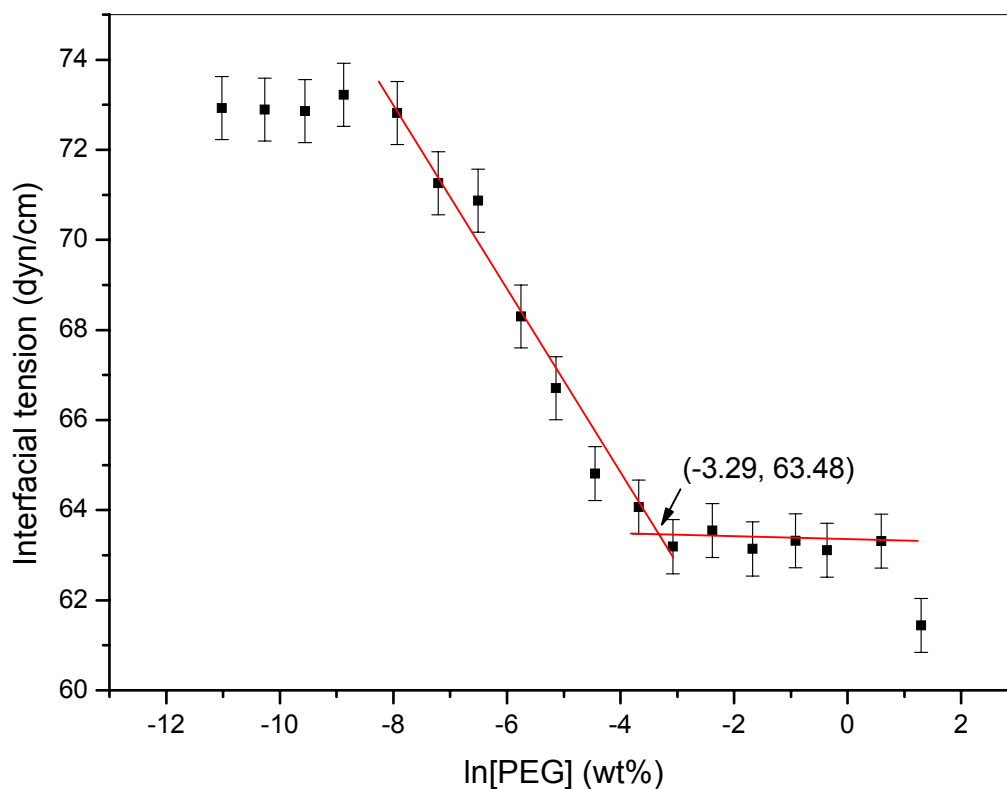
drop method; CMC is 0.00438 wt%.

Figure 3.19 CMC measurement of polymer PEG (070607) in water through pendant drop method; CMC is 0.0373 wt%.

3.3.2 Preliminary application study: Microemulsion polymerization[102]

From all of the above we have confirmed that we were able to make polymerizable copolymers PEG-PS-DVB though a reliably accurate ATRP method. The following discussion aims at using the macromonomer to make nanoparticles with a crosslinked core and PEG corona. We also want to see if those nanoparticles have a thermoreversible gelation property in aqueous solution under certain conditional temperatures and concentration. Scheme 3.2 briefly illustrates our concept of how to make nanoparticles with higher mechanical modulus and similar thermoreversible property in aqueous

solution as F127. For this application, we basically carried an L_1 (oil in water) domain microemulsion polymerization in a ternary system that consists of PEG-PS-DVB, DVB/St (40/60), and water. To be able to determine the microemulsion L_1 domain boundary, we first needed to map the ternary phase diagram. As we have already discussed briefly in the experimental section, when mapping the ternary phase diagram, we used the diblock copolymer PEG-PS instead of PEG-PS-DVB. This is mainly because the diblock copolymer PEG-PS is much more stable than the copolymer PEG-PS-DVB. Fig 3.20 to Fig 3.23 result from the ternary phase diagram mapping of two diblock copolymers (PEG-PS$_{13}$ and PEG-PS$_{22}$) at two different temperatures (25°C and 60°C). These phase diagrams all have the property that the microemulsion L_1 domains are very narrow. We could barely see the boundary in regular ternary phase diagram. This means that the oil solubilizing activity of PEG-PS is not very strong. According to the phase diagrams, under 25°C, PEG-PS$_{13}$ and PEG-PS$_{22}$ can dissolve DVB/St (40/60) up to 0.7 wt% and 1.3 wt%, respectively, while at 60°C the values are 1.8wt% and 2.1 wt%, respectively. The "low oil" loadings are probably due to the hydrophobic segment of PEG-PS being short.
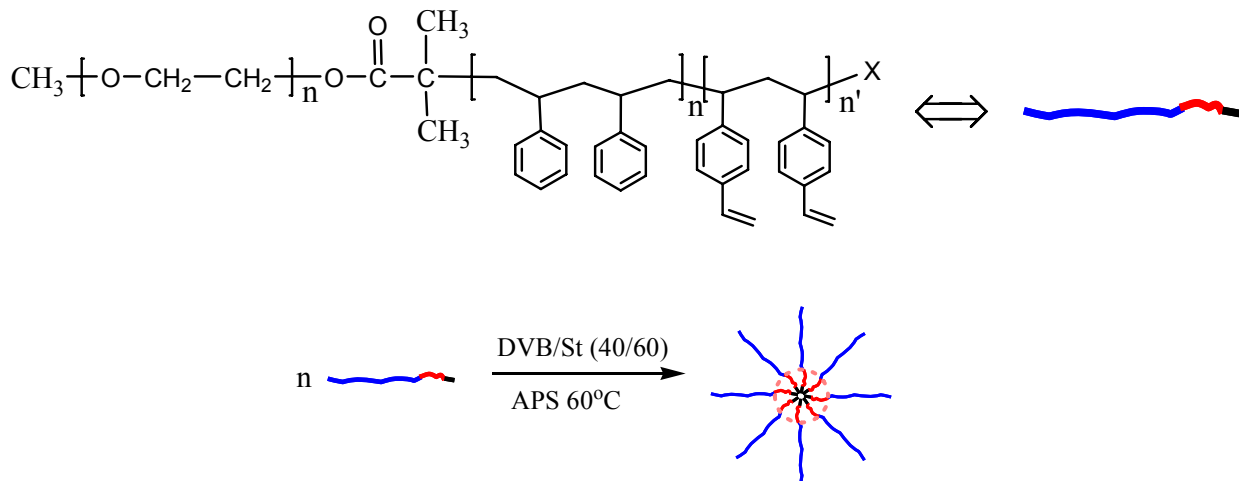
Scheme 3.2 Preparation of nanoparticles with crosslinked core and PEO corona; in this illustration, the number of macromonomers is roughly based on the 102207 sample GPC data.
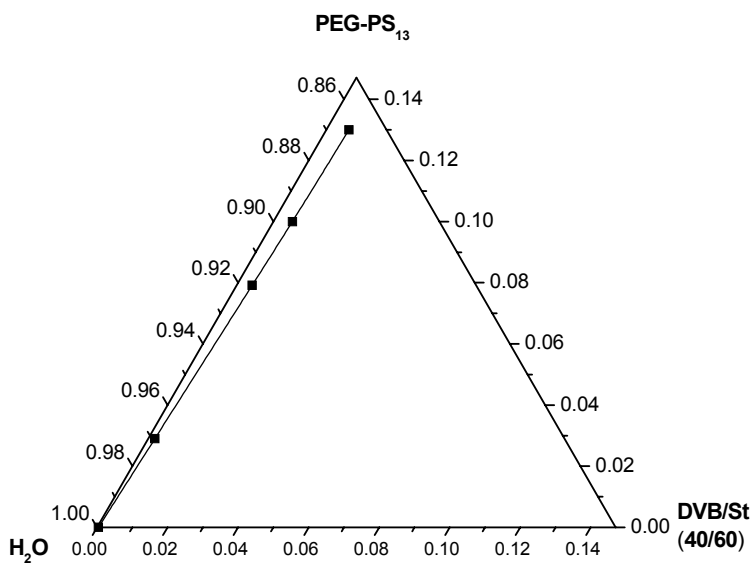

Figure 3.20 Ternary phase behavior between PEG-PS$_{13}$ (030507), DVB/St (40/60), and H$_2$O under 25°C.
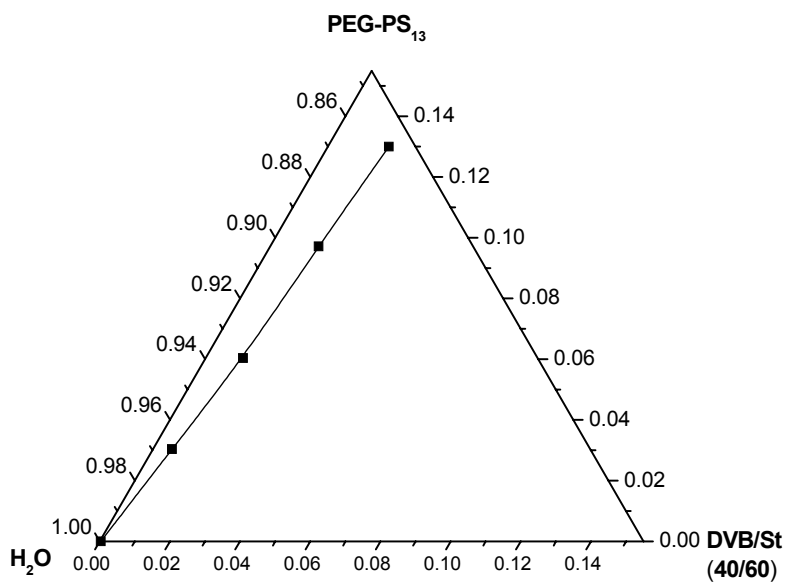
Figure 3.21 Ternary phase behavior between PEG-PS$_{13}$ (030507), DVB/St (40/60), and
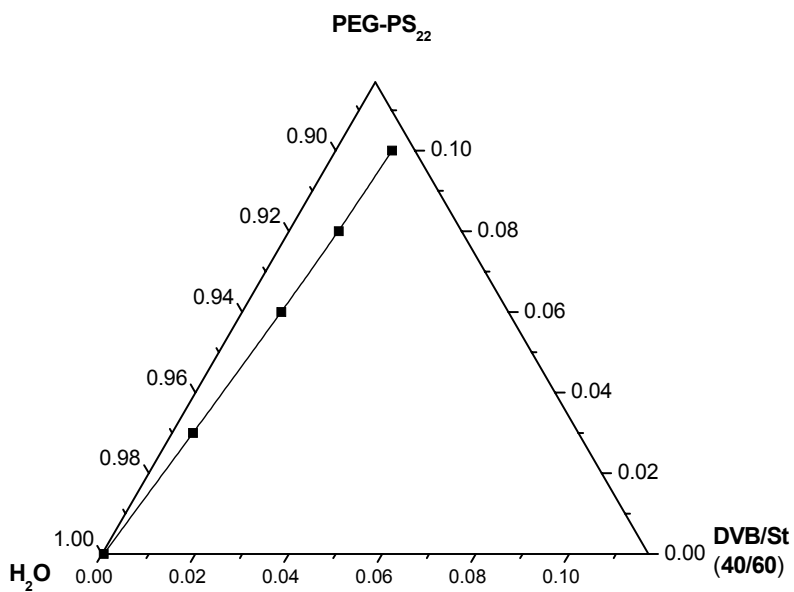
H$_2$O under 60°C.

Figure 3.22 Ternary phase behavior between PEG-PS$_{22}$ (041607), DVB/St (40/60), and
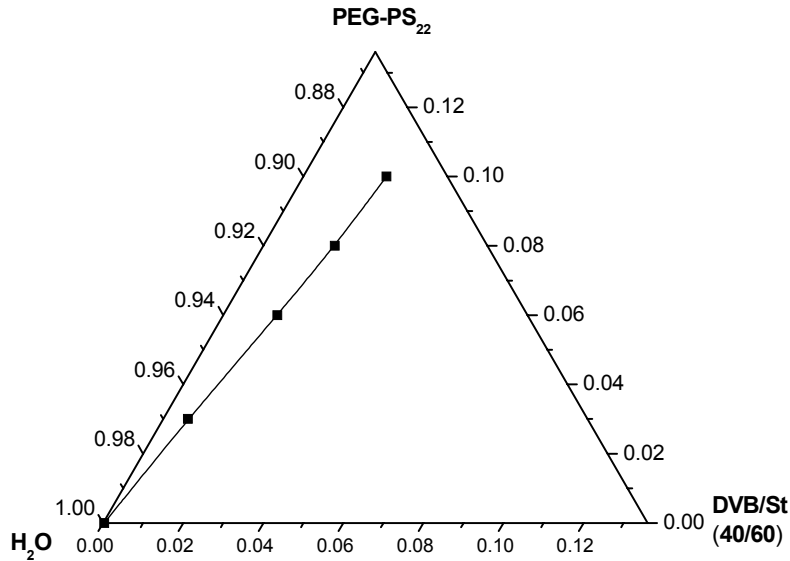
H$_2$O under 25°C.

Figure 3.23 Ternary phase behavior between PEG-PS$_{22}$ (041607), DVB/St (40/60), and H$_2$O under 60°C.

After the diblock copolymer's boundary of the microemulsion L$_1$ domain was found in ternary system, we continued to conduct the microemulsion polymerization experiment in L$_1$ domain using macromonomer PEG-PS-DVB, DVB/St (40/60), and water at 60°C. Specifically, product PEG-PS$_7$-DVB$_2$ (100207), 1.13 wt% (relative to the whole reaction mixture), DVB (40/60), and water were mixed together and formed a homogenous solution at 60°C. The initiator was APS, 1% mole ratio relative to the vinyl groups (the amount of inhibitor in PEG-PS$_7$-DVB$_2$ had been considered for compensational APS) and the reaction time was 25 h. After reaction, the mixture was precipitated in diethyl ether and dried in a vacuum oven at 50°C. NMR measurements (Fig. 3.24) were conducted on the final product, which was labeled as 102207. Obviously, protons at 5.2 ppm and 5.8 ppm, which are due to the vinyl groups (Fig. 3.7), disappeared in the 102207 sample.

This means all the vinyl groups were consumed during the 25 h reaction. As a control, we add 2 wt% of DVB/St (40/60) monomer into the 102207 final product and did the NMR test again; the vinyl group protons were easily observed. Before polymerization, in the reaction mixture, the concentration of DVB/St (40/60) relative to PEG-PS$_7$-DVB$_2$ was actually 13.8% approximately. Since PEG-PS$_7$-DVB$_2$ form micelles containing DVB/St (40/60) in aqueous solution and all the vinyl groups were consumed, there must have been some crosslinked product in some content.
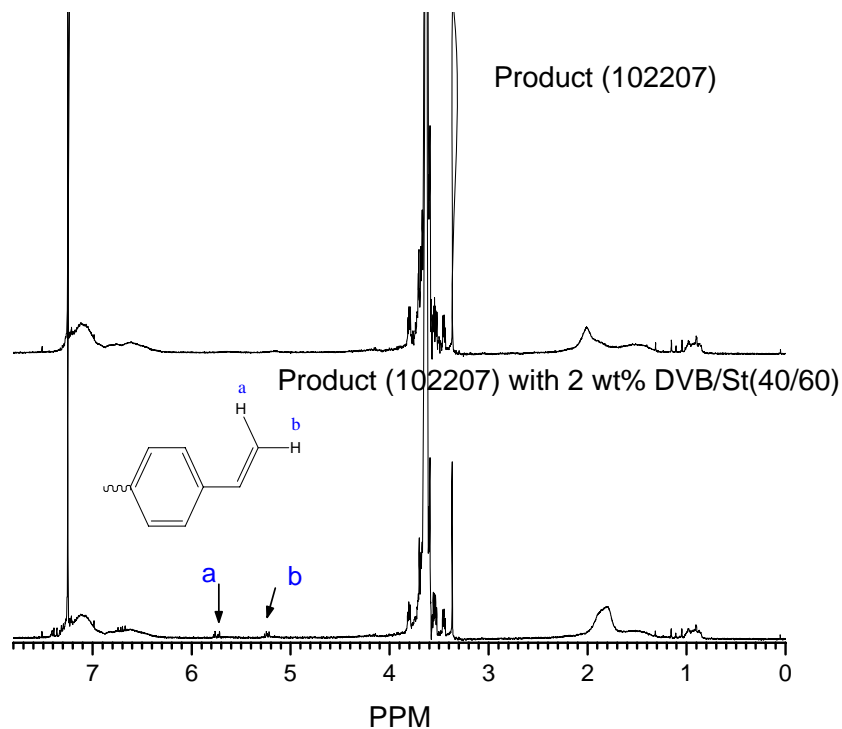

Figure 3.24 Product (102207) NMR and its comparison NMR containing 2 wt% DVB/St monomer.

GPC experiments were also conducted to characterize the 102207 product (Table 3.4, Fig. 3.25, and Fig. 3.26). Fig. 3.26 is just a separate GPC curve separated from Fig. 3.25 for demonstration purpose. Table 3.4 shows that the GPC results (molecular increasing) are consistent with the NMR molecular structure calculation. Sample (102207) looks like it has two main molecular weight distribution peaks; the lower one is almost overlapped with macromonomer PEG-PS$_7$-DVB$_2$, and the higher part has an Mn at 73,542, which could be attributed to the crosslinking reaction of macromonomer PEG-PS$_7$-DVB$_2$ and DVB/St (40/60). According to the molecular weight, the crosslinked sample contains about 8 PEG-PS$_7$-DVB$_2$ macromonomer, and according to Fig. 3.26, there is about 13.45% macromonomer involved crosslinking reaction. (The rest of the macromonomer get reacted but didn't crosslink with each other.) That is to say, in the microemulsion polymerization, only a small fraction (13.5%) of monomer converted to higher molecule weight product. Most parts of monomer were not involved in crosslinking reaction.

Table 3.4 GPC measurements (PS as standards) related to 102207 sample

Sample	Mn	Mw	PDI	Star area(%)
mPEG	6912	7072	1.02	
PEG-PS$_7$(092807)	7923	8448	1.07	
PEG-PS$_7$-DVB$_2$(100507)	8457	8981	1.06	
PEG-PS$_7$-DVB$_2$[a](102207)	73542[b]	83702[b]	1.14[b]	13.45

a) This sample is after PEG-PS$_7$-DVB$_2$ reacted with 1.13wt% DVB/St (40/60) in water.

b) Data are only for the crosslinked part (Fig. 3.26)
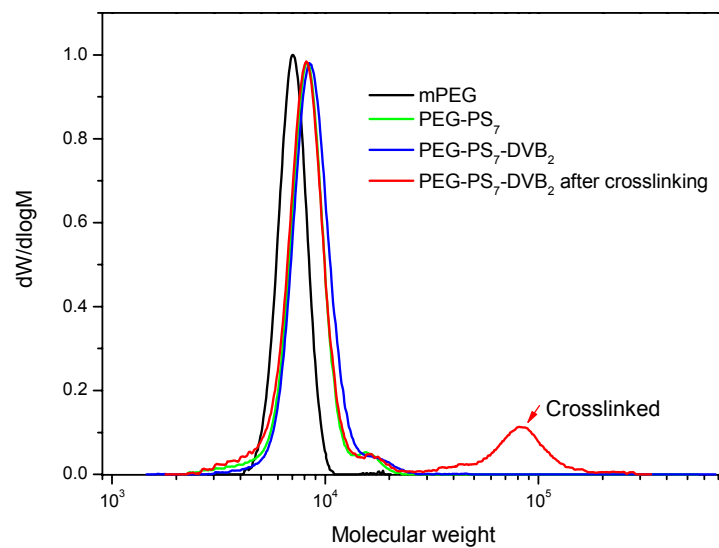
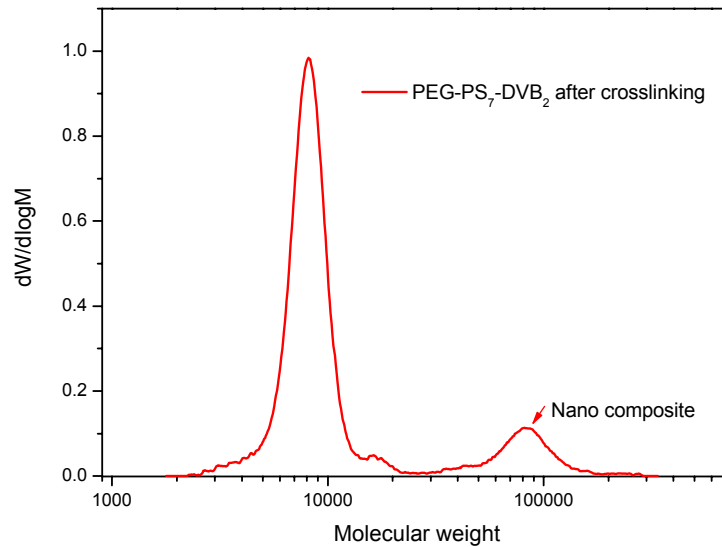Figure 3.25 GPC measurement of a serial of polymers.

Figure 3.26 PEG-PS$_7$-DVB$_2$ (after crosslinking) GPC measurement: the higher

molecular fraction is 13.45% based on the peak enclosed area.

To understand micelles better, we did rough molecule size estimation based on equation (3):

$$S^2 = \frac{1}{6}h^2 \quad\cdots\cdots\cdots\cdots\cdots\cdots\cdots\cdots\cdots\cdots\cdots\cdots\cdots\cdots\cdots\cdots\cdots\cdots\cdots\cdots\cdots\cdots\cdots\cdots\cdots\cdots\cdots\cdots(3)$$

$$(h^2 = n_e l_e^2 \quad n_e = \frac{n}{3} \quad l_e = 2.45l)$$

Here S is radius of gyration, h is the distance of a polymer chain ends, n is chemical bonds number, l is the bonds length, and n_e, l_e are equivalent bond number and length, respectively. This model is built on the assumption of free joint chain and when n is large.

Very roughly, for the PEG molecule that we used, there are about 103 $-CH_2-CH_2-O-$ repeating units; for every repeating unit, there are one C-C and two C-O bonds; the length of C-C and C-O is 0.154 nm and 0.143 nm. If we assume l here is (0.154+0.143+0.143)/3=0.147 nm, then according to the formula (3) above, the radius of gyration of PEG we used is:

$$S = \sqrt{\frac{1}{6}\cdot\frac{1}{3}n\cdot(2.45l)^2} = \sqrt{\frac{309\times(2.45\times0.147)^2}{18}} = 1.49 \; nm$$

Similarly, PEG-PS$_{7.3}$, PEG-PS$_{13}$ and PEG-PS$_{22}$ have radius of gyrations 1.53 nm, 1.55 nm, and 1.59 nm respectively. If we say that PEG-PS$_7$-DVB$_2$ has a 1.6 nm radius of gyration, we estimated that in a 50 nm diameter polymer particle, there are approximately 4200 molecules if they are closely packed. According to Table 3.4 and 3.5, in polymer particle (102207), there are about 9 PEG-PS$_7$-DVB$_2$ molecules crosslinked together. Due to the repulsion between polymer molecules, they can't get crosslinked into a very dense core.

In order to characterize the formed nano crosslinked particles (13.45% in weight fraction, 102207), particle size and TEM measurements were conducted. Table 3.5 shows the particle size and its behavior when diluting a certain concentration aqueous solution of 102207 product. It seems that in aqueous solution, the particles maintain their diameter at around 50 nm until the solution is too dilute to be detected by the particle size analyzer. This behavior supports from another perspective that these particles have crosslinked cores.

TEM results were more apparent than those of particle size measurement. Fig. 3.27 through Fig. 3.30 illustrate four sets of particle images. Core-shell structures can be found in each of them. According to these figures, the approximate particle diameters are in the range of (50 to 100 nm).

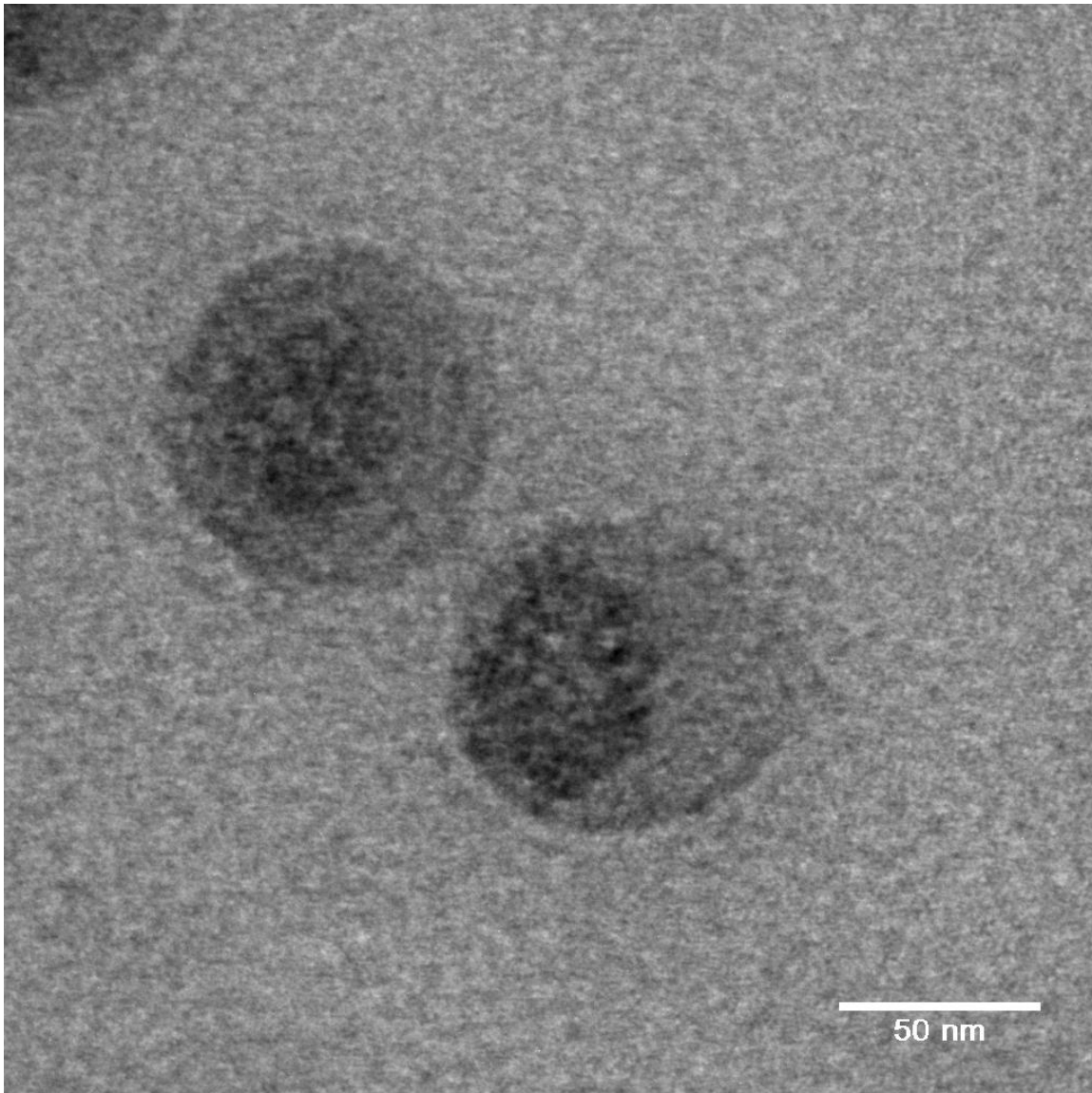Table 3.5 Product (102207) particle size measurement in aqueous solution[a](diluting).

Concentration (wt%)	6.00	1.38	0.44	0.22	0.1	0.05	0.026	0.013	0.007	0.0034	0.0017
Size (nm)[b]		50.3	46.7	44.5	47.4	46.7	47.6	45.8	0	0	0	0

    a) All the samples were filtered before measurement by 500nm Syringe filter

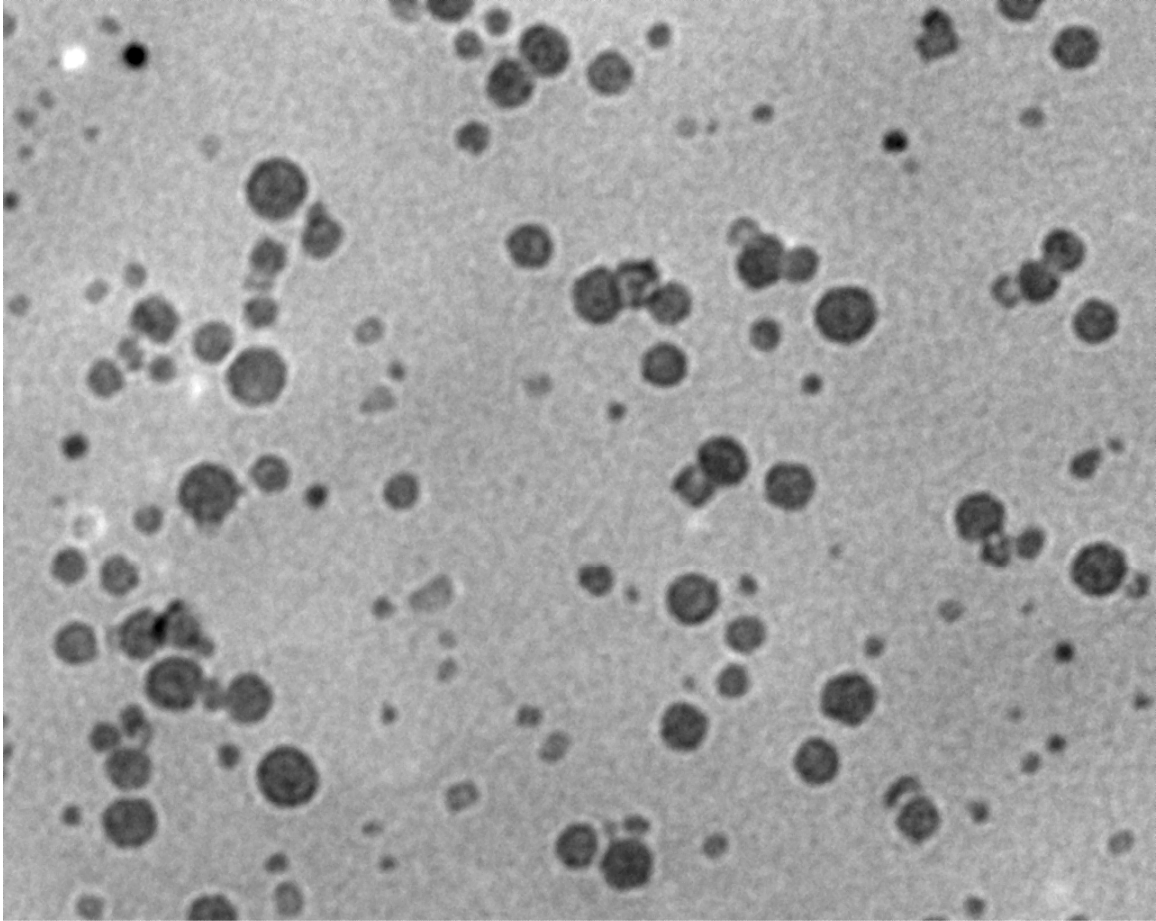   b) Data were obtained on a Brookhaven 90Plus size analyzer.
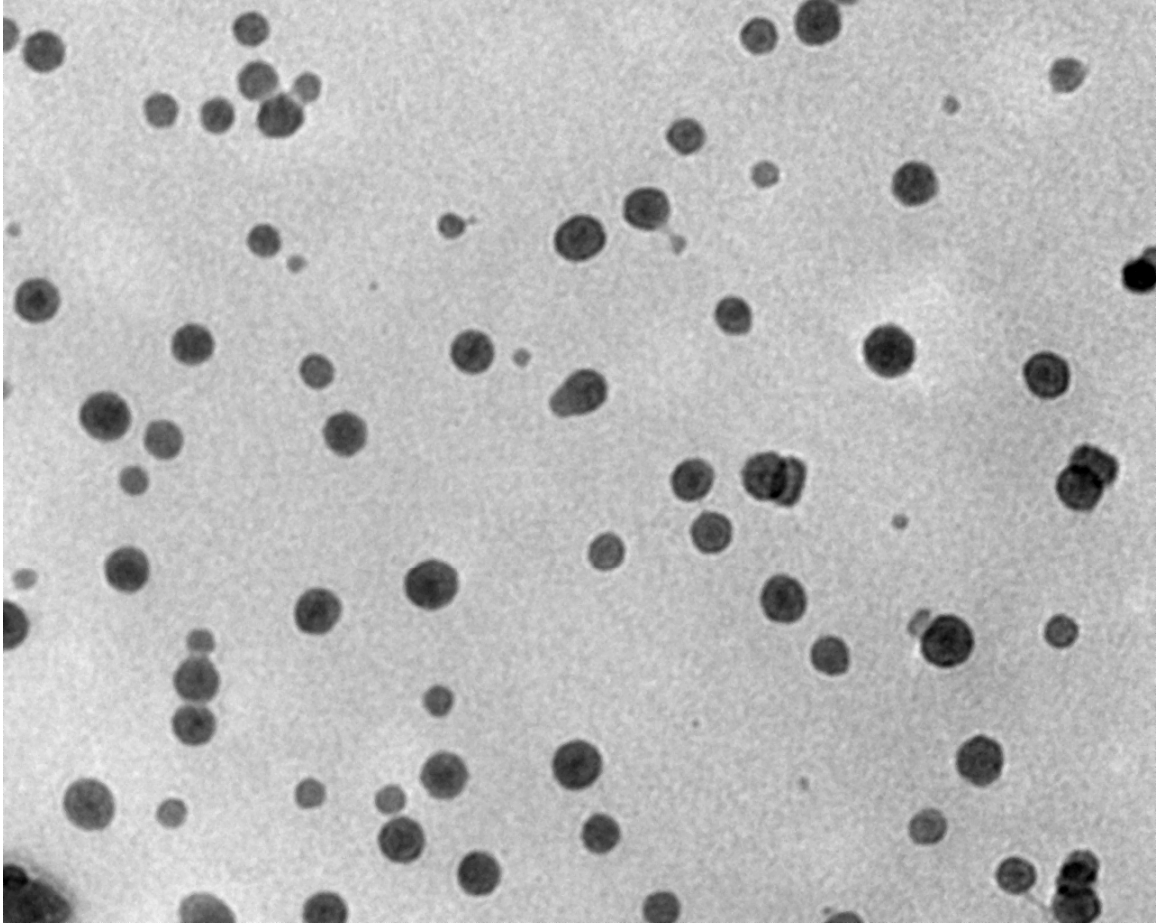
50 nm
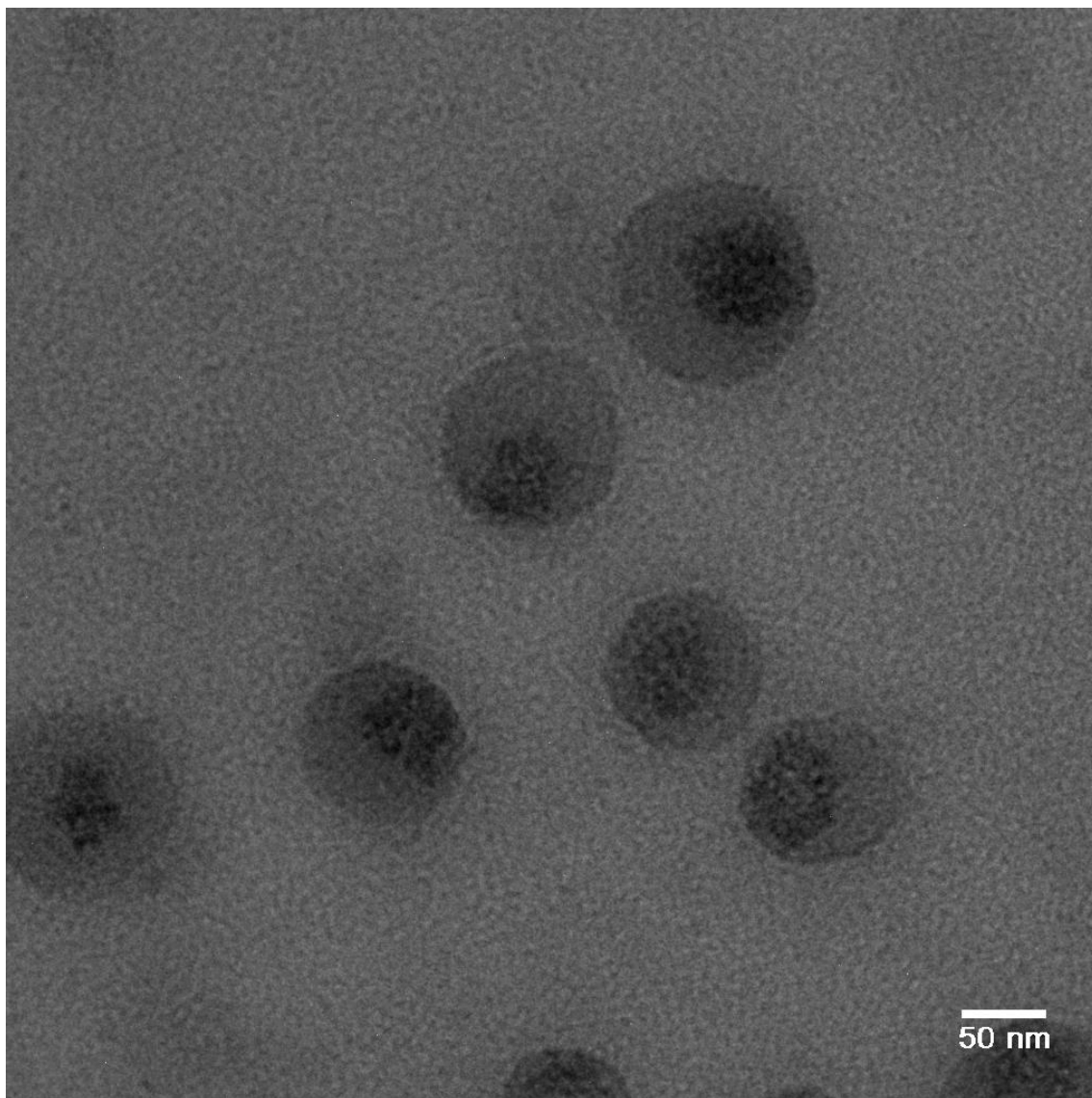
1/2 (Fig 3.27)

2/2 (Fig 3.27)

Figure 3.27 PEG-PS$_{13}$ (030507) TEM images (1 to 2).
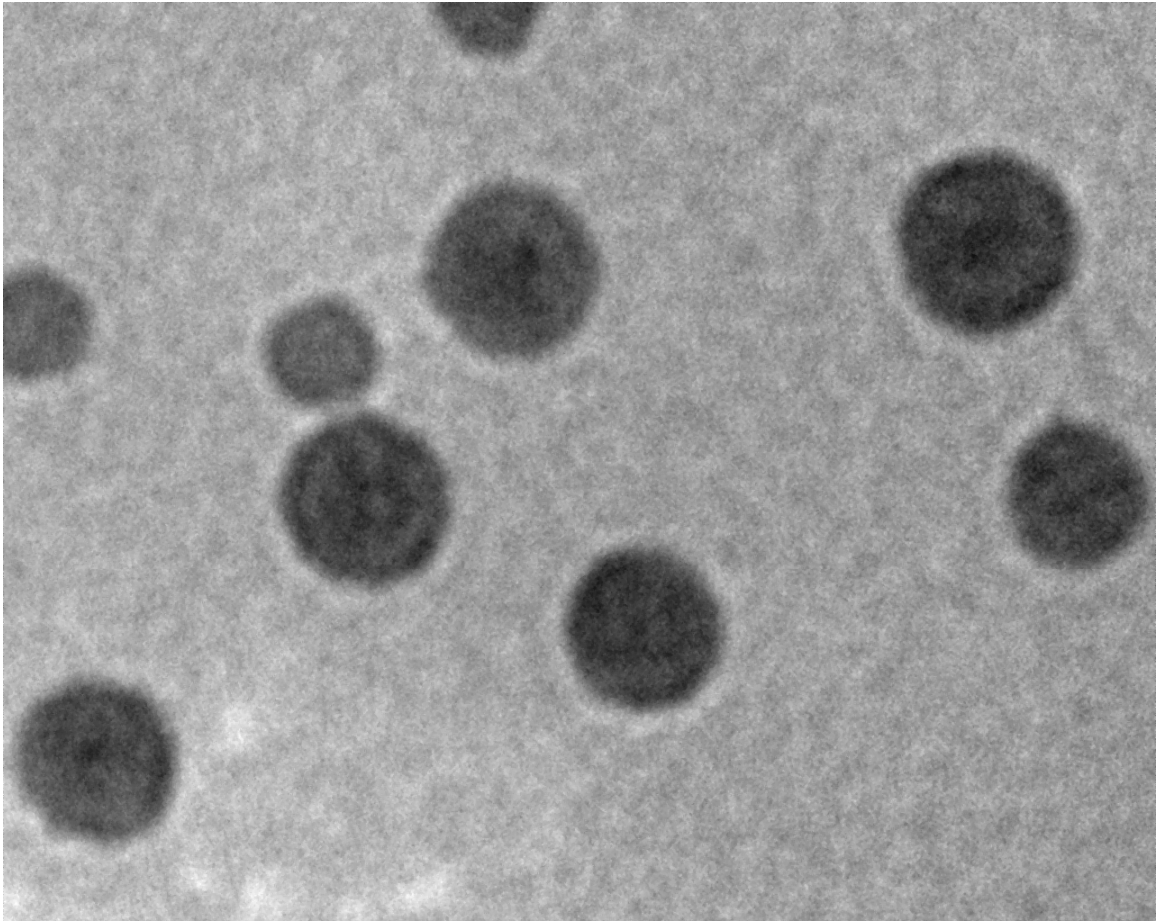
A (Fig 3.28)

B (Fig 3.28)

B2-110707-10.tif
Cal: 1.405pix/nm
12:33 12/07/07
TEM Mode: Imaging

100 nm

HV=300.0kV
Direct Mag: 25000x
X: Y: T:
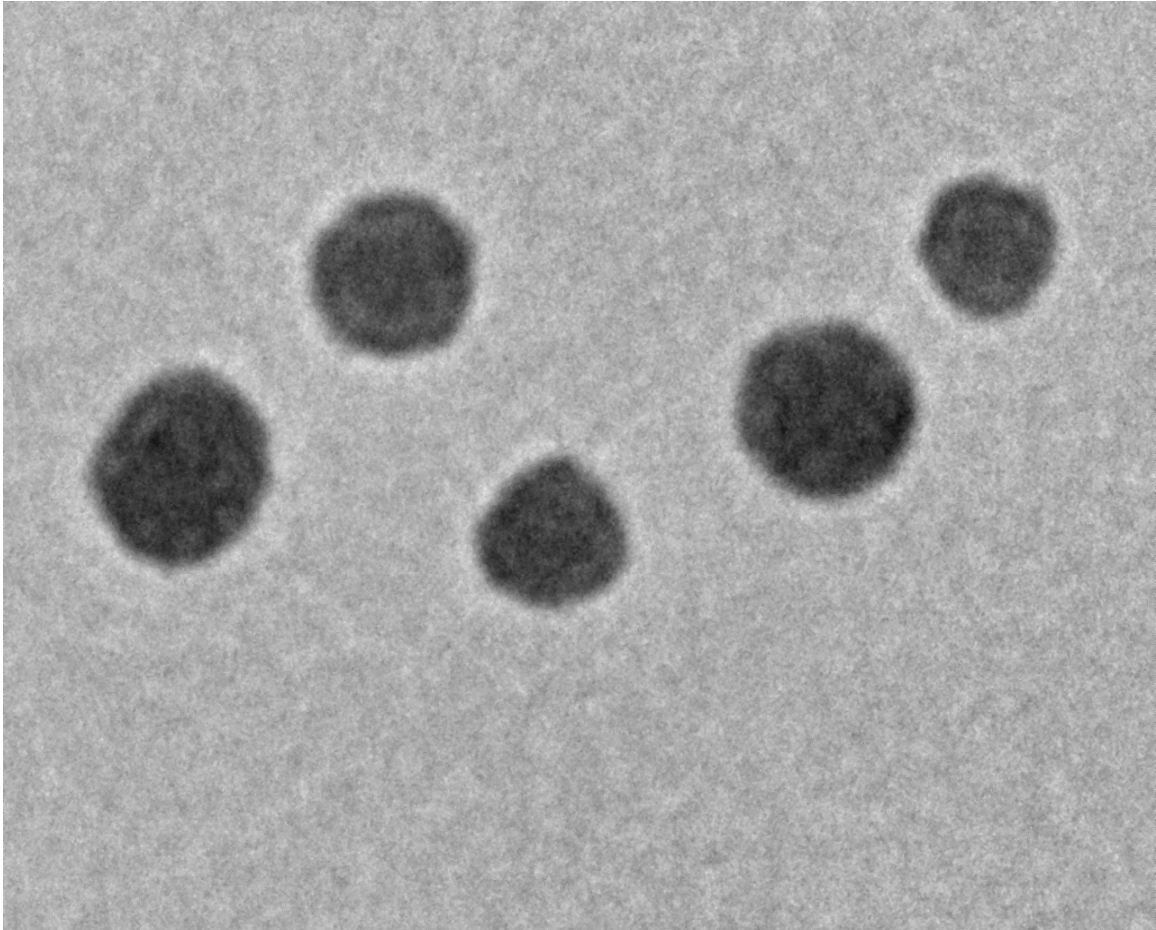University of Michigan

C (Fig 3.28)

D (Fig 3.28)

Figure 3.28 TEM of PEG-PS$_{13}$-DVB$_2$ (100507) polymerizable triblock copolymer in aqueous solution, all scale bars are 100 nm except the right down's is 10 nm (A to D).
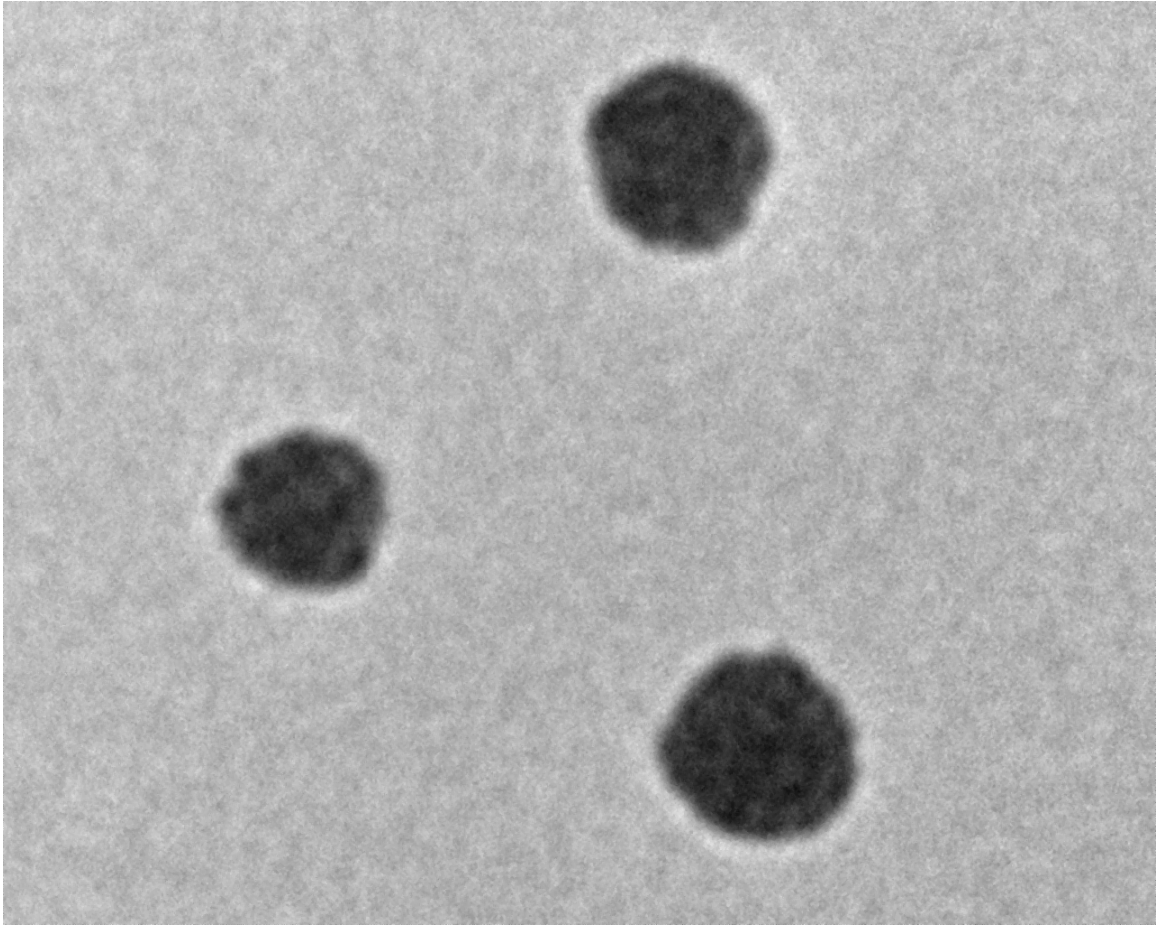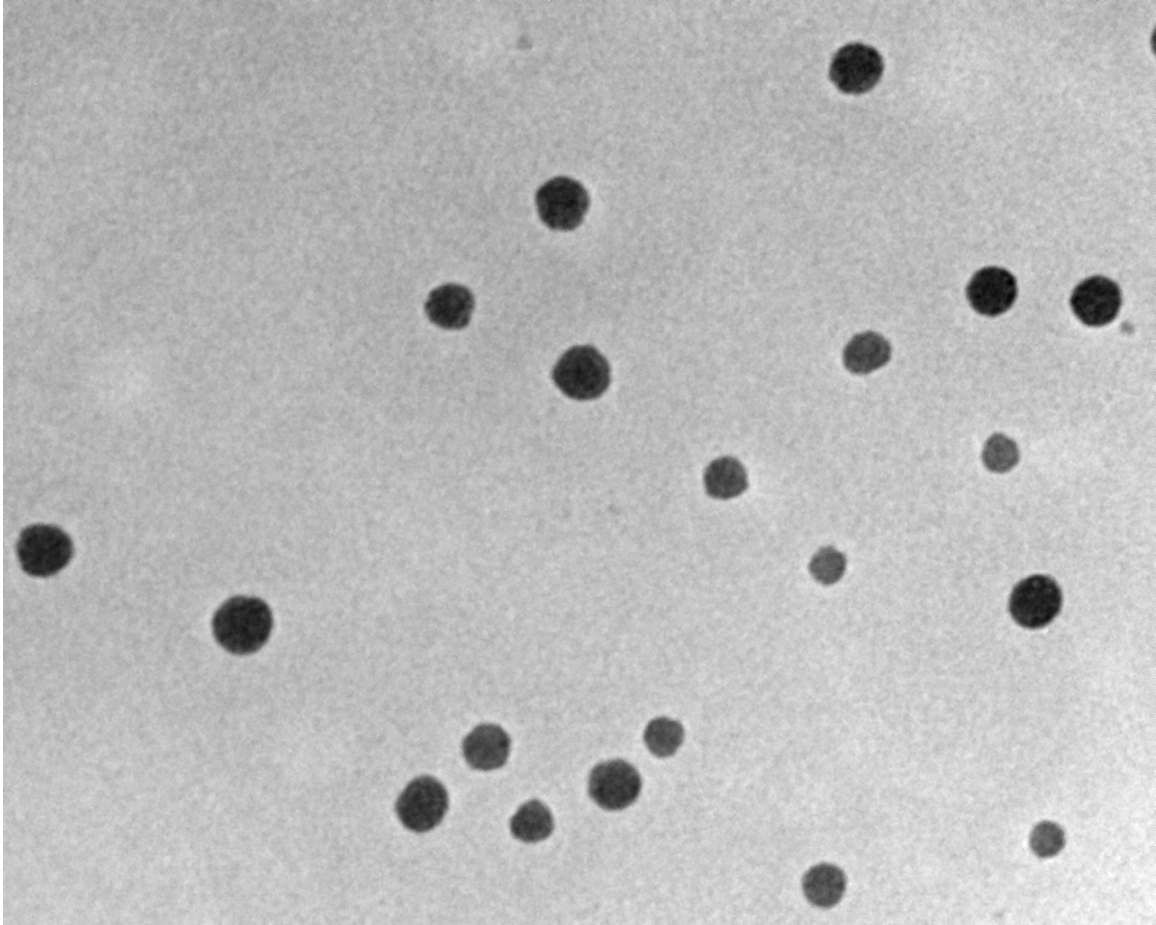
I (Fig 3.29)

II (Fig 3.29)

C2-120707-03.tif
Cal: 562.004pix/micron
12:54 12/07/07
TEM Mode: Imaging

100 nm
HV=300.0kV
Direct Mag: 10000x
X: Y: T:
University of Michigan

III (Fig 3.29)

IV (Fig 3.29)

Figure 3.29 TEM of PEG-PS$_{13}$ (121506) diblock copolymer in aqueous solution, all scale bars are 100 nm (I to IV).
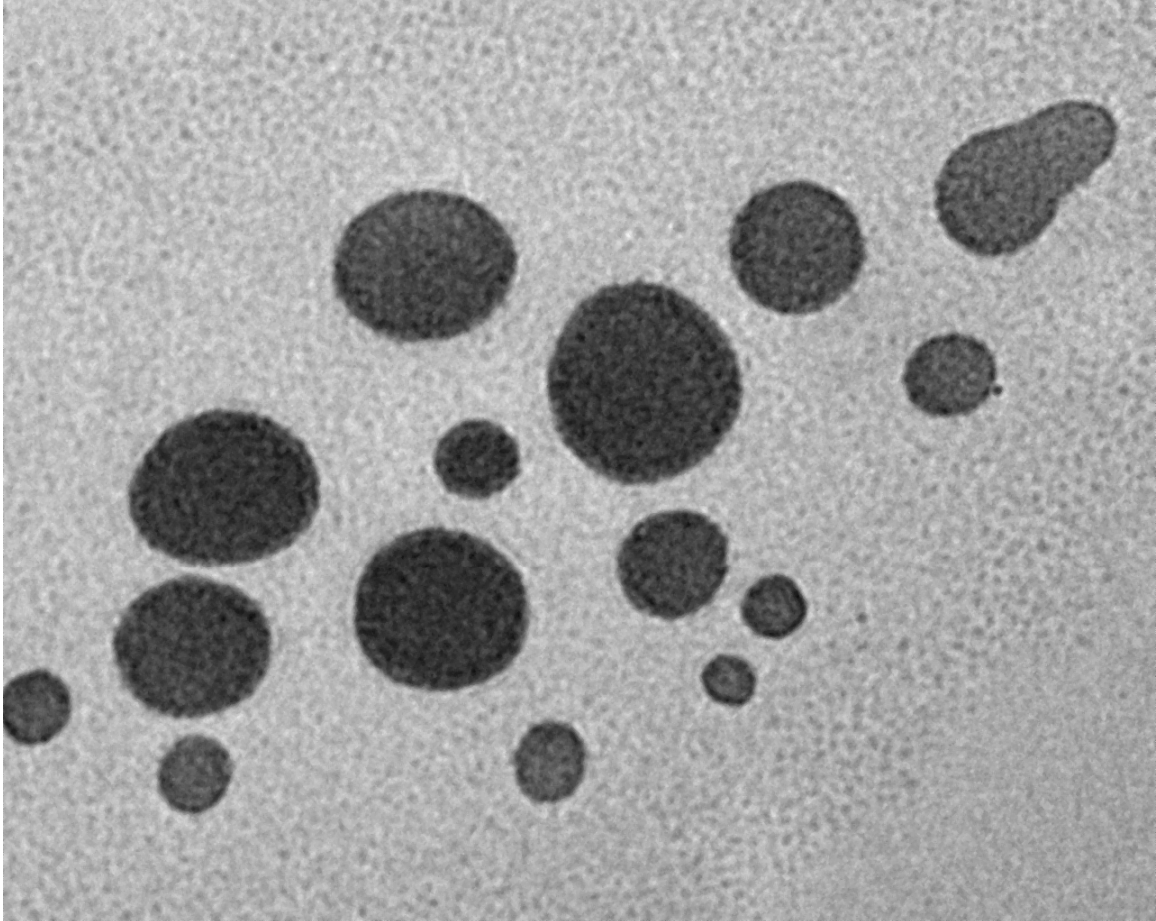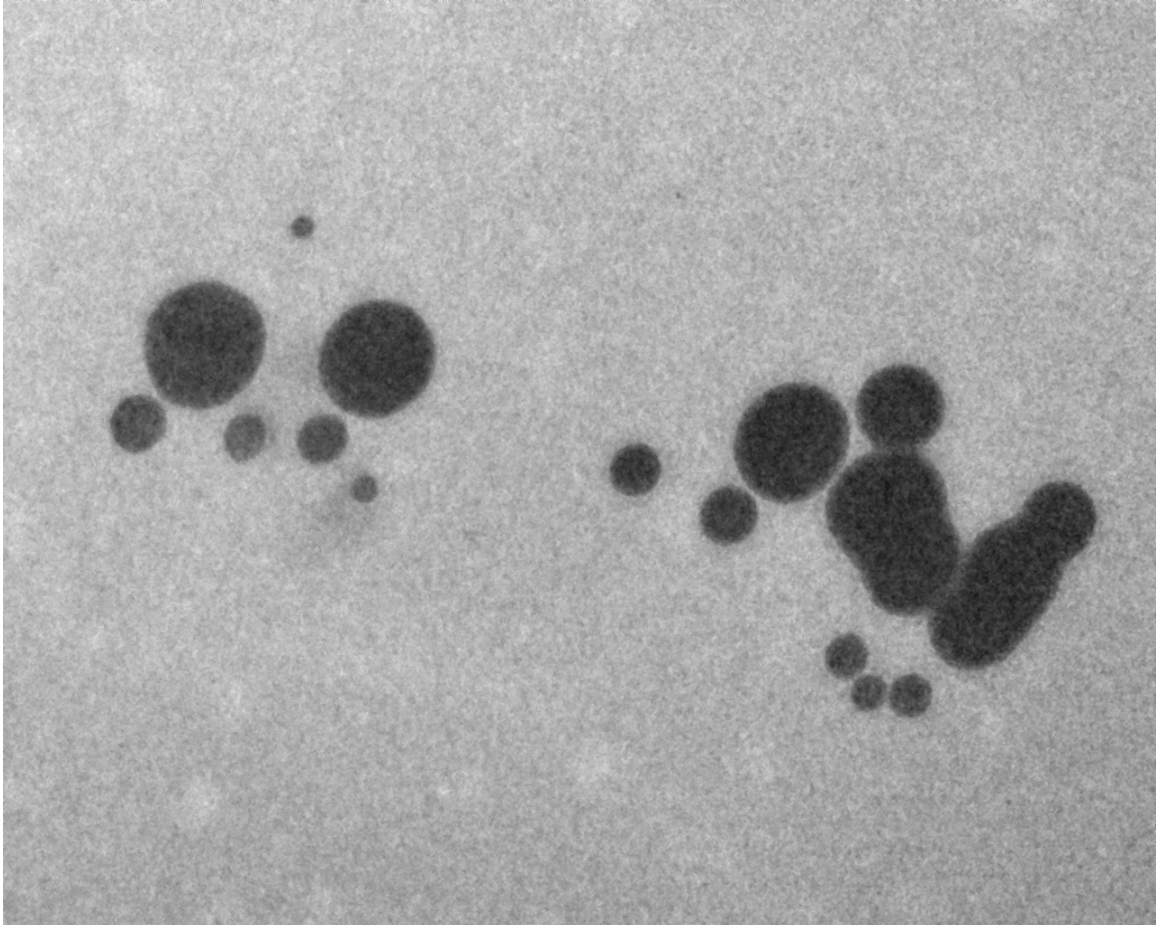
a (Fig 3.30)

E1-120507-04.tif
Cal: 449.604pix/micron
14:31 12/05/07
TEM Mode: Imaging

500 nm
HV=300.0kV
Direct Mag: 8000x
X: Y: T:
University of Michigan

b (Fig 3.30)
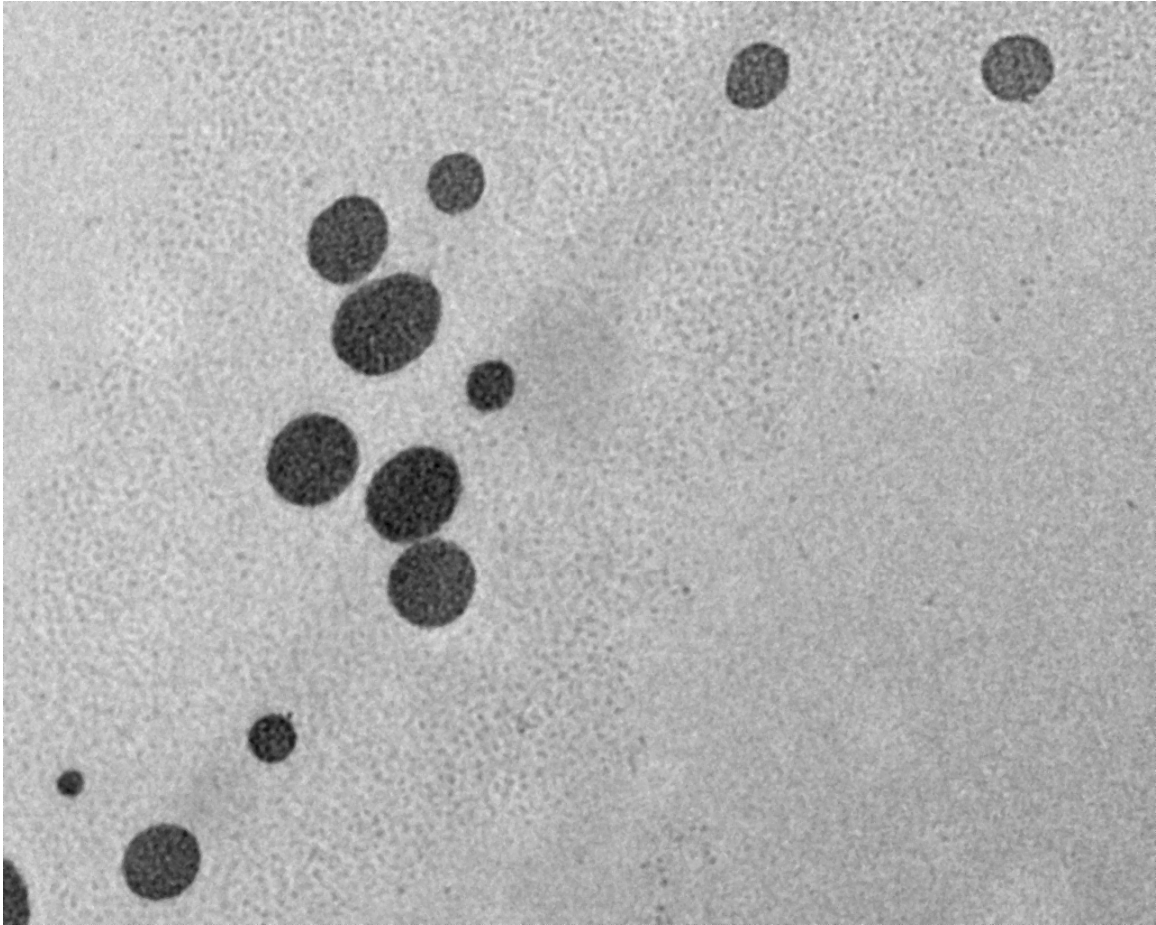
E1-120507-07.tif
Cal: 843.007pix/micron
14:38 12/05/07
TEM Mode: Imaging

100 nm
HV=300.0kV
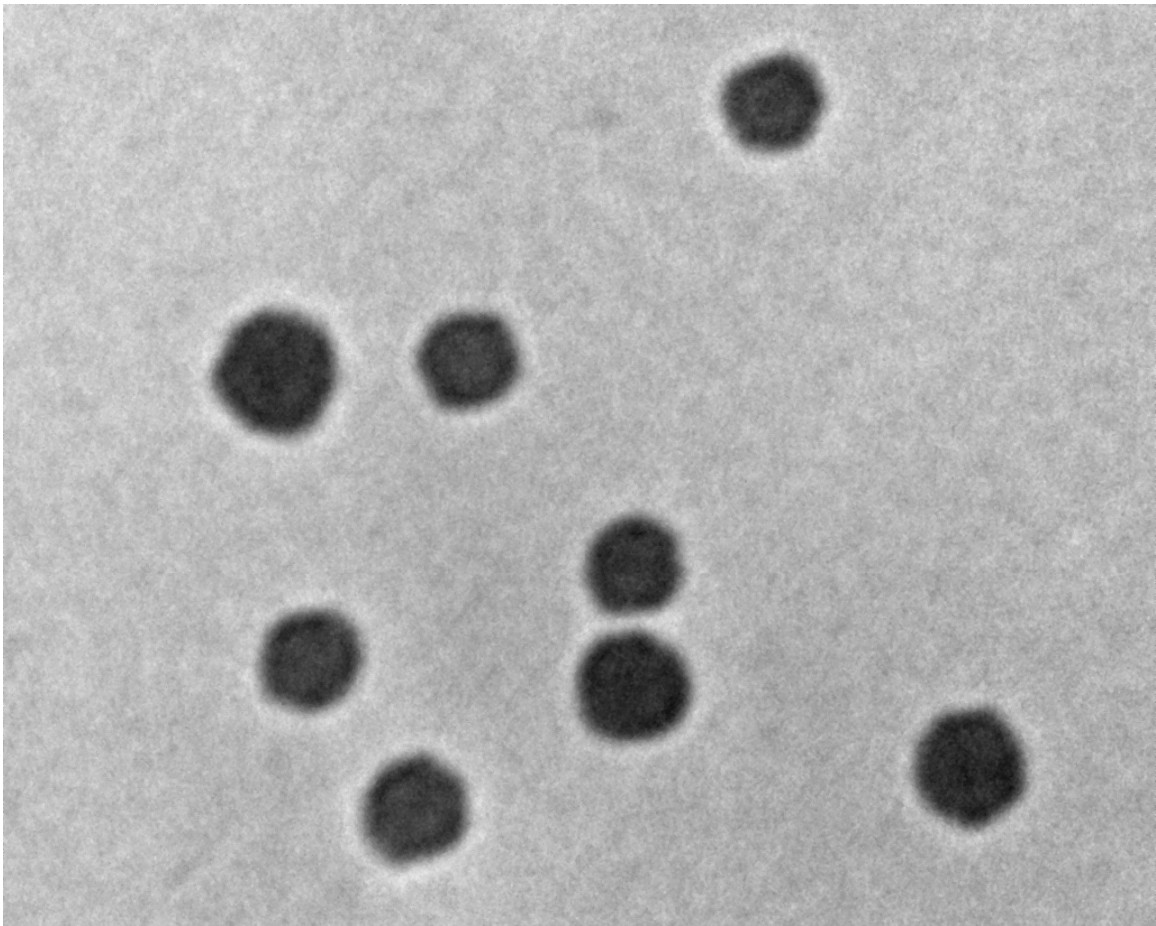Direct Mag: 15000x
X: Y: T:
University of Michigan

c (Fig 3.30)
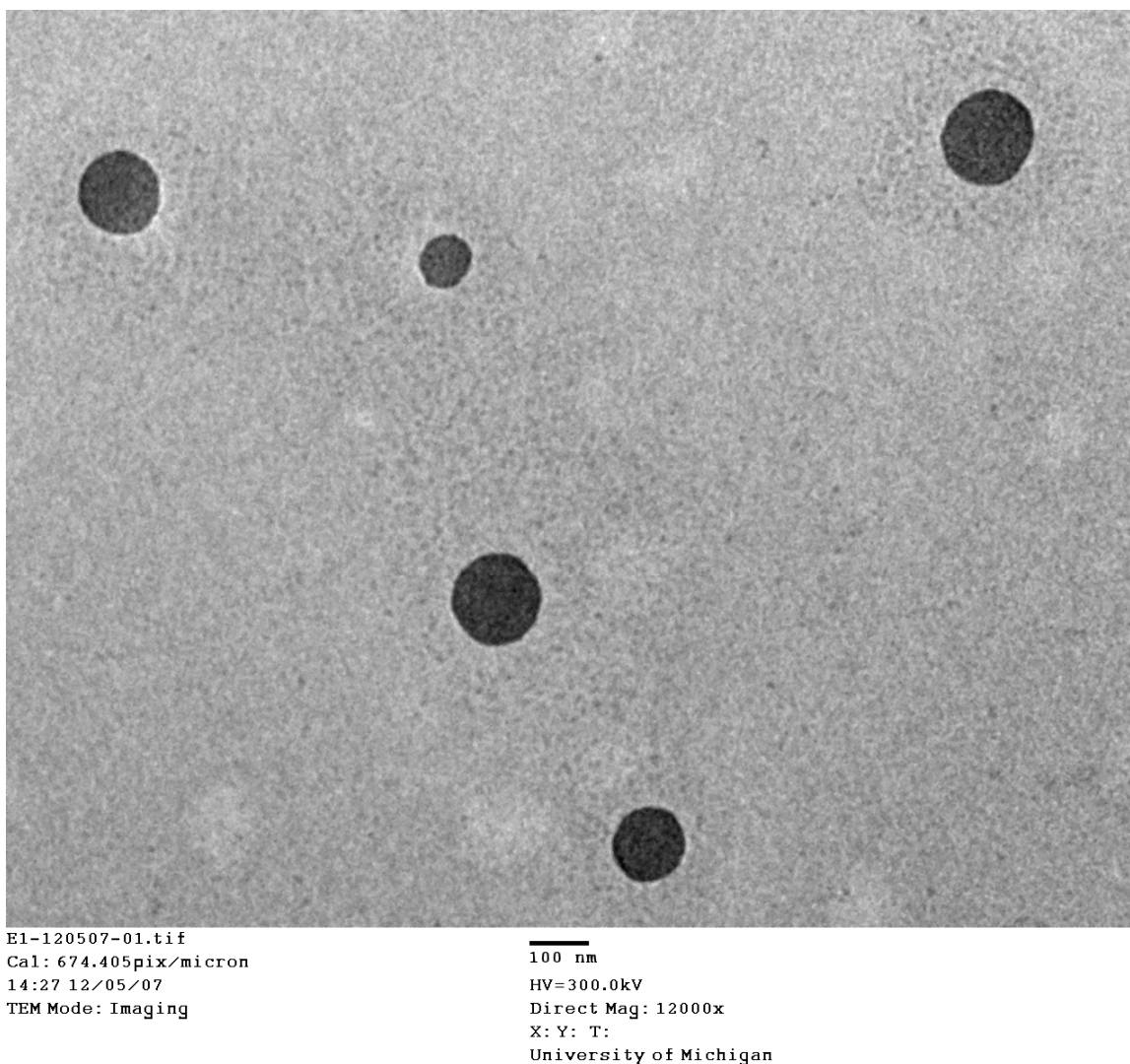
d (Fig 3.30)

e (Fig 3.30)

f (Fig 3.30)

Figure 3.30 TEM of product (102207) in aqueous solution formed by PEG-PS$_{13}$-DVB$_2$ reacting with DVB/St (40/60) in microemulsion polymerization; all scale bars are 100 nm (a to f).

TGA and DSC characterization were also conducted in order to study the thermal properties of the product (102207). Fig. 3.31 shows that the two decomposition temperatures for macromonomer PEG-PS$_7$-DVB$_2$ before and after polymerization were

essentially the same. This again says that the microemulsion polymerization was not efficient and more batches of experiments need to be conduct to improve the product yield. Fig. 3.32 is DSC results for three polymers, which are PEG-PS$_7$ (092807), PEG-PS$_7$-DVB$_2$ (100507) and product polymer (102207). Based on Fig. 3.32, above -40°C, there is no apparent glass transition behavior for all of them according to the figure. (Some researchers[106] claimed that for PEG (Mw 20,000), the Tg is -62.5^{o}C, but obviously, their DSC figure of PEG didn't support them, and we don't want to concentrate on discussing PEG's Tg here.) The quite interesting thing is, on the DSC curves, there is a narrowing "window" that we defined here as the temperature range from melting to crystallizing that appeared on the DSC curve of product polymer (102207) when compared to that of PEG-PS$_7$ and PEG-PS$_7$-DVB$_2$ macromonomer. From the discussion before we knew that the product polymer (102207) contained about 13.45% crosslinked polymer. So a proposed reason for the appearance of the narrowing window result from the polymer (102207) sample is: the polymer is easier to get ordered than pure random polymer chain. The crosslinked polymers can serve as crystal nucleis. Because of this, the polymer (102207) sample becomes easy to crystallize and to melt as well. That's why a narrowing "window" appears on the DSC figure (Fig. 3.32).
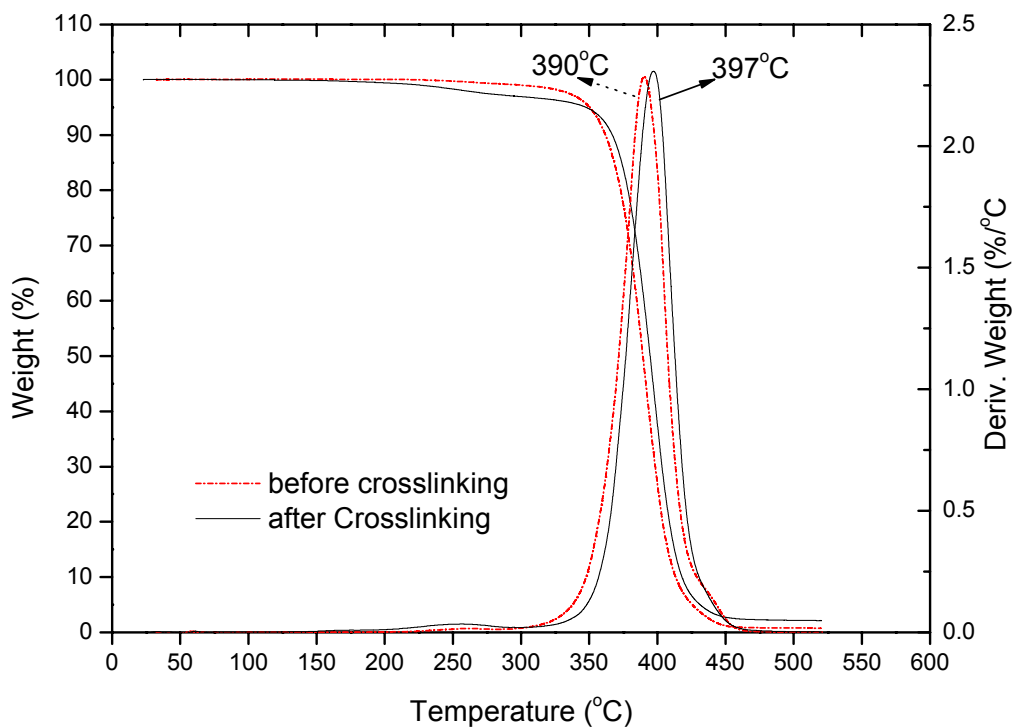
Figure 3.31 Polymer thermal decomposition temperature. Dotted line is PEG-PS$_7$-DVB$_2$

(100207) polymerizable monomer itself. Solid line is PEG-PS$_7$-DVB$_2$ reacted with

DVB/St in microemulsion polymerization (102207). The essentially same decomposition

temperature was due to the low yield (non-efficient) of the microemulsion polymerization.
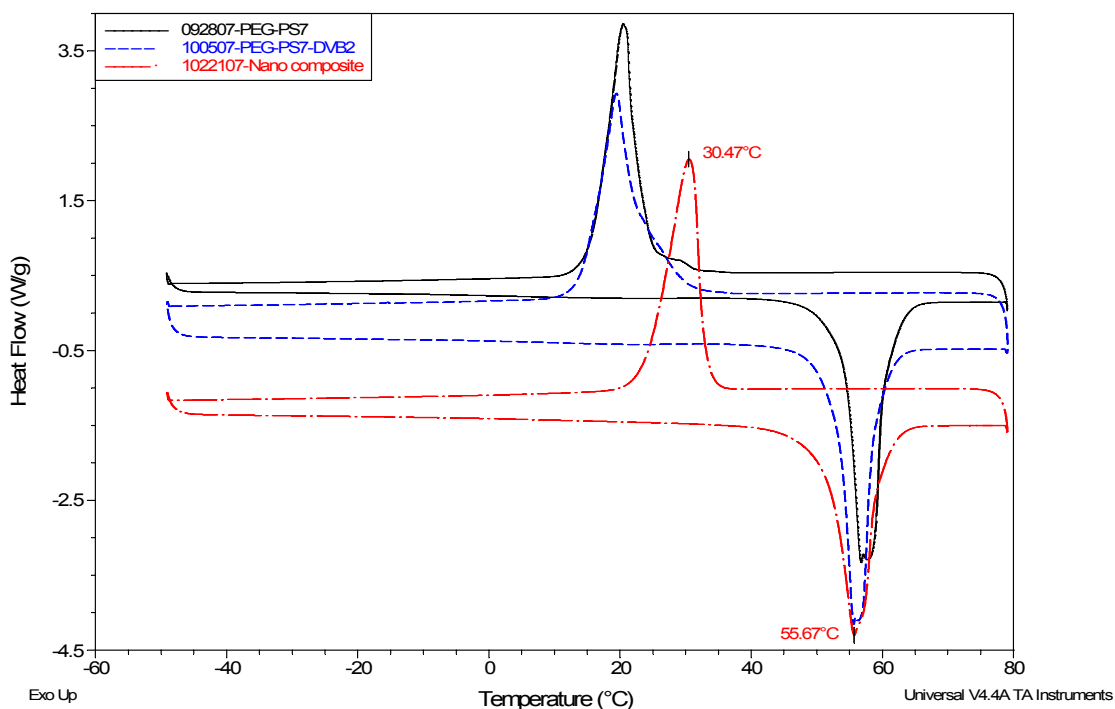
Figure 3.32   DSC measurement for three related polymers: PEG-PS$_7$, PEG-PS$_7$-DVB$_2$
and final polymer (102207)

Using some of the polymer (102207), a 2-D phase diagram (Fig. 3.33) of the polymer

in aqueous solution was mapped carefully following the procedure as described in

Chapter 2 (section 2.2.2). However, there is no apparent thermoreversible behavior

observed from the phase diagram. The phase diagram is essentially similar to that of the

triblock copolymer we studied in Chapter 2 (Fig. 2.1). It has cloud points at about

96°C±1°C all through the 14.7 wt% to 20.6 wt% concentration ranges investigated. The

copolymer (102207) does not liquify when cooling the gel phase (unlike F127). And

samples below 17.7wt% do not have a gel phase. This aspect is similar to F127.[18] Below

-14°C, the samples solidify to an opaque (phase separation) phase for all concentrations studied. The opaque phase always melts at 0°C and forms either a liquid phase (when below 17.7 wt%) or aqueous gel phase (when above 17.7 wt%). The system is unstable between -14°C±1°C and 0°C. Here the "unstable" means when the sample was cooling through 0°C to -14°C, the sample can still flow in the tube if a shear force was applied (will flow directly if concentration was lower than 17.7 wt%). On the other hand, if the procedure was heating up the sample from -14°C to 0°C, the sample will stay in the solid phase (opaque) until the temperature is 0^oC, at which time the sample would liquify or form a clear gel phase, according to its concentration (Temperature hysteresis?).

3.4 Conclusions

Various polymerizable triblock copolymers PEG-PS-DVB were synthesized and characterized through several methods including GPC, NMR, CMC, and DSC. Preliminary applications of these macromonomers were investigated. Microemulsion polymerization of PEG-PS$_7$-DVB$_2$ and DVB/St (40/60) in water was conducted, but only about 13.5% monomers converted higher molecular weight product, which means the polymerization was non-efficient and need to be improved. CMC of our products were measured by pendant drop method. Though all of the tested polymers exhibited amphiphilic molecules properties and most likely form micelles when their concentrations are higher than 0.08 wt%, a further study on the starting material shows that the surfactivities are original from the impurity in PEG.

However, there is no apparent thermoreversible behavior associated with the target polymer in water. This could have much to do with the low yield of the polymerization of the macromonomer PEG-PS-DVB. Further study needs to be done on increasing the yield

of the crosslinking polymer products. Future work should also try smaller molecular

weight mPEG, such as mPEG3000 or mPEG4000.
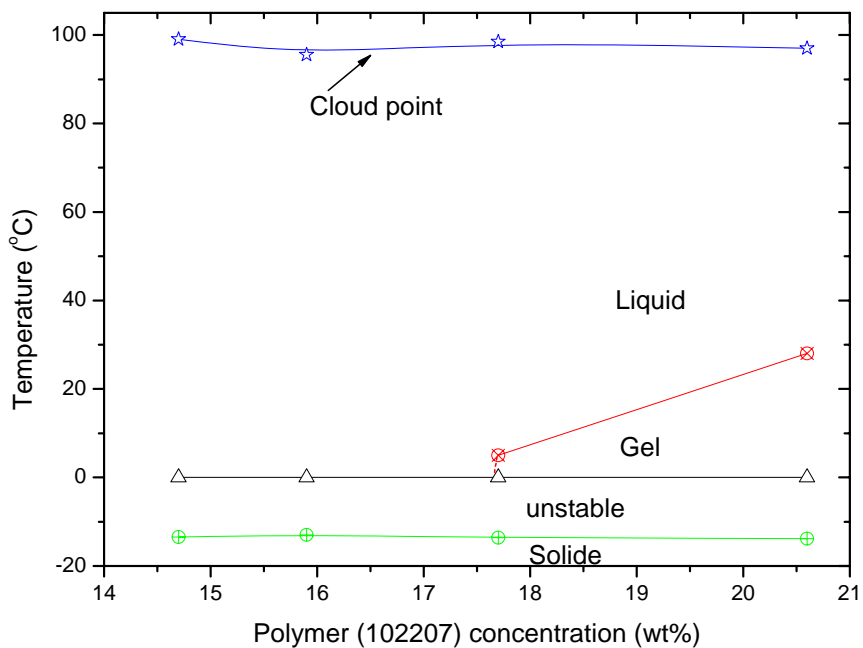
Figure 3.33 2-D phase behavior of 102207 nano composite in aqueous solution. The

nano composite is made by microemulsion polymerization of 10.9% PEG-PS$_7$-DVB$_2$ and

1.13% DVB/St (40/60) in water; initiator is APS (1% mole ration to vinyl groups in the

mixture); reaction time is 25h.

References

1.   Konstantinou, I. K.; Albanis, T. A. *Environment International* **2004,** 30, (2), 235-248.

2.   Chambers, L. D.; Stokes, K. R.; Walsh, F. C.; Wood, R. J. K. *Surface & Coatings Technology* **2006,** 201, (6), 3642-3652.

3.   Holmstrom, C.; Kjelleberg, S. *Fems Microbiology Ecology* **1999,** 30, (4), 285-293.

4.   Evans, S. M.; Leksono, T.; McKinnell, P. D. *Marine Pollution Bulletin* **1995,** 30, (1), 14-21.

5.   Champ, M. A. *Science of the Total Environment* **2000,** 258, (1-2), 21-71.

6.   Karlsson, J.; Eklund, B. *Marine Pollution Bulletin* **2004,** 49, (5-6), 456-464.

7.   Thomas, K. V.; McHugh, M.; Waldock, M. *Science of the Total Environment* **2002,** 293, (1-3), 117-127.

8.   Ranke, J.; Jastorff, B. *Environmental Science and Pollution Research* **2000,** 7, (2), 105-114.

9.   Thomas, K. V. *Journal of Chromatography A* **1999,** 833, (1), 105-109.

10.   Voulvoulis, N.; Scrimshaw, M. D.; Lester, J. N. *Applied Organometallic Chemistry* **1999,** 13, (3), 135-143.

11.   Bingaman, W. W.; Harrington, J. C.; Hurt, S. S.; Jacobson, A.; Mazza, L. S.; Milligan, D. H.; Shade, W. D.; Willingham, G. L. *Abstracts of Papers of the American Chemical Society* **1997,** 213, 88-ENVR.

12.   Wanka, G.; Hoffmann, H.; Ulbricht, W. *Macromolecules* **1994,** 27, (15), 4145-4159.

13. Alexandridis, P.; Hatton, T. A. *Colloids and Surfaces a-Physicochemical and Engineering Aspects* **1995,** 96, (1-2), 1-46.

14. Sharma, P. K.; Bhatia, S. R. *International Journal of Pharmaceutics* **2004,** 278, (2), 361-377.

15. Li, L.; Lim, L. H.; Wang, Q. Q.; Jiang, S. P. *Polymer* **2008,** 49, (7), 1952-1960.

16. Texter, J. *Abstracts of Papers of the American Chemical Society* **2005,** 230, U4335-U4335.

17. Song, M. J.; Lee, D. S.; Ahn, J. H.; Kim, D. J.; Kim, S. C. *Polymer Bulletin* **2000,** 43, (6), 497-504.

18. Bohorquez, M.; Koch, C.; Trygstad, T.; Pandit, N. *Journal of Colloid and Interface Science* **1999,** 216, (1), 34-40.

19. Prudhomme, R. K.; Wu, G. W.; Schneider, D. K. *Langmuir* **1996,** 12, (20), 4651-4659.

20. Lin, Y.; Alexandridis, P. *Journal of Physical Chemistry B* **2002,** 106, (42), 10834-10844.

21. Berglin, M.; Wynne, K. J.; Gatenholm, P. *Journal of Colloid and Interface Science* **2003,** 257, (2), 383-391.

22. Anderson, C.; Atlar, M.; Callow, M.; Candries, M.; Milne, A.; Townsin, R. *Journal of Marine Design and Operations* **2003**, 13.

23. Leo, A.; Hansch, C.; Elkins, D. *Chemical Reviews* **1971,** 71, (6), 616.

24. Malmsten, M., *Surfactants and Polymers in Drug Delivery*. Marcel Dekker: New York, 2002.

25.   Patrick, G. L., *An Introduction to Medicinal Chemistry*. Oxford University Press: New York, 1995.

26.   Sharma, P. K.; Reilly, M. J.; Jones, D. N.; Robinson, P. M.; Bhatia, S. R. *Colloids and Surfaces B-Biointerfaces* **2008,** 61, (1), 53-60.

27.   Herries, D. G.; Bishop, W.; Richards, F. M. *Journal of Physical Chemistry* **1964,** 68, 1842-1852.

28.   Harris, D. C., *Quantitative Chemical Analysis*. W.H. Freeman: New York, 1991.

29.   Lin, S. Y.; Y. Kawashima. *Pharmaceutica Acta Helvetiae* **1985,** 60, (12), 339-344.

30.   Doose, C. A.; Szaleniec, M.; Behrend, P.; M¨uller, A.; Jastorffa, B. *Journal of Chromatography A* **2004,** 1052, 103-110.

31.   Goka, K. *Environmental Research* **1999,** 81, (1), 81-83.

32.   Prud'homme, R. K.; Wu, G.; Schneider, D. K. *Langmuir* **1996,** 12, (20), 4651-4659.

33.   Wu, C.; Liu, T.; Chu, B.; Schneider, D. K.; Graziano, V. *Macromolecules* **1997,** 30, (16), 4574-4583.

34.   Thurn, T.; Couderc, S.; Sidhu, J.; Bloor, D. M.; Penfold, J.; Holzwarth, J. F.; Wyn-Jones, E. *Langmuir* **2002,** 18, (24), 9267-9275.

35.   Peracchia, M. T. F., E.; Desmae¨le, D.; Besnard, M.; Noe¨l, J.P.; Gomis, J.M.; Appel, M.; Angelo, J.; Couvreur, P. *J. Control. Release* **1999,** 60, 121-128.

36.   Andrade, J. D. H., V.; Jeon, S.I. *Adv. Chem. Ser.* **1996,** 248, 51-59.

37.   Storm, G. B., S.O.; Daemen, T.; Lasic, D.D. *Adv. Drug Deliv. Rev.* **1995,** 17, 31-48.

38.   Satomi, T.; Nagasaki, Y.; Kobayashi, H.; Tateishi, T.; Kataoka, K.; Otsuka, H. *Journal of Nanoscience and Nanotechnology* **2007,** 7, (7), 2394-2399.

39.   Kim., S.-W. C. W.-S. K. J.-H. *Journal of Dispersion Science And Technology* **2003,** 24, 475-487.

40.   Bang, J.; Lodge, T. P.; Wang, X.; Brinker, K. L.; Burghardt, W. R. *Physical Review Letters* **2002,** 89, (21), 215505/1-215505/4.

41.   Wanka, G.; Hoffmann, H.; Ulbricht, W. *Macromolecules* **1994,** 27, (15), 4145-9.

42.   Yu, C.; Yu, Y.; Miao, L.; Zhao, D. *Microporous and Mesoporous Materials* **2001,** 44-45, 65-72.

43.   Yu, C.; Fan, J.; Tian, B.; Stucky, G. D.; Zhao, D. *Journal of Physical Chemistry B* **2003,** 107, (48), 13368-13375.

44.   Alexandridis, P.; Olsson, U.; Lindman, B. *Langmuir* **1997,** 13, (1), 23-34.

45.   Alexandridis, P.; Andersson, K. *Journal of Colloid and Interface Science* **1997,** 194, (1), 166-173.

46.   Alexandridis, P.; Andersson, K. *Journal of Physical Chemistry B* **1997,** 101, (41), 8103-8111.

47.   Helfand, E.; Wasserman, Z. R. *Macromolecules* **1976,** 9, (6), 879-88.

48.   Mawson, S.; Yates, M. Z.; O'Neill, M. L.; Johnston, K. P. *Langmuir* **1997,** 13, (6), 1519-1528.

49.   Texter, J.; Ziemer, P.; Rhoades, S.; Clemans, D. *Journal of Industrial Microbiology & Biotechnology* **2007,** 34, (8), 571-575.

50.   Provder, T.; Malliprakash, S.; Amin, S. H.; Majid, A.; Texter, J. *Macromolecular Symposia* **2006,** 242, 279-289.

51.   Dissanayake, I. D.; Dimitrakopoulos, P. *Physical Review E* **2006,** 74, (2).

52.   Malmsten, M.; Lindman, B. *Macromolecules* **1992,** 25, (20), 5446-50.

53.   Malmsten, M.; Lindman, B. *Macromolecules* **1992,** 25, (20), 5440-5.

54.   Sigma-aldrich, *Handbook of Fine Chemicals*. 2007-2008.

55.   Harlow, E.; Lane, D., *Antibodies: A laboratory Manual*. Cold Spring Harbor Laboratory Press: 1988; p 689(726).

56.   Texter, J. *Journal of Non-Crystalline Solids* **2002,** 305, (1-3), 339-344.

57.   Andrade, J. D.; Hlady, V.; Jeon, S. I. *Hydrophilic Polymers* **1996,** 248, 51-59.

58.   Tsukagoshi, T.; Kondo, Y.; Yoshino, N. *Colloids and Surfaces B-Biointerfaces* **2007,** 54, (1), 101-107.

59.   Nam, K.; Kimura, T.; Kishida, A. *Biomaterials* **2007,** 28, (20), 3153-3162.

60.   Klouda, L.; Mikos, A. G. *European Journal of Pharmaceutics and Biopharmaceutics* **2008,** 68, (1), 34-45.

61.   Sun, Y. H.; Qiu, Y. X.; Yu, X. J.; Feng, L. X. *Chemical Journal of Chinese Universities-Chinese* **1996,** 17, (4), 642-645.

62.   Connal, L. A.; Vestberg, R.; Hawker, C. J.; Qiao, G. G. *Macromolecules* **2007,** 40, 7855-7863.

63.   Ohshima, T.; Kogami, Y.; Miyata, T.; Uragami, T. *Journal of Membrane Science* **2005,** 260, (1-2), 156-163.

64.   Lu, H.; Lovell, L. G.; Bowman, C. N. *Macromolecules* **2001,** 34, (23), 8021-8025.

65.   El-Nashar, D. E.; Turky, G. *Polymer-Plastics Technology and Engineering* **2003,** 42, (2), 269-284.

66.   Ide, N.; Fukuda, T. *Macromolecules* **1999,** 32, (1), 95-99.

67.   Matyjaszewski, K.; Davis, T. P., *Handbook of Radical Polymerization*. Wiley: Hoboken, 2002.

68.   Matyjaszewski, K., *Controlled/Living Radical Polymerization. From Synthesis to Materials (ACS Symp. Ser. 944)*. ACS: 2006.

69.   Braunecker, W. A.; Matyjaszewski, K. *Progress in Polymer Science* **2007,** 32, (1), 93-146.

70.   Matyjaszewski, K.; Gnanou, Y.; Leibler, L., *Macromolecular Engineering: Precise Synthesis, Materials Properties, Applications*. Wiley-VCH: Weinheim, 2007; p 730 pp.

71.   Georges, M. K.; Veregin, R. P. N.; Kazmaier, P. M.; Hamer, G. K. *Macromolecules* **1993,** 26, (11), 2987-8.

72.   Hawker, C. J.; Bosman, A. W.; Harth, E. *Chemical Reviews (Washington, D. C.)* **2001,** 101, (12), 3661-3688.

73.   Chiefari, J.; Chong, Y. K.; Ercole, F.; Krstina, J.; Jeffery, J.; Le, T. P. T.; Mayadunne, R. T. A.; Meijs, G. F.; Moad, C. L.; Moad, G.; Rizzardo, E.; Thang, S. H. *Macromolecules* **1998,** 31, (16), 5559-5562.

74.   Moad, G.; Rizzardo, E.; Thang, S. H. *Australian Journal of Chemistry* **2006,** 59, (10), 669-692.

75.   Wang, J.-S.; Matyjaszewski, K. *J. Am. Chem. Soc.* **1995,** 117, (20), 5614-15.

76.   Kato, M.; Kamigaito, M.; Sawamoto, M.; Higashimura, T. *Macromolecules* **1995,** 28, (5), 1721-3.

77.   Matyjaszewski, K.; Xia, J. *Chem. Rev.* **2001,** 101, (9), 2921-2990.

78.   Tsarevsky, N. V.; Matyjaszewski, K. *Chemical Reviews (Washington, DC, United States)* **2007,** 107, (6), 2270-2299.

79.   Minisci, F. *Acc. Chem. Res.* **1975,** 8, (5), 165-71.

80.   Curran, D. P. *Synthesis* **1988**, (7), 489-513.

81.   Clark, A. J. *Chemical Society Reviews* **2002,** 31, (1), 1-11.

82.   Kabachii, Y. A.; Kochev, S. Y.; Bronstein, L. M.; Blagodatskikh, I. B.; Valetsky, P. M. *Polym. Bull.* **2003,** 50, (4), 271-278.

83.   Le Grognec, E.; Claverie, J.; Poli, R. *J. Am. Chem. Soc.* **2001,** 123, (39), 9513-9524.

84.   Kotani, Y.; Kamigaito, M.; Sawamoto, M. *Macromolecules* **1999,** 32, (8), 2420-2424.

85.   Matyjaszewski, K.; Wei, M.; Xia, J.; McDermott, N. E. *Macromolecules* **1997,** 30, (26), 8161-8164.

86.   Braunecker, W. A.; Itami, Y.; Matyjaszewski, K. *Macromolecules* **2005**, 9402-9404.

87.   Percec, V.; Barboiu, B.; Neumann, A.; Ronda, J. C.; Zhao, M. *Macromolecules* **1996,** 29, (10), 3665-8.

88.   Wang, B.; Zhuang, Y.; Luo, X.; Xu, S.; Zhou, X. *Macromolecules* **2003,** 36, (26), 9684-9686.

89.   Uegaki, H.; Kotani, Y.; Kamigaito, M.; Sawamoto, M. *Macromolecules* **1997,** 30, (8), 2249-2253.

90.   Lecomte, P.; Drapier, I.; Dubois, P.; Teyssie, P.; Jerome, R. *Macromolecules* **1997,** 30, (24), 7631-7633.

91.   Tang, W.; Matyjaszewski, K. *Macromolecules* **2006,** 39, (15), 4953-4959.

92.   Coessens, V.; Pintauer, T.; Matyjaszewski, K. *Progress in Polymer Science* **2001,** 26, (3), 337-377.

93.   Antonietti, M.; Basten, R.; Lohmann, S. *Macromolecular Chemistry and Physics* **1995,** 196, (2), 441-66.

94.   Chow, P. Y.; Gan, L. M. *Advances in Polymer Science* **2005,** 175, (Polymer Particles), 257-298.

95.   Co, C. C.; Cotts, P.; Burauer, S.; de Vries, R.; Kaler, E. W. *Macromolecules* **2001,** 34, (10), 3245-3254.

96.   Hentze, H. P.; Kaler, E. W. *Current Opinion in Colloid & Interface Science* **2003,** 8, (2), 164-178.

97.   Stoffer, J. O.; Bone, T. *Journal of Polymer Science, Polymer Chemistry Edition* **1980,** 18, (8), 2641-8.

98.   Atik, S. S.; Thomas, J. K. *Journal of the American Chemical Society* **1981,** 103, (14), 4279-80.

99.   Candau, F.; Leong, Y. S.; Fitch, R. M. *Journal of Polymer Science, Polymer Chemistry Edition* **1985,** 23, (1), 193-214.

100.   Reining, B.; Keul, H.; Hocker, H. *Polymer* **1999,** 40, (12), 3555-3563.

101.   Deng, Y. H.; Yu, T.; Wan, Y.; Shi, Y. F.; Meng, Y.; Gu, D.; Zhang, L. J.; Huang, Y.; Liu, C.; Wu, X. J.; Zhao, D. Y. *Journal of the American Chemical Society* **2007,** 129, (6), 1690-1697.

102.   Texter, J.; Oppenheimer, L. E.; Minter, J. R. *Polym. Bull. (Berlin) FIELD Full Journal Title:Polymer Bulletin (Berlin, Germany)* **1992,** 27, (5), 487-94.

103. Matyjaszewski, K.; Patten, T. E.; Xia, J. H. *Journal of the American Chemical Society* **1997,** 119, (4), 674-680.

104. Li, J. R.; Xu, J. R.; Zhang, M. Q.; Rong, M. Z.; Zheng, Q. *Polymer* **2005,** 46, (24), 11051-11059.

105. Taton, D.; Gnanou, Y.; Matmour, R.; Angot, S.; Hou, S.; Francis, R.; Lepoittevin, B.; Moinard, D.; Babin, J. *Polymer International* **2006,** 55, (10), 1138-1145.

106. Wang, F. Y.; Ma, C. C. M.; Wu, W. J. *Journal of Applied Polymer Science* **2001,** 80, (2), 188-196.